UNIVERSITY
OF TRENTO - Italy
DEPARTMENT OF INDUSTRIAL ENGINEERING

XXVI cycle

Doctoral School in Materials Science and Engineering

Color masterbatches for polyamide 6 fibers. Optimization of compounding and spinning processes. Physical-chemical characterization of industrial products.

Mauro Buccella

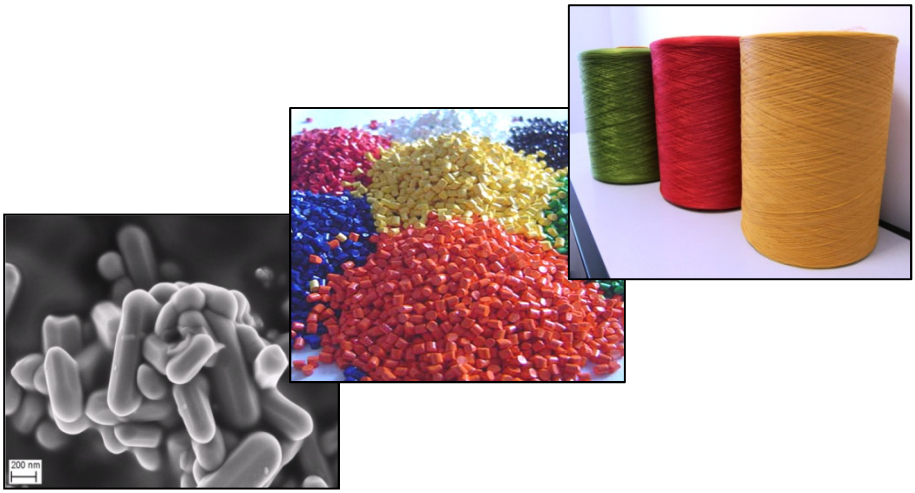

April 2014

UNIVERSITY
OF TRENTO - Italy
DEPARTMENT OF INDUSTRIAL ENGINEERING

XXVI cycle

Doctoral School in Materials Science and Engineering

Color masterbatches for polyamide 6 fibers. Optimization of compounding and spinning processes. Physical-chemical characterization of industrial products.

Mauro Buccella

Academic Tutors:

Prof. Luca Fambri

Ing. Andrea Dorigato, PhD

Industrial Tutor:

Dott. Mauro Caldara

April 2014

ABSTRACT

In the last years the coloration industry has become increasingly important because it strongly influences the market of the plastic materials.

The request of objects with new and particular colors, sometimes with imperceptible differences, combined with high physical and chemical performances, has made the coloration technology more sophisticated and complex. Moreover, the recent legislations (i.e. REACH standard) suggest the use of products with lower human health impact. Therefore, a continuous research and development of new colorants and technologies is needed, in order to obtain environmental friendly manufacturing processes and market products.

As concerns the carpet sector, the solution dyed process of the fibers is industrially preferable rather than the coloration through batch of raw yarns. This is because the first process involves the production of monoconcentrated color masterbatches, their mixing in order to obtain the final color masterbatch and its addition into the polymer matrix during fiber spinning. On the other hand, the production of carpet from raw fibers shows higher environmental impact because the dyeing baths contain colorants and additives environmentally harmful and difficult to remove with water treatments. The solution dyed process is more difficult from an industrial point of view, because during the melt spinning three problems can occurred: (i) clogging of filtration system during spinning due to agglomerates, deposits and degraded material, (ii) formation of polymer drops under the spinneret due to degradation phenomena that can cause premature fibers breakage and (iii) fibers breakage during drawing process.

The objective of this work is the investigation of the industrial production process of the Color Masterbatches and of the parameters that influence the pigment dispersion into the polymer matrix. In particular, the project is focused on the production

process optimization in order to increase the quality of the final product and to minimize their environmental impact.

The three steps of the solution dyed bulk continuous process were investigated: (i) production of monoconcentrated masterbatch, (ii) production of color masterbatch and (iii) mass pigmentation during melt spinning process.

In the first part of the work, a detailed microstructural characterization was performed to assess the different morphologies and surface properties of the most important color pigments used in the automotive sector. The most problematic monoconcentrated masterbatches were industrially produced using different processing set-up, related to different specific mechanical energy applied to the material during the production. Furthermore, a detailed analysis of the pigment dispersion state in the matrix was performed, through the evaluation of the filterability, the Relative Color Strength (RCS) and the rheological behavior of the monoconcentrated masterbatches. Moreover the thermal stability of the products was investigated by chemical characterization and rheological measurement. The industrial production process for each monoconcentrated masterbatch was optimized, obtaining a product quality improvement and a significant production cost reduction.

In the second part of the work, the blue color masterbatch was selected because it is a critical product for the melt spinning process. This color masterbatch has the peculiarity to clog the filtration system during spinning process, and a frequent change of filters is thus required. This monoconcentrated color masterbatch was produced in two different ways: standard and optimized processes.
These two color masterbatches were fully characterized, from a coloration, chemical and rheological point of view, in order to determine the effect of monoconcentrated production process and so of the pigment dispersion on the subsequent industrial production step. The use of the optimized monoconcentrated masterbatch allowed to

reduce the clogging power of the product of about 30%, and to increase its thermal stability. Furthermore even the monomer concentration, that is related to the drop formation under the spinneret and to the filament breakage, was reduced.

The third part was focused on the characterization of the industrial yarn colored with the standard and the optimized blue masterbatches, in order to evaluate the effect of the pigment dispersion on the final products. The optimized yarn showed an improvement of the mechanical properties, in particular of the elastic modulus, compared with the standard product. This is very important because, for the yarns used in the carpet industry, the higher elastic modulus, the higher carpet resistant to the compressive stresses during its service life. The pigment dispersion improvement enhanced the heterogeneous nucleation activity of polyamide 6 during the melt spinning, resulting in a higher content of the more stable α phase compared to the γ crystalline phase. The thermal and UV degradation resistance were also improved.

Finally, in order to confirm the good experimental results obtained on the optimized blue yarn at the laboratory scale, an industrial test was performed and the most problematic aspects of the process were critically analyzed. The use of the optimized blue masterbatch to color the industrial yarn allowed to markedly reduce the clogging phenomenon on the extruder filter of about 70%, reducing the number of filter substitutions and so the production stops. Moreover, the filament breakage frequency during the spinning were reduce of about 45%, increasing the productivity of the process, the stability of the product and reducing the production co

TABLE OF CONTENTS

LIST OF FIGURES

LIST OF TABLES

INTRODUCTION

This research project was developed from a collaboration between Aquafil S.p.A. (Arco, Italy) and the University of Trento. Aquafil is a multinational company specialized in Polyamide 6 polymerization, fiber spinning and compounding production [1].

The first polyamide, nylon 66 or polyamide 66, was synthesized by W.H. Carothers at Du Pont laboratory in 1934. Afterwards in 1938, at I.G. Farbenindutrie, Schlack developed nylon 6, or polyamide 6, obtained by ring opening polymerization of caprolactam. Polyamides or nylons were the first synthetic polymer used for fiber applications and their rapid market growth was determined by their similar appearance of silk. For this reason they were initially used in the textile and carpet sector and only later for engineering purposes, because of their excellent mechanical and chemical properties [2-5].
Industrially there are two different macro categories of fibers used in the carpet sector: raw and solution dyed yarns. Raw fibers are made only by polyamide 6 and a low amount of titanium dioxide to make the appearance dull. This yarns are transformed in carpets by tufting process and colored by immersion in dyeing baths containing water, acid and metal-complex colorant and additives. On the other hands, solution dyed fibers are colored during spinning process by addition the so called color masterbatch, made by polyamide 6, color pigments and antioxidants [6]. From an industrial point of view, the production of solution dyed fibers is more difficult and critical compared to the production of raw fibers (not colored). In fact, the first process involves the production of monoconcentrated color masterbatches, their mixing in order to obtain the final color masterbatch and their addition into the polymer matrix during fiber spinning.

Considering these two processes the production of carpet from raw fibers shows higher environmental and human health impact compared to those produced from solution dyed process. This because dyeing baths contain colorant and additives environmentally harmful and difficult to remove with water treatments.
Due to the recent legislation (i.e. REACH standard [7]) that suggest the use of product with lower human health impact, the solution dyed process is industrially preferable rather than the raw fibers production.
These two processes show an important difference in the production efficiency and this can be related to the color masterbatch addition. The major effects that characterized the solution dyed spinning process are: (i) clogging of filtration system during spinning due to agglomerates, deposits and degraded material, (ii) formation of polymer drops under the spinneret due to degradation phenomena that can cause premature fibers breakage and (iii) fibers breakage during drawing process.
On the basis of these considerations, the aim of this work is the investigation and understanding the specific materials-process-property relationship in an industrial reality, in order to optimize the production processes and minimize the environmental impact. In particular, the project concerns the improvement and the production process optimization of the color masterbatches and their use in the so called solution dyed process of synthetic fibers.

This thesis is divided in four chapters. In the first chapter a short general theoretical introduction about the color from physical point of view, the color pigments and the color masterbatches, is reported. The second chapter is focused on the materials analyzed, on their preparation methods and on experimental technologies used to evaluate the properties of the samples. In the third chapter the analysis of the results on pigments, monoconcentrated color masterbatch, color masterbatch and fibers are reported. These result were discussed in order identify the best production process, at least from qualitative point of view. Finally the fourth chapter regards the conclusions about the entire research project and the suggestions to improve the production process.

1. BACKGROUND

1.1. PHYSICAL PROPERTIES OF COLOR

Color is the visual perception generated by nerve signals that the photoreceptors in the retina send to the brain when they are hit by an electromagnetic radiation in the visible spectrum [8]. Different wavelengths are perceived to be different colors. Generally speaking, the presence of color requires three fundamental factors: (i) the light source, (ii) the object that interacts with the electromagnetic radiation emitted by the source, and (iii) the human eye that observes the phenomenon [9]. Color is a very complex phenomenon because it is influenced by physical, chemical, psychological and physiological processes [10, 11].

1.1.1. ILLUMINANT

An object is visible and colored only if an electromagnetic radiation interact with its surface and the reflected spectrum reach the retina of human eye [8].
The electromagnetic spectrum is divided in different frequency intervals, that denote different nature of radiant energy, as it is reported in Figure 1.1. The human eye is sensitive only to a small frequencies interval, called visible light, with wavelength between 380 to 760 nm [12]. The visible spectrum is reported in the Figure 1.1 and each frequency corresponds to a specific color perceived by the eye.
Visible light can be generated in different ways and each source shows different spectral emission. When there is no gap in the visible spectrum of light, the source and the spectrum is called continuum, and the light is white. The sunlight, the incandescence and the fluorescence are the typical continuum sources of white light.

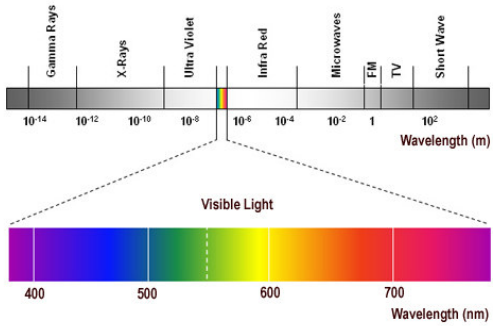

Figure 1.1: Electromagnetic spectrum of light

Even if the color of the object that they illuminate appears quite similar, there are slight differences between these sources, because of their different emission spectrum [13, 14], as reported in Figure 1.2.

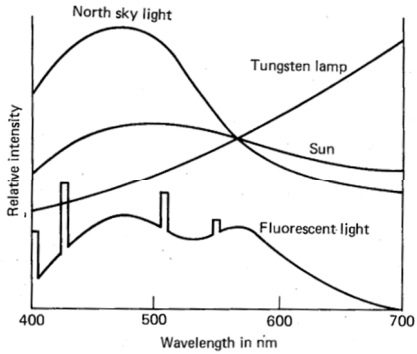

Figure 1.2: Spectral distribution curves for different white light sources in the visible spectrum [15]

There are two main ways in order to create light radiation: (i) incandescence and (ii) luminescence. In the first case, the tungsten filament in the lamp is heated at elevated temperature applying electrically power because of joule effect, and the vibrational energy of its atoms is converted into optical energy (light radiation). Luminescent light is also called cold light because it is not generated from heating

sources. The electrons stream, produced by electrical power, collides with the atom gas in the lamp and excites them to an higher energy level. This higher state is unstable and so the excited electrons come back to a more stable lower energy level. This motion release a photon in the ultraviolet (UV) region of the spectrum at 253.7 and 185 nanometers (nm). This photon are absorbed by electrons in the atom of interior coating of lamp that, in the same way, emit photon in the visible spectrum [15, 16].

1.1.2. OBJECT

An object appears colored because it interacts with the light, absorbing some wavelength radiations and reflecting some others [17].
The interaction of light with bulk matter is a phenomenon related to the surface and physical properties of materials (see in Figure 1.3). When the electromagnetic radiation reaches the object, a part of the incoming beam is reflected in two ways. The specular reflection occurs when there is a smooth surface like mirror and the angle of incidence is equal to the angle of reflection and the color is the same of incoming light. Part of incoming light penetrates into the object near the surface and can be absorbed by the molecular chromophoric groups or reflected back toward the surface. This reflected light interacts with the particles and is scattered in all direction producing a diffuse reflection [18]. The diffuse radiation reveals the color of object strongly compare specular reflection because it is generated from a deep interaction with the matter. The other part of radiation penetrates deeply inside the material and can be absorbed or scattered [19].
The absorbed light can be converted into heat due to atoms bond vibration or/and can be reemitted as fluorescence [8]. Obviously the fluorescence phenomenon modifies the color of object and so it has to be taken into account for color matching.

If the material is transparent the incoming beam is deflected when it enters into the materials due to different refractive index and when it reaches the opposite surface of the object it can be internally reflected or transmitted [8] .

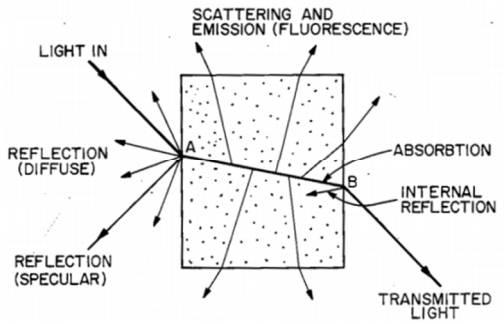

Figure 1.3: Schematic representation of light-matter interaction [8]

An object appears in a particular color because it reflects the light with a specific wavelength and absorbs the other part of radiation. For example, a blue object reflects blue light radiation and absorbs all other wavelength of spectrum as it is represented in Figure 1.4.

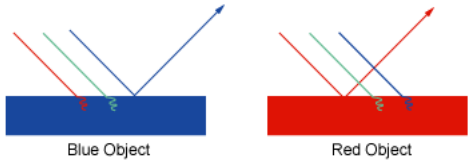

Figure 1.4: Representation of light reflection for colored materials

1.1.3. THE OBSERVER

The observer of the color is the human eye, in particular their photosensitive parts, able to collect the light radiation and to produce specific stimuli elaborated by the brain [17]. In Figure 1.5 the scheme of the human eye is reported.

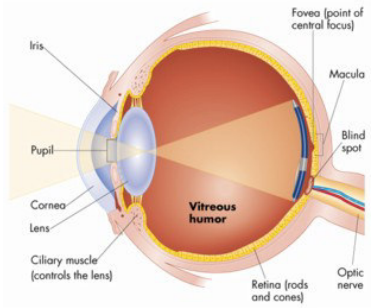

Figure 1.5: Scheme of human eye

The photoreceptor cells in the retina are rods and cones. The rods are more sensitive compared to cones and they are responsible of the night vision, with low light intensities. They detect the light in all the spectrum of visible light with the sensitivity peak at 500 nm of wavelength but they are not sensitive to color and give a monochromatic vision with neutral color perception, white, gray and black [20]. On the other hand the cone cells are sensitive to bright light for the day vision and their response is more complicated. The cones give three different peak of light sensitivity, related to three different color perception. L cones show the peak at 560 nm of wavelength in the range of red color, M cones are sensitive to green color with a peak at 530 nm and S cones have the sensitivity peak at 420 nm in the blue

color region of spectrum [11, 17, 21]. In Figure 1.6 the normalized absorbance of eye photoreceptors are reported.

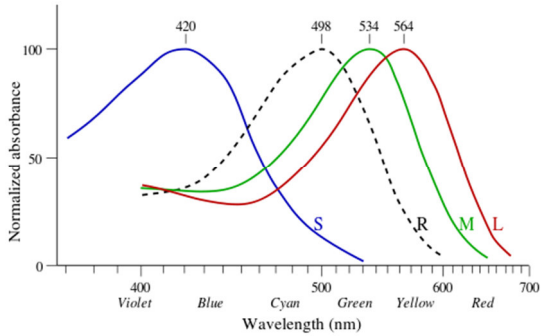

Figure 1.6: Normalized absorbance of cones and rods photoreceptors

For these reasons the human color vision is trichromatic but it is strongly influenced by a lot of variables like age, memory, cultural background. Moreover important variation with the human population in the cone cells sensitivity are detected.

1.2. COLOR MATCHING

Because of numerous processes and variables that are involved in the color perception phenomenon, standard method was developed in order to measure color in an objective way. Light sources and observers have been standardized by the Commission Internationale de l'Eclairage (CIE).

The standard illuminant used in the color measurements are the incandescent light (A), the north sky daylight (D65) and the cool white fluorescent light (F2) [18]. They are described by spectral power distribution D(λ). The standard colorimetric observer was described using the color matching functions (λ), (λ) and (λ), obtained from specific experimental procedures by CIE in 1931 [22]. These functions represent the spectral tristimulus values related to the sensitivity of the

three types of cones [18]. In Figure 1.7 the three color matching function are reported.

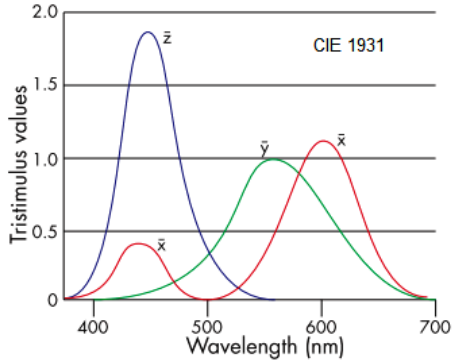

Figure 1.7: Color matching functions

The three color matching functions give the amount of the X, Y and Z primary imaginary colors required to define the spectral stimulus of unit radiance for the standard observer and the unit plane of the tristimulus color space XYZ (Figure 1.8a) is called CIE 1931 system or (x,y)-chromaticity diagram (Figure 1.8b) [23].

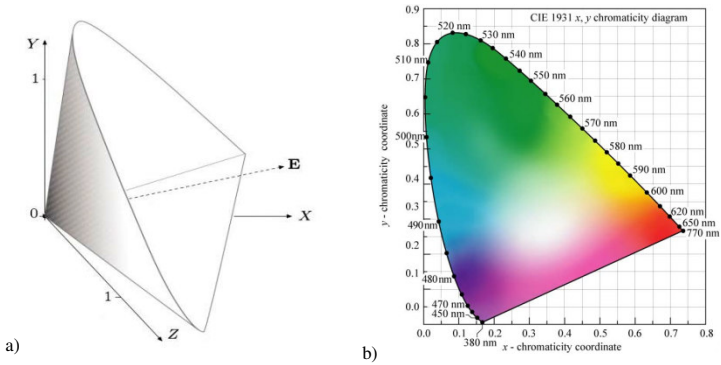

Figure 1.8: (a) Tristimulus color space XYZ and (b) (x,y) chromaticity diagram [24]

The chromaticity coordinates used to describe the pure color hue and saturation, are reported in the Equations (1), (2) and (3):

$$x(\lambda) = \frac{\tilde{x}}{\tilde{x}(\lambda) + \tilde{y}(\lambda) + \tilde{z}(\lambda)} \quad (1)$$

$$y(\lambda) = \frac{\tilde{y}}{\tilde{x}(\lambda) + \tilde{y}(\lambda) + \tilde{z}(\lambda)} \quad (2)$$

$$z(\lambda) = \frac{\tilde{z}}{\tilde{x}(\lambda) + \tilde{y}(\lambda) + \tilde{z}(\lambda)} \quad (3)$$

With the condition in Equation (4):

$$x(\lambda) + y(\lambda) + z(\lambda) = 1 \quad (4)$$

In 1976, CIE introduced a new color model, called CIELab in order to linearize the color representation with respect to the human color perception and to produce a more intuitive color system [23, 25] . Today the CIELab is the most used system to measure color in the industry by spectrophotometers. CIELab color space is a sphere and the new coordinates, derived from a transformation of tristimulus values, are reported in the Equations (5), (6) and (7):

$$L^* = 116 \cdot \left(\frac{Y}{Y_n}\right)^3 - 16 \quad (5)$$

$$a^* = 500 \cdot \left[\left(\frac{X}{X_n}\right)^{\frac{1}{3}} - \left(\frac{Y}{Y_n}\right)^{\frac{1}{3}}\right] \quad (6)$$

$$b^* = 500 \cdot \left[\left(\frac{Y}{Y_n}\right)^{\frac{1}{3}} - \left(\frac{Z}{Z_n}\right)^{\frac{1}{3}}\right] \quad (7)$$

Where L* represents the difference between light (where L*=100) and dark (where L*=0), a* represents the difference between green (-a*) and red (+a*), and b*

represents the difference between yellow (+b*) and blue (-b*), as reported in Figure 1.9. Moreover the angle between a* and b* axes represents the color Hue and the radial distance from the center of the sphere is the color Saturation or the Chroma.

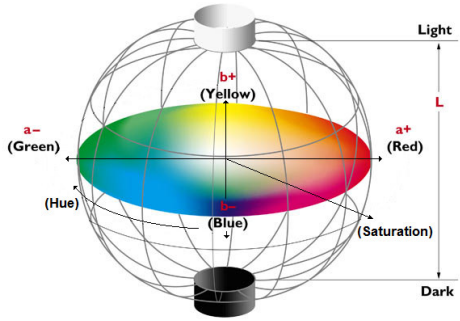

Figure 1.9: Representation of Lab color space

In order to evaluate the color differences between two samples (ΔE*) CIE developed a formula using color coordinates in Lab space (Equation (8)) [23, 26, 27]:

$$\Delta E^*_{ab} = \sqrt{(L^*_2 - L^*_1)^2 + (a^*_2 - a^*_1)^2 + (b^*_2 - b^*_1)^2} \qquad (8)$$

Where $\Delta E^*_{ab} \approx 2{,}3$ corresponds to a just noticeable difference [28].

In 1984 a new color difference formula (Equation (9)), based on LCh model, was developed and recommended for industrial pass/fail evaluation by Color Measurement Committee (CMC):

$$\Delta E^*_{CMC(l:c)} = \sqrt{\left(\frac{L^*_2 - L^*_1}{l \cdot S_L}\right)^2 + \left(\frac{C^*_2 - C^*_1}{c \cdot S_C}\right)^2 + \left(\frac{\Delta H^*_{ab}}{S_H}\right)^2} \qquad (9)$$

Where S_L, S_C and S_H are the compensation of lightness, chroma and hue respectively. The factors l (lightness) and c (chroma) allowing the users to weight the difference based on the ratio of l:c that is deemed appropriate for the application. Commonly used values are 2:1 for acceptability [29] and 1:1 for the detection limit. This formula is more reliable and in agreement with the observer vision and it includes the weighting functions in order to compensate the lightness, chroma and hue differences in relation to nature and use of the product evaluated [29].

1.3. COLOR MEASUREMENTS

The most important technique to evaluate the color of products both in industrial and in research fields is the spectrophotometer [11]. Spectrophotometers are instruments for measuring reflectance, transmittance or absorbance of a sample as a function of wavelength [30]. Light reflected by a material is collected in an integration sphere, normalized to the source light of the reflectance, and calibrated with the measurement of a perfect diffuse white (pdw) standard (100% reflection) and a black box (zero reflection) over the entire wavelength spectrum of visible light. The result of this test is the reflection factor (RF) defined as the ratio between the reflectance of sample and of reference, reported in Equation (10) [31].

$$RF(\lambda) = \frac{R(\lambda)(sample)}{R(\lambda)(pdw)} \tag{10}$$

The reflectance factor is usually referred to a % Reflectance. Reflectance spectra are related to color using established international conventions and according to the Commission Internationale d'Eclairage (CIE) (1986) method. The tristimulus values L, a and b, that describe color with complete unambiguity, are calculated. Even the Hue, Saturation and ΔE are measured in order to optimize the color matching process [32]. A schematic representation of the spectrophotometer is shown in Figure 1.10.

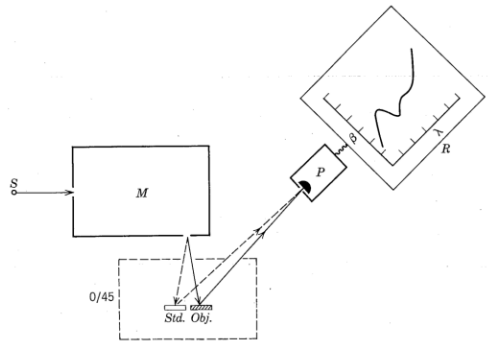

Figure 1.10: Schematic diagram showing the principal component of spectrophotometer. S: light source; M: monochromator; Obj.: sample to be measured; Std.: standard of reflectance factor; P: photocell; R: read out unit [11]

1.4. COLORATION TECHNOLOGY

Since prehistory coloration technology has played an important role in our society from on anthropological, aesthetic, functional and economic point of view [33, 34]. Also the market of plastic materials is strongly influenced by the coloration industry, because of the growing demand of innovative color products with high physical, chemical and mechanical performances.

The coloration of plastic materials can be made basically in two ways: using soluble dyes or color pigments [35]. Soluble dyes are organic substances that can be solubilized with the plastic substrate. Their good chemical affinity with the polymer matrix results in the absence of visible particles and in the retention of the transparency of the compounded materials. In the Figure 1.11 the dyes solubilization phenomenon is represented.

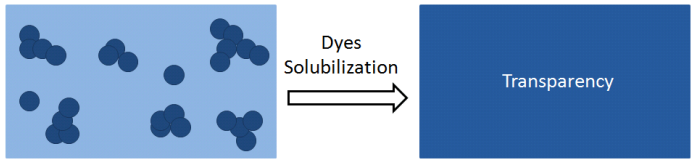

Figure 1.11: Schematic representation of dyes solubilization

Color pigments are very fine and insoluble particles that maintain their original properties both during the manufacturing processes and during the whole life of the plastic product [10, 35]. Pigments impart color to the plastic medium by a selective light absorption in the visible spectrum [33]. In Figure 1.12 the dispersion process of pigments is reported.

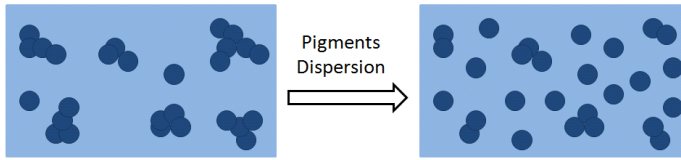

Figure 1.12: Schematic representation of pigments dispersion

1.4.1. PIGMENT PROPERTIES

Color pigments show three structural levels (Figure 1.13). The primary particles are obtained during their synthesis and have small particle size and tend to aggregate. The aggregates are formed by primary particles that tend to collapse because of their high surface energy. This results in a reduction of specific surface area. Finally, agglomerates can be obtained by the physical bonding between aggregates [36-39].

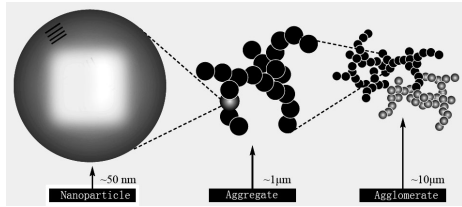

Figure 1.13: Representation of primary particle, aggregate and agglomerate [40]

Color pigments used in plastic industry can be divided into two groups: inorganic and organic pigments. Their primary particles can have different shapes: cubes, platelets, needless or different irregular shapes [41-43]. In Figure 1.14 the primary particle with different geometry, their aggregate and agglomerate are shown.

The primary particles of the most used pigments are composed by tiny molecular crystals, and show dimensions ranging from 20 to 500 nm [41]. For this reason they are called nano colorants [36].

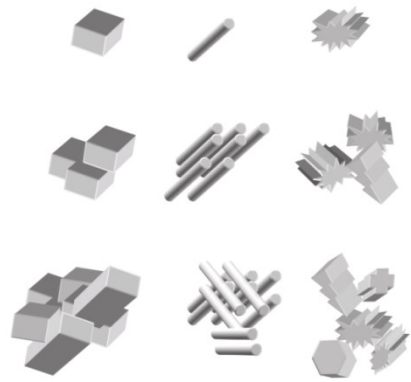

Figure 1.14: Primary particles and aggregates with different geometry [41]

In order to specifying the nature of a colorant, the Color Index (CI), defined by Society of Dyers and Colorists and the American Association of Textile Chemists, can be used.

Generally speaking, color pigments for plastic have to satisfy some requirements: (i) total insolubility in the polymer in which they are incorporated, (ii) easy dispersion within the matrix, (iii) chemical stability under severe thermo-mechanical processing conditions, (iv) compatibility with the other additives used, (v) non-toxicity and (vi) environmental friendliness [36, 41].

Except for titanium dioxide (TiO_2), inorganic pigments are characterized by high light absorption and low scattering. They present high stability at elevated temperatures (up to 300 °C), but they possess a lower "color strength" compared to organic pigments. Generally speaking, inorganic pigments can be easily dispersed in polymers even at low shear stresses, because their good wettability of the primary particles reduces the agglomeration phenomena [36]. The most commonly used inorganic pigments in the plastic industry are CI Pigment White 6 (TiO_2) and CI

Pigment Black 7 (Carbon Black) [44-46]. Organic pigments are polycyclic molecules containing chromophoric groups. Due to their insolubility in most polymeric matrices, they show a lower dispersability with respect to organic pigments, especially in polyolefins. Their heat resistance is often limited to 280 °C [36]. Unlike inorganic pigments, it has been also found that organic pigments play a marked nucleating activity in polymer matrices, increasing crystallization kinetics [47-53]. The most utilized organic pigments are blue and green copper phthalocyanine (CI Pigment Blue 15:3 and CI Pigment Green 7) and violet dioxazine (CI pigment violet 23) [36, 54, 55].

1.4.2. MASS PIGMENTATION OF SYNTHETIC FIBERS

Generally speaking, color pigments are not used in powder form, but they are compounded with polymer for the production of monoconcentrated masterbatches, with a filler concentration ranging from 5 to 40 wt%. These concentrates are added into to the polymer through an extrusion process in the so-called "mass coloration" or “solution dyed” process [36, 41], as reported in Figure 1.15.

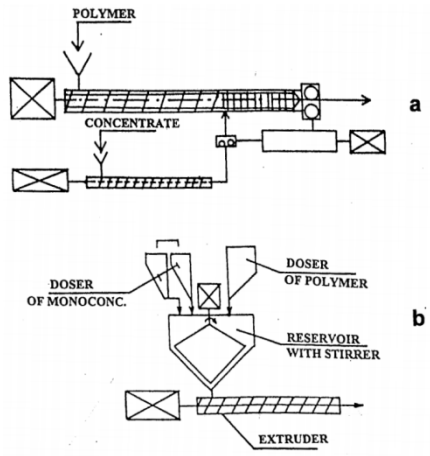

Figure 1.15: Schematic diagram of mass pigmenting in melt spinning process.
(a) Injection method and (b) metering of concentrate chips before melting [36]

Compared to the use of color powders, monoconcentrated masterbatches present several advantages in term of safety (i.e. avoiding of dust in the working place) and in terms of product quality (i.e. better pigments dispersion, higher color strength, reduced cleaning time) [35, 56, 57].

Mass coloration process is composed by two steps: (i) preparation of the color masterbatch and (ii) its addition to the polymer matrix [36].

The extrusion process during monoconcentrated masterbatch production promotes pigments dispersion, and involves four steps: (i) aggregates and agglomerates of pigment primary particles breakdown thanks to elevated shear stress generated (ii) improves the particles wetting from melt polymer, (iii) produces a uniform particles distribution within matrices and (iv) stabilizes the dispersion in order to prevent flocculation phenomenon [36, 58-60].

The dispersion degree of the pigments in the polymer matrix and their tendency to agglomerate depend on the physical properties of pigment particles (i.e. size, shape, surface properties, crystalline structure, chemical composition of the primary crystals) [41, 61]. The smaller particles size of color pigment the higher color strength of masterbatches [38] (Figure 1.16).

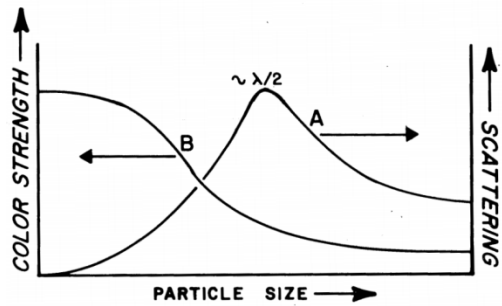

Figure 1.16: The variation of scattering (A) and the color strength (B) with the particle size [8]

On the other hand, pigment aggregation during the production process leads to some technical limitations like reduction of the mechanical properties, breakage during

spinning, difficulties in obtaining the desired color and economical disadvantages due to the increase of the production times and scraps [41, 61, 62].

Moreover, pigments constituted by smaller primary particles possess an higher surface energy and thus have a higher tendency to agglomerate or to absorb other chemical species (i.e. solvents or surfactants) [33, 63]. As demonstrated from the studies of Deshmukh et all. [35] and Ahmed et all. [41], the most critical pigments to disperse in a polymer matrix are CI Pigment Blue 15:3, CI Pigment Green 7 and CI Pigment Violet 23.

The evaluation of the pigments dispersion within the matrix is a key point for the color masterbatch quality. Direct investigation techniques are microscopical analysis and X-ray fluorescence (EDX), while indirect methods such as Filter-Test, Color Strength and Rheology [41], are more representative because they are related with the production process and with the optical properties of the yarns [36].

Quite surprisingly, only few articles dealing with the analysis of the production process of monoconcentrated masterbatch and of the optimization of pigments dispersion in polymer matrices can be found in the open literature. For instance, Joshi et al. studied the effect of surfactant agent on the particles dispersion by measuring torque variation in the extruder during the compounding process [59]. Suresh et al. investigated pigments dispersion in a low density polyethylene matrix comparing different kinds of monoconcentrated masterbatches [35]. Ahmed et al. compared the mechanical properties of polypropylene fibers obtained by using pigments in powder form and monoconcentrated masterbatches [41]. A detailed description of pigment and their effects on the fibers produced through a spinning process was made by Marcincin [36]. Moreover, Wo et al. investigated the effect of phthalocyanine pigments on the crystallization behavior of polypropylene [47].

1.5. EXTRUSION PROCESS

The extrusion is one of the most important processes for plastic materials, in order to produce semi-finished and finished products for industrial or consumer applications [64]. About 60% of polymer chips in the world market are produced through an extrusion process [65].

This process is used not only to produce continuous articles, such as sheets, tubes, profiles, fibers, films but also to mix together different polymers and to introduce additives in a polymer. In fact, during the extrusion process, high shear stresses are generated and these forces allow the additive to penetrate and disperse homogeneously in the molten polymer [66].

During this process the material, in granular or powder form, is introduced into the hopper and immediately reaches the screw, driven by a motor-reducer system with safety coupling. The screw, rotating within the cylinder, pulls the material towards the extrusion head. During the process the polymer is melted by friction forces along screw and by the heat produced by heating bands controlled by thermocouples. There is also a cooling circuit to prevent both the premature softening of the pellets in the hopper, which could lead the feeder clogging, and prevent the overheating of the polymer during the process [67]. The extrusion line is composed by polymer feeder, extruder, die, cooling system and cutter [68], as reported in the Figure 1.17.

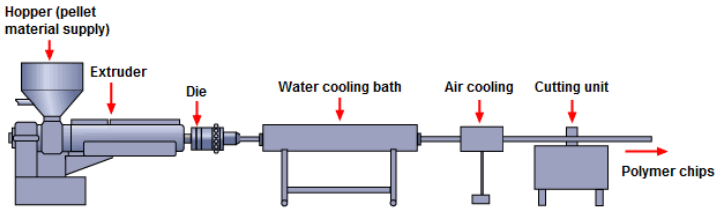

Figure 1.17: Scheme of extrusion line

The two main types of extruder are single screw and twin screw [69]. The first one is represented in Figure 1.18.

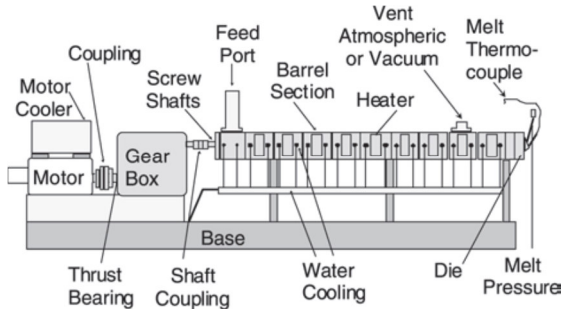

Figure 1.18: Schematic representation of single screw extruder [64]

The diameter (D) and the length (L) of the screw are the key parameters of the extruder. The first one defines the maximum flow rate, while the length/diameter ratio (L/D) defines the mixing capability of the extruder. In the cylinder usually there are heating zones, consisting of electrical resistors, to favor the homogeneous melting of the polymer, while the cooling is produced by water or air. The screw is an Archimedean screw built in alloy steel with high toughness, one side is connected with the motor and the other one usually has a conical shape (tip) to link up with the head of the extruder [70].

The screws for polyamides are generally made up of three areas: feed, compression and metering zones, as represented in Figure 1.19 :

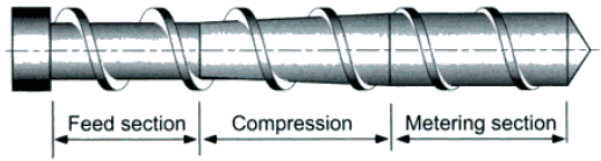

Figure 1.19: Sections of screw [71]

Feed zone: polymer in granules or powder form inside the hopper falls by gravity into the heated cylinder where the screw rotation begins to transport and to melt the material. In this area the screw threads height is larger, in comparison with the other sections, and constant. The granules occupy a very high volume due to high voids.
Compression zone: the molten polymer is compressed and transported by the screw threads. The melting is due to two contributions: the heat exchange and friction with the walls of the extruder. In this area the height of the threads decreases and then increases the diameter of the core of the screw, resulting in an increase of the pressure and compression of the polymer. The compression in this area eliminates the cavities and gas incorporated into the molten polymer.
Metering zone: in this area pressure required to push the molten polymer through the die is generated. The height of the thread is defined as a function of the mixing and processing requirements [71]. Usually, for Polyamide 6 the metering zone is 30% of total length, in order to optimize the polymer performances [70].

Another important parameter of the screw extruder is the compression ratio (RC), given by the ratio between the radial heights of the screw thread in feeding and metering zones, which determines its pumping capacity. Typical values are in the range between 2 and 6, while the height in the first zone is equal to 0.1-0.2 D. Another aspects of the screw are the width of the threads, the pitch and the connection angles between threads and screw core. Usually the screw pitch is constant and the width of the threads is proportional to the screw diameter. The angles of connection between threads and core are important for optimizing production, because they significantly affect the material transport and mixing within the cavity [71]. There are many kinds of screws designed in order to solve specific problems. The vented screw, for example, is used to remove volatiles and/or moisture from polymers (Figure 1.20).

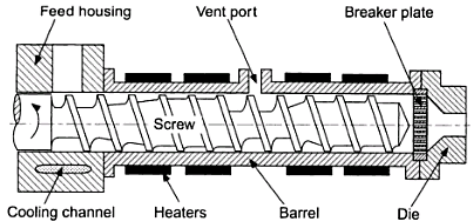

Figure 1.20: Schematic representation of vented screw [71]

There are screws equipped with special devices to improve the mixing of the material, particularly useful for fibers and reinforcing fillers addition, ensuring their optimal dispersion. The screws barrier are characterized by the presence of additional threads to the top of the transition zone, which allow to operate the separation of the solid and the melt.

The twin screw extruder is used essentially for materials sensitive to thermal degradation or for particular operations, such as venting and the compounding production. The twin screw extruder shows some advantages compare to single screw extruder: higher capacity, narrow range of the residence time, auto cleaning of screws and possibility to work with thermally sensible materials [72].

The screws can be counter-rotating and co-rotating. The solution with counter-rotating screws, visible in Figure 1.21, is the most favorable for the polymer flow and it is generated by the interpenetration of the screws surfaces.

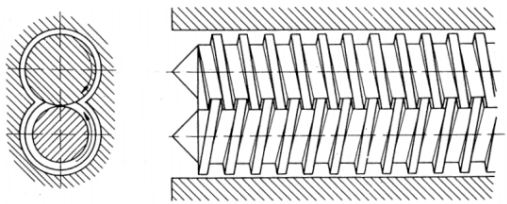

Figure 1.21: Schematic representation of counter-rotating screws [73]

The co-rotating screws extruder, shown in Figure 1.22, is less effective for two basic reasons: in the contact zone the circumferential speed of the screws are directed in

opposite directions while the compartments between the two threads in the same area are considerably larger.

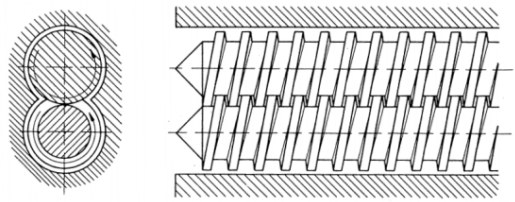

Figure 1.22: Schematic representation of co-rotating screws [73]

Both types of extruder are manufactured in low rotation speed (some tens of revolutions per minute) and high speed version (some hundreds of revolutions per minute). The first are suitable for the profiles extrusion, while the second is widely used in the mixing operation, such as color masterbatch production.
In the interaction area between the screws the pressure increases, because of the reduction of the channel section and of the variation of flow direction. Moreover significant shear stresses are generated. The pressure increase in the interaction zone determines the greater mixing degree of the material [74].

1.6. MELT SPINNING PROCESS

The melt spinning is a process based on continuous steady state elongation of flow used to produce fiber [75]. Polyamides (PA) were the first polymer used for fiber production due to their similarity with silk fibers and nowadays they are widely used in different sector, from textiles and carpet to reinforcements of tires [2, 3].
In the melt spinning process the raw materials, polyamide and masterbatches, are melted and mixed together through an extrusion process. Polymer melt is metered and forced to pass through filtration system, composed by different layers of stainless steel screens and sintered plates. The aim of this operation is to remove

impurities, gels and large additive agglomerates that could cause fibers breakage in the next operation steps [76, 77]. After filtration, the molten polymer passes through a spinneret with a large number of holes, usually from 50 to 200, to extrude filaments [70, 78]. The cross section of these holes can be circular or with different geometry (trilobal, pentalobal, etc.) (Figure1.23), in order to achieve special effects such as luster, opacity, air permeability, insulation, reduce weight, and so on [76, 79, 80].

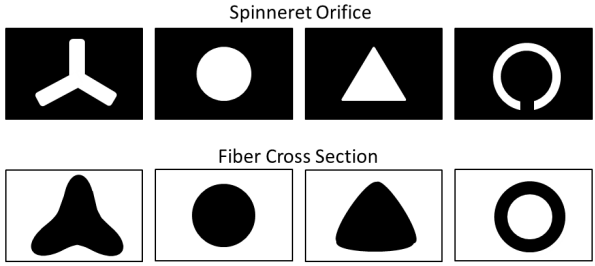

Figure 1.23: Scheme of spinneret orifice and the relative fiber cross section

The extruded filament are cooled in quench ducts by a cross current of air and collected in a single fiber by a so called convergence guide [70]. After conditioning a spin finish, composed by aqueous emulsion of lubricant and bactericides, is applied to fiber in order to reduce friction and abrasion between polymer and metal [70, 76, 79]. The spun yarn are therefore drawn by a so called high rotational speed godet (4000 m/min) to obtain a draw ratio from 2 to 5, depending to the fibers application, increasing the mechanical performance of material. The draw ratio (DR) is defined as the take up velocity of godet (v_f) and extrusion velocity (v_i) ratio, as reported in Equation (11):

$$DR = \frac{v_f}{v_i} \tag{11}$$

Another important step for polyamide fibers, used in wearing and carpet market, is the texturing operation. This produces mechanical distortions on the filaments that imparts to the wire: similar feature of natural fibers; high torque and abrasion

resistance, this means extreme durability; high elasticity and excellent volume; great covering power; excellent thermal insulation; excellent moisture absorption and high evaporation rate; excellent tactile sensation. The last operation, before the fibers are wound on bobbins, is the entangling process obtained by a jet air that produce a physical cohesion between filament [76]. The schematic diagram of melt spinning line is reported in Figure 1.24.

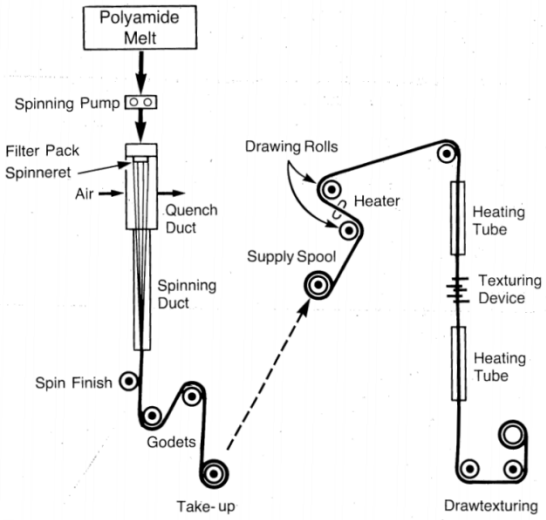

Figure 1.24: Schematic diagram of spinning line [76]

In the melt spinning process the extrusion, the quenching and the drawing conditions strongly influence the structure of fibers, which is directly linked to the final properties [81]. Generally speaking the spinning process transforms semicrystalline polymers into high oriented fibers with high modulus, because of the velocity gradient along the spinning axes [82-84].

When the melt polymer exits from spinneret the die swell phenomenon occurs (Figure 1.25). The diameter of filament is larger than the hole and this is due to the relaxation of viscoelastic forces under which the molten polymer is subjected after the spinneret capillaries [70, 80, 85-87].

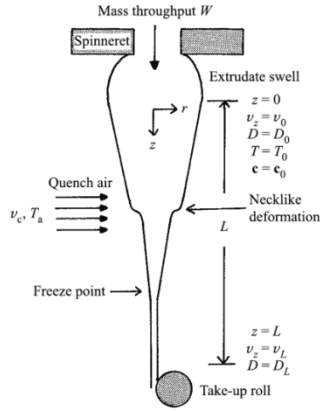

Figure 1.25: Representation of filament swelling [86, 87]

After swelling, in the first zone, the macromolecules do not show orientation due to relaxation phenomenon and the filament diameter starts to decrease under natural flow [85]. In the second zone, because of the maximum high elongational flow gradient achieved, the polymer chains orientation begins and the crystallization is accelerated. After the necklike deformation, represented in Figure 1.26, high molecular orientation occurs due to high drawing and the crystallization proceeds until the freeze point [85, 87-89].

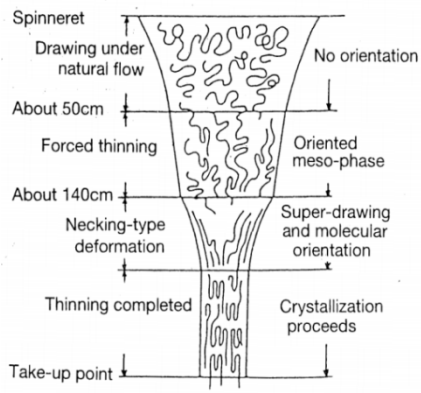

Figure 1.26: Fiber structure in high speed spinning [76]

Polyamide 6 can crystallize in α and γ form depending on the spinning conditions, but the more stable structure is the α form. During melt spinning process of nylon 6 the extensional flow and the plastic deformation produce a microfibrillar morphology in which crystalline and amorphous regions are alternated [90-92]. In Figure 1.27 the model of microfibrillar morphology of nylon 6 is reported.

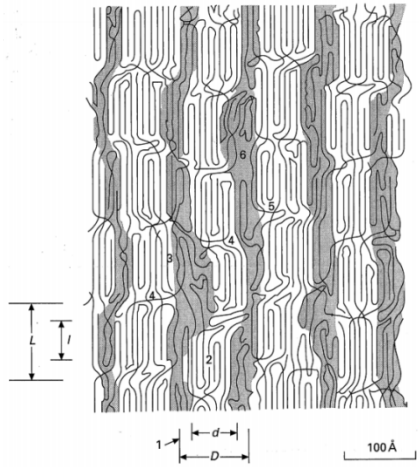

Figure 1.27: Model of microfibrillar nylon 6 morphology [79, 90]
(1) Fibrils, (2) crystallites, (3) partially extended molecules,
(4) tie molecules in the interlamellar region, (5) free chain ends and (6) amorphous region [90]

2. EXPERIMENTAL

2.1. MATERIALS

2.1.1. POLYAMIDE 6

Polyamides (PAs), also known as Nylon, are one of the most important commercial engineering plastics [93].

PA66 was the first polyamide synthesized by W.H. Carothers at the laboratories of Du Pont in the USA and it was introduced on the market by the same company, under the trade name of Nylon® 66 in 1939. Schlach, following the work of Carothers, at the laboratories of IG Farbenindustrie, synthesized PA6 in 1939 and produced the first monofilament. It began to be produced industrially in 1940 and marketed under the trade name of Perluran® [70]. Today PA66 and PA6 represent 97÷98% of the polyamides produced and world the production volume exceeds 5 million tons per year.

From a chemical point of view, Polyamide 6 is a linear polymer constituted by amide (-CONH-) repeating units, polymerized by the ring opening polymerization (ROP) of Caprolactam (CPL) [94-96]. In Figure 2.1 the chemical formula of caprolactam and the polyamide 6 repeating unit are reported.

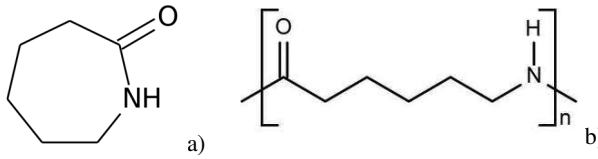

a) b)

Figure 2.1: Chemical structure of caprolactam and polyamide 6 repeating unit

Every year, about 4.3 million tons of CPL are produced worldwide to synthesize Nylon 6. Because of their good drawability and their fibers similar to silk, polyamides were initially used in the production of socks, carpets, rugs [97, 98]. Only subsequently, because of their excellent mechanical and chemical properties, they were applied for engineering purposes, and nowadays PAs are widely used in fiber, film, packaging and molding applications [70]. In Europe, about 1.3 million tons of PA are utilized for textile yarns, industrial yarns and flooring. Polyamide fibers dominate the scenario of recycled carpet materials, and it is therefore evident the strategic interest in polyamide carpet recycling [94, 99-102].

Generally speaking, PA6 shows excellent resistance to fatigue, impact, good toughness and low friction coefficient. Moreover PA6 has good chemical resistance against many fuels, oils and it is inert to biological attack [5]. For these good properties PA6 is widely applied in many industrial sectors, such as automotive, chemical and textiles. Concerning the automotive field, it is used for the production of gear wheels, cooling fans, filters petrol, connectors of electric wires, tanks for fluid and thanks to the low friction coefficient, for bearings and supports [103]. In the chemical field polyamide is used for the production of pipes, hoses, hydraulic systems. Generally speaking, PA6 is characterized by a high degree of crystallinity, and melting temperature above 200 °C. The main limitation is the sensitivity to water, which may cause hydrolytic degradation at high temperatures and in the presence of acids and poor dimensional stability for unreinforced polyamides.

The polyamides are semicrystalline polymer and the crystal surfaces are formed by lamellae, consisted of folded chains, which are linked together to form aggregates called spherulites.

The production processes, such as spinning, generates a polymer chain orientation that leads to breakdown the lamellae and spherulites, with the formation of new crystalline structures called fibrils. On the other hand, the products obtained without drawing are characterized by low orientation and the crystal structures are spherulites. The higher orientation is reached on the surface, because of the higher shear stresses during the process. The Nylon 6 can crystallize in two different forms:

α and β phases [104, 105]. In α phase macromolecules are arranged in a zig-zag conformation, with opposite direction and form a planar structure of hydrogen bonds. The resulting crystalline structure of PA6 is monoclinic and each cell contains four repeating units, as shown in Figure 2.2.

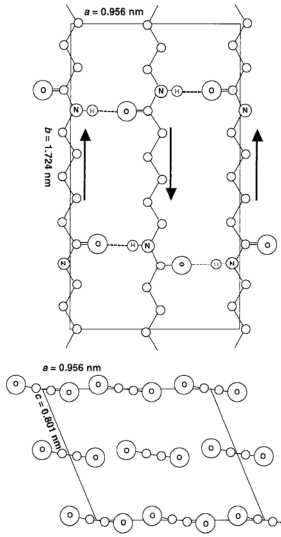

Figure 2.2: α crystalline cell of polyamide 6. β=67.5°

The second the stable crystalline phase of polyamide 6 is the γ form [106]. This is characterized by chains with the same direction and the structure is monoclinic, as represented in Figure 2.3.

The α/γ ratio changes in dependence on heating and cooling conditions of the material. At temperature higher than 160°C the transition from γ to α occurs because γ phase shows lower thermal stability compare to α crystals. Regarding fiber spinning process the winding speed strongly influences the crystallization behaviour. Winding speed higher than 2500 rpm promotes the formation of γ phase for undrawn filament, while α crystals grow slowly at lower temperature during conditioning. The drawing process causes a transition from γ to α crystals [52].

Higher molecular weight produces a reduction of crystallization rate due to the lower mobility of the macromolecular chains.

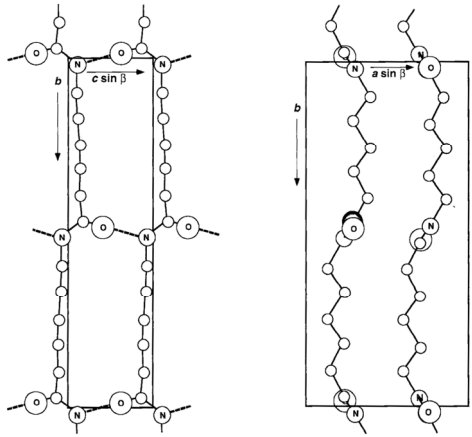

Figure 2.3: γ crystalline cell of polyamide 6.
A=0.933nm; b=1.688nm; c=0.478nm; β=67.5°

The Polyamide 6 used in this work was supplied in chips by Aquafil S.p.A. It was prepared in a continuum process through a VK reactor. The trade name of the product is AQ24401® and it is characterized by a relative viscosity of 2.4, a density of 1.14 g/cm^3 and a melting temperature of 222 °C, as reported in Table 2.1.

Properties	Test method	Typical value
η_{rel}	ISO 307	2,4
Density ρ [g/cm^3]	ISO 1183/A	1,14
Melting Temperature [°C]	ISO 11357-3	222±2

Table 2.1: Technical datasheet of AQ24401

Aquafil AQ24401 is used as polymer matrix for color pigment addition to produce the so called color masterbatches. In turn, these products are applied during the solution dyed bulk continuous filament process in order to color the industrial yarn. Finally the colored fibers are processed, through tufting machine, to produce carpet for automotive or residential sectors.

2.1.2. COLOR PIGMENTS

Color pigments are fine colored particles used in plastic industry to impart color to a specific substrate. In Aquafil S.p.A. Polyamide 6 and color pigments are mixed together by an extrusion process in order to obtain the monoconcentrated masterbatches, containing only one type of pigment. Different monoconcentrated masterbatches are mixed through another extrusion process for the production of color masterbatch, with the specific color, hue and saturation to satisfy the costumer request. In this work the most important color pigments, used in the automotive industry to produce carpets for car, were analyzed.

The color pigments can be divided in two main groups: inorganic and organic pigments. Organic pigments are mainly used for applications needing high tinting strength and brilliant shades while inorganic pigments are mainly useful where high opacity is needed. Table 2.2 shows the inorganic pigments considered in this research.

Pigment (CI)	Color	Trade name	Supplier	Molecule	CAS number
PW6	White	Hombitan LO-CR-S-M W/O SI	Sachtleben Chemie GmbH	TiO_2	13463-67-7
PBk7	Black	Black Pearls 4560	Cabot Corporation	Carbon black	
PBr24	Yellow	Sicotan Yellow K 2001 FG	BASF	Chrome antimony titanium buff rutile	68186-90-3
PR101	Brown	Bayferrox 110M	Bayer Chemicals	Iron oxide α-Fe_2O_3	1309-37-1

Table 2.2: Inorganic color pigments

In Table 2.3 the inorganic pigments analyzed in this work are reported.

Pigment (CI)	Color	Trade name	Supplier	Molecule	CAS number
PB15:3	Blue	Heliogen Blue K 7090	BASF	Cu-phthalocyanine beta	147-14-8
PG7	Green	Heliogen Green K 8730	BASF	Cu-phthalocyanine halogenated	1328-53-6
PR149	Red	Paliogen Red K 3580	BASF	Perylene	4948-15-6
PV23	Violet	CROMOPHTAL Violet GT	BASF	Dioxazine	6358-30-1

Table 2.3: Organic color pigments

2.1.2.1. White Pigment (PW6)

The most important white pigment used in plastic industry is titanium dioxide (TiO_2) in its anatase crystal form. The general properties of this pigment, reported in the datasheet, are shown in the Table 2.4.

Pigment (CI)	**Color**	**Chemical formula**	**MW**	**Density [g/cm^3]**	**Particle size** (Photocentrifuge) **[nm]**	**SSA [m^2/g]**
PW6	White	TiO_2	79,90	3,8	300	12-17

Table 2.4: Technical datasheet of PW6

For its high refractive index, PW6 is primarily used as a white pigment in paint and plastic industry to make dull the appearance of color products. The primary particles have very small dimensions and it is easy to disperse in polymeric matrices because of its low flocculation tendency.

PW6 shows high color clarity, high chemical resistance to organic solvents and high thermal stability. Titanium dioxide shows high photoreactivity because it absorbs the ultraviolet radiation that can degrades the polymer matrix and the organic pigments. The UV radiation is converted into heat and can create radical sites on the pigment surface that can lead to the breakdown and degradation of the macromolecules [56]. For this reason, the TiO_2 used as pigment in plastic matrix undergoes to surface treatment. The PW6 used in this work, Hombitan LO-CR-S-M W/O SI, was covered by a first inorganic coating and a second organic coating in order to reduce its photoreactivity, as represented in Figure 2.4. Despite of its good feature, TiO_2 is relatively cheap [56, 107-109].

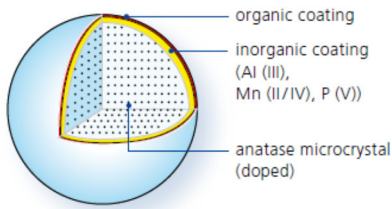

Figure 2.4: PW6 pigment particle

2.1.2.2. Black Pigment (PBk7)

Carbon black is widely used in many industrial sectors for many purposes such as rubber reinforcement, plastic pigmentation, paints and coatings [110]. It is an amorphous form of carbon obtained by an oxidative decomposition of hydrocarbons under controlled conditions [108, 111]. The carbon atoms are arranged in blocks of graphene layers with reduced dimensions and these units are organized in a turbostratic structure to form spherical particles with a range of diameter from 10 to 100 nm [111]. Table 2.5 shows the technical datasheet of PBk7.

Pigment (CI)	Color	Chemical formula	Density [g/cm^3]	SSA [m^2/g]
PBk7	Black	C (Carbon)	~ 2	80-110

Table 2.5: Technical datasheet of PBk7

The primary particles of PBk7 are very small with a corresponding high specific surface area and surface energy. For this reason, in order to minimize the free energy of the system, the primary particles tends to flocculate and to form aggregates.
The color strength of carbon black is high and is proportional to its specific absorbance, that depends on the refractive index and the size of the independent structural units [112, 113].

2.1.2.3. Brown Pigment (PBr24)

Brown Pigment PBr24 is a solid, complex inorganic yellow pigment. It is based on titanium dioxide with chromium (III) and antimony (V) ions partially replacing titanium ions in the rutile lattice. It is produced by a solid state reaction at 1000-1200°C between metal oxide, hydroxide and carbonates. PBr24 has a density around 4.5 g/cm^3 g and a specific surface area of 4 m^2/g, as reported in the Table 2.6.

Pigment (CI)	Color	Chemical formula	Density [g/cm^3]	Particle size (Disc Centrifuge) [nm]	SSA [m^2/g]
PBr24	Yellow	(Ti,Cr,Sb)O_2	4.5	688	4

Table 2.6: Technical datasheet of PBr24

This pigment is used for coloring plastics, ceramics, building materials and coatings. The estimated world production amounts to 10,000 – 15,000 tons. It is practically inert and has a melting point above 1000°C. The primary particles are larger compare to the organic pigment and thus they are easy to be dispersed into a polymeric matrix because they do not tend to flocculate. It shows low color strength.

2.1.2.4. Red Pigment (PR101)

Pigment Red 101 is iron oxide (Fe_2O_3) and shows a brown color. It can be natural, called hematite, or synthetic produced from calcination of iron hydroxide with hydration water elimination. Depending on calcination degree its crystals can have different shapes. The properties of PR101 are reported in Table 2.7.

Pigment (CI)	Color	Chemical formula	Density [g/cm^3]	Particle size[a] [nm]
PR101	Brown	Fe_2O_3	5	90

Table 2.7: Technical datasheet of PR101
a: measured by Electron microscope

PR101 particles are really small and they show low tendency to flocculate. This pigment can be dispersed easily in a polymer medium. The color depends by the particles dimensions: the bigger the particles, the brighter the color.
This pigment shows high resistance to chemical agents, solvent and heat but a really low color strength. Their strong UV absorption gives additional light and weather protection to substrate and binder. It is really cheap [107].

2.1.2.5. Blue Pigment (PB15:3)

Copper Phthalocyanines (CuPc) are the most important and the most widely used blue pigments in the market [35]. They are primarily applied to color inks, paints and plastic and they are also used to synthetic fibers and paper coatings [62, 114-116]. Copper Phthalocyanine shows two crystal structure available on the market. The alpha form is the CI PB15:1 and the beta form is the CI PB15:3. The beta crystal is more stable and it was taken into account in this work [117]. The properties of PB15:3 are reported in Table 2.8.

Pigment (CI)	**Color**	**Chemical formula**	**Density [g/cm^3]**	**Particle size** (Disc Centrifuge) **[nm]**	**SSA [m^2/g]**
PB15:3	blue	$C_{32}H_{16}CuN_8$	1,6	220,8	65

Table 2.8: Technical datasheet of PB15:3

Copper Phthalocyanine pigments are manufactured from phthalic anhydride, urea, cupric chloride and ammonium molybdate or from ammonoxidation of oxylene and a cupric salt. The chemical structure of this pigment is shown in the Figure 2.5.

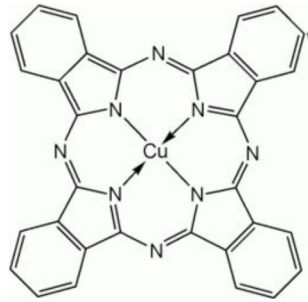

Figure 2.5: Chemical structure of PB15:3

The primary particles of this pigment are very small and constituted by tiny molecular crystal with a typical dimensions range from 20 to 500 nm [118]. Because

of this CuPc shows a significant tendency to flocculate. In plastic coloring the effectiveness of PB15:3 strongly depends on the level and on the stability of the dispersion. Copper Phthalocyanine pigments show high color strength, high solvent resistant and heat stability compared to the other blue dyes.

2.1.2.6. Green Pigment (PG7)

The PG7 is a Copper Phthalocyanine molecule polychlorinated by 14-16 atoms of chlorine. CuPc green dominates the market of green pigment and, like PB15:3, it is primarily applied to color inks, paints and plastic and they are also used to synthetic fibers and paper coatings [62, 114-116]. The properties of PG7 are summarized in Table 2.9.

Pigment (CI)	**Color**	**Chemical formula**	**Density [g/cm^3]**	**Particle size** (Disc Centrifuge) **[nm]**	**SSA [m^2/g]**
PG7	green	$C_{32}H_3N_8Cl_{15}Cu$	2,1	201	61

Table 2.9: Technical datasheet of PG7

PG7 pigment is produced from copper Phthalocyanine by a multiple substitution of hydrogen atoms of the benzo rings by chlorines [119, 120], and the resulting chemical structure is shown in Figure 2.6.

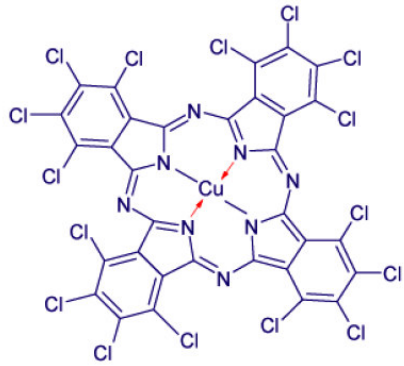

Figure 2.6: Chemical structure of PG7

Phthalocyanine green pigments are composed by a very tiny molecular crystal primary particles that are difficult to disperse into the polymeric matrix. For this reason, they have a tendency to flocculate. PG7 pigments are characterized by high tinctorial strength, good solvent resistance, high chemical and heat stability.

2.1.2.7. Violet Pigment (PV23)

The dioxazine violet is the most used violet pigment in paint industry and coloration of plastic [54]. The pigment is usually used at low concentration because of its high tinting strength to impart bluer hue to the undertone of the white. The properties are reported in Table 2.10.

Pigment (CI)	Color	Chemical formula	Density [g/cm^3]	SSA [m^2/g]
PV23	violet	$C_{34}P_{22}Cl_2N_4O_2$	1,46	57,8

Table 2.10: Technical datasheet of PV23

The dioxazine violet is obtained by the reaction of chloranil with aminoethyl carbazole [33, 35]. The Figure 2.7 shows the chemical structure of this pigment.

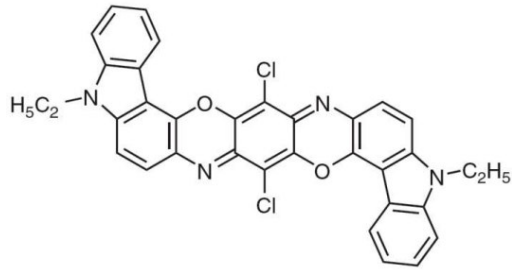

Figure 2.7: Chemical structure of PV23

The primary particles are really fine with high specific surface energy and they tend to flocculate in order to reduce the surface energy of the system [107]. This pigment

shows a good resistance to solvent and light, and an excellence thermal stability [107, 121].

2.1.2.8. Red Pigment (PR149)

PR149 is a perylene diimide pigment primarily used in the coloration of plastics [54]. The limitation is that this pigment affects the shrinkage of injection molded articles and high concentration must be avoided because it can interact with hindered amine light stabilizers (HALS), reducing the thermal and UV stability of the product. In the Table 2.11 the main properties of PR149 are summarized.

Pigment (CI)	**Color**	**Chemical formula**	**Density [g/cm^3]**	**Particle size[a]** (Disc Centrifuge) **[nm]**	**SSA [m^2/g]**
PR149	red	$C_{40}H_{26}N_2O_4$	1,4	125	76

Table 2.11: Technical datasheet of PR149

The chemical structure of PR149 is reported in Figure 2.8.

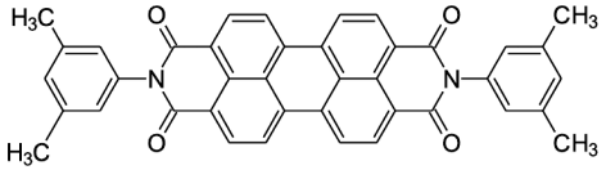

Figure 2.8: Chemical structure of PR149 [122]

As for the other organic pigments, the properties of perylene pigments are strongly dependent on particles size and their dispersion in the medium, crystal morphology and surface properties of particles [122]. The morphology of the PR149 primary particles is acicular and shows a small dimensions.

This pigment have good general properties: excellent solvent resistance, heat and light stability and good chemical stability [107].

2.2. MATERIALS PROCESSING

In this work the effects of color pigments addition into the industrial products were analyzed at three different levels: (i) the production of monoconcentrated masterbatch, (ii) the production of color masterbatch and finally (iii) on the fibers produced by solution dyed process.

2.2.1. MONOCONCENTRATED MASTERBATCH

Monoconcentrated masterbatches are composite materials, also called concentrates, obtained by a melt compounding process, with a high amount of additives (5-50% wt.), higher than in the final products [123, 124]. Polymer matrix and one type of color pigment are mixed by an extrusion process, in order to obtain a fine dispersion of particles into the polymer [35]. Monoconcentrated masterbatches are marketed in chips form and they are used in later production step for coloring plastic materials and, as mentioned before, their use is recommended in comparison to the use of powder pigment or soluble dyes [125].

For masterbatch production a co-rotating twin screw machines are commonly used in the industry because they have modular configurations and are thus quite flexible for adapting to changing tasks and material properties [126].

During extrusion two mixing phenomena occur: (i) dispersing mixing that breaks down the agglomerate in aggregate and primary particles and (ii) distributive mixing that produce an homogeneous distribution of pigment into the polymeric matrix. Generally speaking, the distributive mixing is achieved at low shear rate processes while the dispersive mixing is obtained by high shear processes [64, 74, 127, 128]. The schematic representation of these two mixing phenomena is shown in the Figure 2.9.

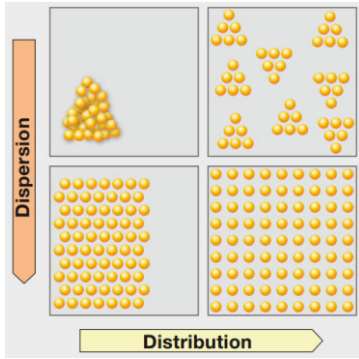

Figure 2.9: Distributive and dispersive mixing representation

The eight monoconcentrated masterbatches, obtained starting from the eight color pigments taken into account, were produced in Aquafil S.p.A. through its industrial process. The schematic layout of the monoconcentrated masterbatch process is represented in Figure 2.10.

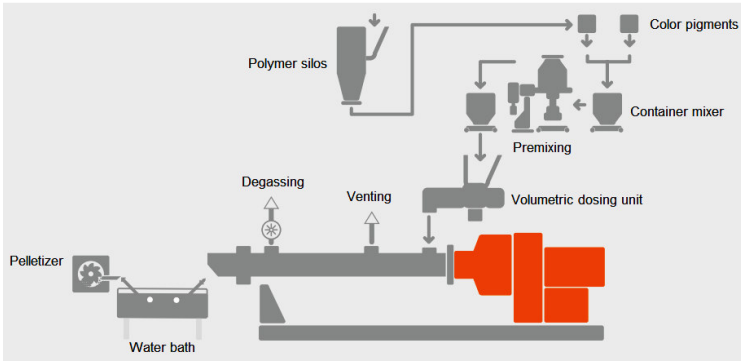

Figure 2.10: Schematic representation of monoconcentrated masterbatch process

The polymer powders, stored in the controlled atmosphere silos, and the color pigments have been weighted and moved into a container mixer. By a so called turbo-mixer machine the powders compound is premixed to make the materials

feeding as much uniform as possible. Through a volumetric dosing unit the compound is fed into extruder in which the real mixing occur. At the end of extrusion, the polymer mixed with the pigments is forced to pass through a spinneret and the filaments produced are cooled down by water and by air before going into pelletizer, that produces the chips of monoconcentrated color masterbatch (~3 mm). The Figure 2.11 shows a picture of a yellow monoconcentrated masterbatch.

Figure 2.11: Yellow monoconcentrated masterbatch

In Table 2.12 the monoconcentrated masterbatches studied in this work with their pigment concentration are reported.

Monoconcentrated Masterbatch	**Notation**	**Pigment Concentration [%]**
Monoconcentrated white masterbatch PW6	Mono PW6	20
Monoconcentrated black masterbatch PBk7	Mono PBk7	30
Monoconcentrated brown masterbatch PBr24	Mono PBr24	40
Monoconcentrated red masterbatch PR101	Mono PR101	50
Monoconcentrated blue masterbatch PB15:3	Mono PB15:3	25
Monoconcentrated green masterbatch PG7	Mono PG7	25
Monoconcentrated violet masterbatch PV23	Mono PV23	25
Monoconcentrated red masterbatch PR149	Mono PR149	25

Table 2.12: Pigment concentration in the monoconcentrated masterbatches

The industrial extruder used in this work was a TM-M58 model produced by F.lli Maris S.p.A. and its technical characteristics are shown in Table 2.13.

Parameter	Value
Nominal diameter	58 mm
Number of lobes screw	2
Max screw speed	602 rpm
Max screw torque	860 Nm
L/D ratio	44
Throughput	300 Kg/h
Number of thermal zones	12
Engine power	110 kW

Table 2.13: Technical specification of TM-M58 extruder

Each monoconcentrated masterbatch was extruded using different process parameters because of the different physical-chemical nature of the color pigments. These parameters allow to obtain a continuous production process, with the production of filaments with constant cross section, avoiding also pressure fluctuations and filament breakage.

In Table 2.14 the extrusion parameters used for each monoconcentrated masterbatch are reported.

	Screw rotation speed [rpm]	Throughput rate [Kg/h]	Energy consumption [%]
Mono PW6	450	290	80%
Mono PBk7	400	240	80%
Mono PBr24	400	240	80%
Mono PR101	400	240	80%
Mono PB15:3	350	210	75%
Mono PG7	350	210	75%
Mono PV23	350	210	75%
Mono PR149	400	240	80%

Table 2.14: Process parameters used for monoconcentrated masterbatches production

The monoconcentrated masterbatches were obtained using different production set-up in order to evaluate the best process parameters combination to reach a better pigment dispersion, to reduce the masterbatch waste and to increase the productivity of the industrial plant.

The different production processes were evaluated in term of Specific Mechanical Energy (SME), by the Equation (12):

$$SME = \frac{n \cdot P \cdot O}{n_m \cdot Q} \ [kWh\ kg^{-1}] \qquad (12)$$

Where n is the screw speed, n_m is the maximum screw rotations, P is the electric power, O is the engine loading and Q is the extruder capacity. SME represents the energy transfer from drive motor to the frictional heating for melting, mixing and die pressurization in the compounding process [129]. It is a measure of extrusion energy consumption and provides some information about extruder efficiency [130-137].

Table 2.15 shows the four different process set up analyzed and used to produce monoconcentrated color masterbatches.

	Notation	**Filtration system**	**Number of extrusions**
Process 1	1 E-W-F	Yes	1
Process 2	1 E-W/O-F	No	1
Process 3	2 E-W/O-F	No	2
Process 4	3 E-W/O-F	No	3

Table 2.15: Production processes set up for monoconcentrated masterbatches

In Table 2.16 the specific mechanical energies involved in the production processes for each monoconcentrated masterbatch are reported.

	1 E-W-F	1 E-W/O-F	2 E-W/O-F	3 E-W/O-F
Mono PW6	0,228	0,228	0,455	-
Mono PBk7	0,238	0,254	0,508	-
Mono PBr24	0,238	0,254	0,508	-
Mono PR101	0,238	0,254	0,508	-
Mono PB15:3	0,229	0,247	0,494	0,740
Mono PG7	0,229	0,247	0,494	0,740
Mono PV23	0,229	0,247	0,494	0,740
Mono PR149	0,238	0,254	0,508	-

Table 2.16: SME for all production processes of monoconcentrated masterbatches

2.2.2. COLOR MASTERBATCH

Final color masterbatches were obtained by an extrusion of different monoconcentrated masterbatches in order to produce the color requested from the costumer. Even in this case the twin screw extruder is the most commonly equipment used in industry for its flexibility.

The industrial extruder used in this work was a EBC40HT model produced by Comac S.r.l and the technical characteristics are reported in Table 2.17.

Parameter	Value
Nominal diameter	42 mm
Number of lobes screw	2
Max screw speed	1200 rpm
Max screw torque	470 Nm
L/D ratio	48
Throughput	220 Kg/h
Number of thermal zones	10
Engine power	98 kW

Table 2.17: Technical specifications of EBC40HT extruder

In this work, after an industrial production analysis, a critical color masterbatch was chosen. In particular the Blue Masterbatch was selected, and its composition is reported in Table 2.18.

Monoconcentrated Masterbatch	Amount
Polyamide 6	20 %
Monoconcentrated black masterbatch	17 %
Monoconcentrated blue masterbatch	29 %
Monoconcentrated violet masterbatch	27 %
Stabilizer monoconcentrated masterbatch	7 %

Table 2.18: Blue Color masterbatch formulation

This kind of color masterbatch has the peculiarity to clog the filtration system during spinning process and a frequent change of filters is needed. This, obviously reduces the production output of industrial plant and reduces the stability and quality of the final product. Moreover it can promote the drop formation on spinneret during melt spinning and consequently the fibers breakage.

This color masterbatch was produced in two different ways. The first, called Standard Blue Color Masterbatch (BM-S), was obtained using monoconcentrated masterbatches produced in the standard way (1 E-W-F). The second, called Optimized Blue Color Masterbatch (MB-O), was composed by monoconcentrated masterbatches obtained from the optimized process, that was different for each concentrate. The notation of the samples is reported in Table 2.19.

Sample	Notation
Blue Color Masterbatch Standard	BM-S
Blue Color Master Optimized	BM-O

Table 2.19: Blue color masterbatch notation

These two color masterbatches were fully characterized, from color, chemical, rheological and mechanical point of view, in order to determine the effect of

monoconcentrated production process and so of the pigment dispersion on the subsequent industrial step. Particular attention was focused on the clogging power of color masterbatch and on the filament breakage during melt spinning process.

2.2.3. FIBER SPINNING

In Aquafil the spinning process, called bulk continuous filament, is composed of three macro steps: spinning, drawing and texturization. A schematic representation of this process is reported in Figure 2.12.

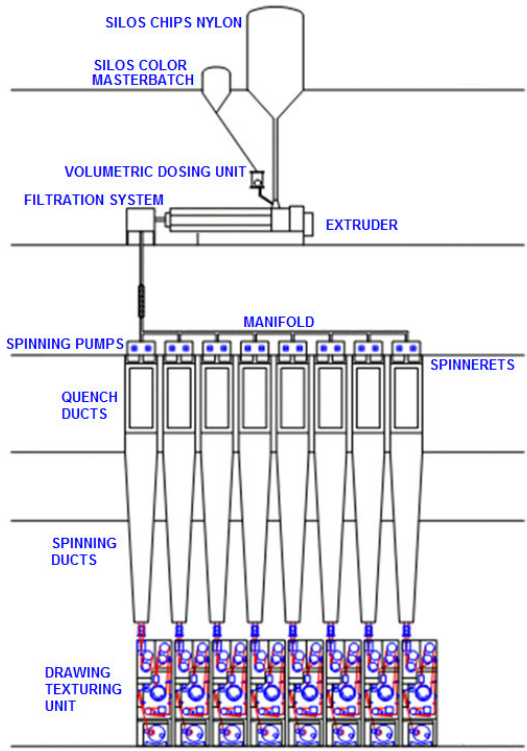

Figure 2.12: Melt spinning plant scheme

The process is composed by these steps:

- Storage: polymer and color masterbatch are stored in silos under nitrogen atmosphere in chips form, to prevent the thermo-oxidation and moisture absorption.
- Extrusion: polymer chips fall by gravity into feed extruder while color masterbatch is dosed through a volumetric metering device, composed by vibrational plates. The polyamide melts at a temperature ranging from 250°C to 280°C and at pressure between 50 and 150 bar, depending on the compositions.
- Filtration: the extruded compound is forced to pass through a filter made of sintered material, which has to remove agglomerates and gels from molten polymer before spinning.
- Spinning: through manifold the compound is transferred to the spinning pumps that dose polymer in each spinning unit, depending on the title to reach. The polymer passes through a spinneret filtration system for the impurities removal, to minimize the probability of spinneret clogging, but also to impart high shear stresses to homogenize the temperature and disaggregate the gels and agglomerates [138, 139]. The compounded materials pass through the spinneret holes with high pressure and the produced filament falls by gravity.
- Cooling: the filaments fall by gravity through the duct and are cooled down by a cross-flow of air with temperature, humidity and speed controlled. Under the spinneret the first drawing process occurred due to the gravity.
- Drawing: under ducts an emulsion of lubricant are applied to filaments, around 0.3-1% by weight of the finished product, in order to reduce friction and to impart an antibacterial and antistatic effect.

  The real thermo-mechanical drawing process occurs between two pairs of heated cylinders, called godets, that wound the filaments. In particular, the first pair works at a low temperature and a low speed while the second pair works at high temperature and high speed of rotation. The speed ratio between the two pairs is called draw ratio and usually for the nylon 6 it is around 3 [70, 85, 139-142].

- The filaments go into the texturing unit, composed by a lamellae room and a nozzle, where through pressure and temperature permanent plastic deformation of yarns is performed. The hot filaments are cooled down by a rotation drum where, through an aspiration of air, the deformation is fixed.

  The filaments undergo to entangling process by jet air that produce a physical cohesion between filaments to produce yarn. This operation improves the processability of fibers and their optic effect on the carpet.
- Collection: the wires are collected on cylindrical bobbins. In this phase it is very important the tension of yarns on pack. In fact, the wire should be relaxed, non-tensioned, to avoid permanent deformation which could compromise the subsequent processing and the optical effect of the final carpet.

Figure 2.13 shows the drawing-texturing unit:

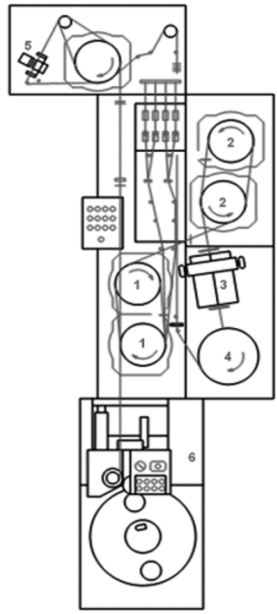

Figure 2.13: Representative scheme of drawing-texturizing unit.
First couple of godets (1); second couple of godets (2); texturing unit (3); cooling drum (4); texturizing unit (5); collection unit (6)

The standard and the optimized blue color masterbatches were used to color the yarns in the solution dyed fibers spinning process in order to evaluate the effect of monoconcentrated masterbatch optimization on the final industrial product.
The yarn colored by BM-S was identify as Standard Blue Yarn (BY-S), while the yarn colored by BM-O was identify as Optimized Blue Yarn (BY-O).
The notation of the samples is reported in Table 2.20.

Sample	Notation
Blue Yarn Standard	BY-S
Blue Yarn Optimized	BY-O

Table 2.20: Blue Yarns notation

These two industrial blue yarns were mechanical characterized and their thermal and UV resistance were evaluated by measuring the variation of their mechanical, color and microstructural properties with the exposure time.

2.3. EXPERIMENTAL ACTIVITIES

2.3.1. MICROSTRUCTURAL CHARACTERIZATION

2.3.1.1. Density measurements

Density measurements were performed on the color pigments by using a Micromeritics® Accupyc 1330 helium pycnometer, at a temperature of 23 °C. A testing chamber of 3.5 cm^3 was utilized for all the samples. In order to obtain a reproducible evaluation of powders density, 300 measurements were performed on every sample, and the average of the last 80 measures was considered as the plateau density of the material. In this way, possible overestimation of the real density due to the helium absorption on the surface of the pigments was avoided. The results were then compared with the datasheet.

2.3.1.2. Evaluation of the pigment surface properties

In order to evaluate the influence of the surface morphology of the color pigment on their dispersion in the polymer matrix, BET surface area and porosity measurements were conducted, following ASTM D 6556 standard. An ASAP® 2010 Accelerated Surface Area and Porosimetry machine, was utilized. Surface properties were evaluated referring to the nitrogen gas physisorption process, setting a saturation pressure of 738.57 mmHg and a bath temperature of 77.35 K. Adsorption/desorption curves reported the adsorbed nitrogen volume vs. the relative pressure, and from the interpolation of the linear part of the adsorption curve the BET (Brunauer, Emmett, Teller) surface area was calculated [143, 144], as reported in Equation (13) and in Equation (14).

$$\frac{P}{V_a\,(P_a - P)} = \frac{1}{V_m C} + \frac{C-1}{V_m C}\left(\frac{P}{P_0}\right) \tag{13}$$

$$s = \frac{V_m \sigma\, N_A}{m\, V_0} \tag{14}$$

Where P and P_0 are the applied and the saturation pressure, respectively, V_a is the volume of the adsorbed gas at the pressure P, V_m is the adsorbed gas when the whole surface is covered with a mono-molecular layer, and C is a constant depending on the probing gas (98.0 for nitrogen). s is the area of a single gas molecule, N_A is the Avogadro constant, m is the mass of the adsorbing sample and V_0 is the molar volume of the gas.

From the comparison of the absorption/desorption curves is was also possible to analyze the possibility of having an internal porosity in the sample, while following BJH (Barrett-Joiner-Holenda) [145] method it was possible to determine the pore size distribution and the surface area contribution associated to pores of different dimensions. According to this theory the pores dimension is related to the relative pressure, and in the case of N_2 at 77 K Equation (15) and Equation (16) are valid during the absorption and desorption process respectively.

$$t = \left(\frac{13.99}{\left(0.034 - log\left(\frac{P}{P_0}\right)\right)}\right) \cdot 0.05 \tag{15}$$

$$t = 3.54 \cdot \left(\frac{-0.5}{ln\left(\frac{P}{P_0}\right)}\right) \cdot 0.333 \tag{16}$$

where t is the pore thickness, expressed in nm.

From BET analysis it is possible to evaluate the everage primary particle diameter (d_{BET}) by Equation (17):

$$d_{BET} = 6000/(S_{BET} \cdot \rho) \quad (17)$$

where S_{BET} is the specific surface area determined by BET method in m^2/g and ρ is the density in g/cm^3.

2.3.1.3. Microscopy techniques

Field emission scanning electron microscope (FESEM) was utilized in order to evaluate the morphology of the color pigments. The pigment powders were observed at different magnifications by using a Zeiss® Supra 60 FESEM, at a low acceleration voltage of 4 kV in order to avoid the surface charging. A little amount of the powders were deposited on the metallic support and two kinds of samples were prepared. The first was used as prepared while the second was surface threated by a thin layer of gold in order to increase the conductivity of the sample.

2.3.1.4. Light Scattering analysis

Dynamic Light Scattering was performed on the color pigment powders in order to evaluate the dimension of the filler aggregate, using a Malvern® Zetasizer Nano S. The samples were prepared by dispersing the pigment powder into the water at a concentration of 5 $g \cdot l^{-1}$. The resulting dispersion underwent to a sonication process for 20 minutes in order to produce a better and stable dispersion for the analysis and to break up the agglomerates.

From the correlation function the diffusion coefficient of the particles was calculated and by the Stokes-Einstein equation (Equation (18)) the hydrodynamics radius of aggregates was derived.

$$R_h = \frac{K_B\, T}{6\pi\eta D} \tag{18}$$

Where K_B is the is the Boltzmann constant, T is the temperature, η is the shear viscosity of the solvent and D is the diffusion coefficient [146-151].

2.3.1.5. Differential Scanning Calorimetry (DSC)

Differential Scanning Calorimetry (DSC) was utilized in order to detect the influence of the color pigments on the melting and crystallization behaviour of the monoconcentrated masterbatches.

These tests were carried out using a TA Instrument DSC Q20 and all measurements were performed on 10 mg of sample, under a nitrogen flow of 100 ml/min.

The samples were first heated at a rate of 20°C/min from 30°C to 260°C, and then cooled to 0°C. A second heating was performed at the same rate until 350°C. The melting enthalpy (ΔH_m) was determined from the corresponding peak areas in the heating and cooling thermograms. The crystallinity content (X_c) of monoconcentrated masterbatches based on Polyamide 6 matrix was calculated, as reported in Equation (19) [152]:

$$X_c = \frac{\Delta H_m}{\Delta H_u} \cdot 100 \tag{19}$$

Where ΔH_m is the melting enthalpy of the sample, measured by DSC, and ΔH_u is the melting enthalpy of 100% crystallinity Polyamide 6, taken as 190 J/g [153, 154].

DSC was also used to performed an isothermal crystallization kinetics analysis on the monoconcentrated masterbatches and on the color masterbatch in order to evaluate the influence of the pigment dispersion.

The first heating was performed at 20°C/min from 30 °C to 260 °C, then the temperature was maintained for 5 minutes in order to delete the thermal history of the sample. The cooling was performed at different rate: 3, 4.5, 6, 10, 20 and 30 °C/min. Finally a heating cycle was performed from 0 °C to 350 °C at 10 °C/min.

The crystallization temperature can be related with the cooling rate (v) by an Arrhenius-type equation, from which the activation energy of crystallization (E_{act}) can be calculated (Equation 20).

$$\ln v = \ln v_0 - \left(E_{act} \cdot \frac{c}{R}\right) \cdot \frac{1}{T} \qquad (20)$$

Where v_0 is pre-exponential factor, c is a constant reported in literature and R is the gas constant [155-162].

2.3.1.6. Infrared (IR) Spectroscopy

Infrared spectroscopy (IR) was conducted on the monoconcentrated masterbatches and on the color masterbatches after thermal treatment in order to evaluate the formation of different functional groups because of thermo-oxidation degradation of the polymer matrix, promoted by color pigments. Moreover, from IR analysis conducted on the industrial yarn, the ratio between the crystalline α-phase and the amorphous (and γ-phase, if present) component was evaluated [2]. In fact, in the polyamide 6 IR spectrum, these phases are related to the peaks at 1200-1190 cm^{-1} and at 1189-1170 cm^{-1}, respectively. These tests were conducted by using a Perkin Elmer® Spectrum 100 FTIR Spectrometer in a scanning interval between 650 and 4000 cm^{-1}.

2.3.2. FILTERABILITY DETERMINATION

The dispersion of pigments inside the polymer matrix, directly correlated to the industrial filterability of the monoconcentrated masterbatches, was evaluated through Filter-Test measurement, according to EN 13900-5 standard [54, 163]. Monoconcentrated masterbatches were processed through an extruder (L = 33.6 cm, L/D = 24, rotational speed = 20 rpm, barrel temperature profile = 270 / 270 / 270 / 275 °C), and the molten polymer was forced to pass through a filter having a size of 25 µm. The increment of pressure due to the filter clogging was measured [35, 36]. Filter-Tests provided the so called FPV (Filter Pressure Value) and FPVII (Plateau Filter Pressure Value), defined as reported in Equation (21) and (22) :

$$FPV = \frac{P_2 - P_1}{M} \tag{21}$$

$$FPV\ II = \frac{P_3 - P_1}{M} \tag{22}$$

where P_1 is the initial pressure, P_2 is the maximum pressure, P_3 is the second pressure plateau after pressure peak and M is the mass of pigment passed through the filter. A low value of FPV indicates that the extrusion process led to an homogeneous dispersion of the pigments in the matrix, while elevated FPV are related to a bad filler dispersion within PA6. From an industrial point of view, FPV gives an idea of the masterbatch processability and of its suitability for the spinning process, while FPVII provides information about filter clogging phenomenon. In particular, a slight pressure drop after the pressure peak indicates a physical clogging of the filter, due to the packing effect of the aggregates, while a marked pressure decrease may be due to the presence of unstable agglomerates or gels that were broken down and pushed through filter from the molten polymer flow.

2.3.3. COLOR MEASUREMENTS

2.3.3.1. Color Difference evaluation

The color difference (ΔE*) indicates the distance between two points in the Lab Color Space, using the Equation (8), introduced in the paragraph 1.2. Through an Hunterlab® Colorquest XE Spectrophotometer the color coordinates of the two industrial yarns, obtained from standard and optimized color masterbatches, were measured. In this way the thermal and UV stabilities of the two products were evaluated by measuring the color variation during the thermal and UV aging.

2.3.3.2. Color Strength evaluation

The color strength identifies the property of a pigment to impart color to a substrate under specific processing conditions [10, 164]. The reflectance curves of samples were determined through a Hunterlab® Colorquest XE Spectrophotometer. The measured reflectance of an optically infinite thick layer $R_\infty(\lambda)$ is related to the ratio of the absorption coefficient K(λ) and the scattering coefficient S(λ) for diffuse light according to the two-flux radiation theory of Kubelka-Munk (KM) [18], as reported in Equation (23):

$$\frac{K(\lambda)}{S(\lambda)} = \frac{[1 - R_\infty(\lambda)]^2}{2 \cdot R_\infty(\lambda)} \qquad (23)$$

From Equation (22) the absorption coefficient K(λ) over the whole interval of visible light was calculated and weighted with the tristimulus curves, and the pigment amount necessary to obtain the same reference color intensity was calculated. The relative color strength (RCS) was determined comparing the (K/S)

ratio of the sample and that of a standard reference [54], as reported in Equation (24).

$$RCS = \frac{(K/S)_{sample}}{(K/S)_{reference}} \cdot 100 \quad (24)$$

RCS determination is an indirect method to have an idea of the pigment dispersion inside the matrix: the higher RCS values, the better dispersion is achieved [165].

2.3.4. PHYSICAL-CHEMICAL CHARACTERIZATION

2.3.4.1. Rheological measurements

Dynamic rheological measurements were performed by using a Dynisco Polymer LCR 52M capillary rheometer, setting a chamber temperature of 260 °C and a shear rate ($\dot{\gamma}$) interval between 100 and 10000 s^{-1}. Before testing, pelletized samples were dried in vacuum oven at 120 °C for 24 h, to ensure a moisture content less than 0.1% [166]. The samples were maintained in the rheometer for two different residence times (3 and 23 minutes), in order to detect if the pigment promotes the thermo-oxidative degradation of the matrix or if it tends to agglomerate for prolonged processing times. These intervals were chosen according to the requirements of the industrial processing of polyamides. In particular, a time of 3 minutes is required to completely melt PA6 in the rheometer oven at 260 °C, while an interval of 23 minutes is the typical residence time at elevated temperature for a melt spinning process. Apparent viscosity curves (η_{app}) were fitted through the Cross equation [167-173] (Equation (25)), in order to determine the values of the zero-shear rate viscosity (η_0) and of the C parameter, that is proportional to the cohesive energy of the particles under shear stresses [36].

$$\eta_{app} = \eta_{\infty} + \frac{\eta_0 - \eta_{\infty}}{1 + (C\dot{\gamma})^m} \quad (25)$$

where η_{∞} is the viscosity at the second Newtonian plateau at elevated shear rates and m is a coefficient related to the slope of the pseudo-plastic interval of the rheological curve.

2.3.4.2. Relative and Intrinsic viscosity of solubilized polymer

Relative viscosity tests were carried out through an Ubbelohde viscometer at 25.0 °C according to ISO 307 standard on monoconcentrated masterbatches and on color masterbatches chips, thermal treated at 260°C at different residence time, in order to evaluate the degradation phenomenon. About 0.4 g of samples were previously dried for 30-60 minutes in oven at 90 °C and solubilized at 50 °C with sulfuric acid (purity 95.7%), at a concentration of 5 $g \cdot l^{-1}$, 7.5 $g \cdot l^{-1}$ and 10 $g \cdot l^{-1}$. The solution was then put in a water bath at 25 °C for 20 minutes and then tested at the same temperature [174-176].

The relative viscosity (η_{rel}) is defined as the ratio between the flow time of a polymer solution (t) and the flow time of the pure solvent (t_0) through a capillary, as reported in the Equation (26):

$$\eta_{rel} = \frac{t}{t_0} \quad (26)$$

By measuring the relative viscosity at different concentration the reduced viscosity (η_{red}) and the inherent viscosity (η_{inh}) were calculated using the Equation (27) and Equation (28).

$$\eta_{red} = \frac{\eta_{rel} - 1}{c} \quad (27)$$

$$\eta_{inh} = \frac{ln\,\eta_{rel}}{c} \quad (28)$$

Where c is the solution concentration. The plots of reduced viscosity and inherent viscosity converge at zero concentration to the intrinsic viscosity (η_i) of the polymer, defined in the Equation (29) [177, 178].

$$\eta_i = \lim_{c \to 0} \frac{\eta_{rel} - 1}{c} \quad (29)$$

2.3.4.3. End-groups analysis

End groups analysis was performed on extruded pellets, in order to investigate the effect of the different processing conditions on the chemical properties of the monoconcentrated masterbatches. These tests were performed by using a Mettler DL50 automatic titrator coupled with an electronic voltmeter [140]. About 0.8 g of samples were solubilized in 20 ml of 2,2,2 trifluoroethanol (TFE) at 55 °C. -NH_2 groups titration was performed at 25 °C through a HCl 0.02 N solution, while -COOH titration was carried out with a NaOH 0.02 N solution. The adopted testing methods and the relative parameters have been optimized, and the absolute error associated to each measurement is in the order of 1 mmol·kg^{-1}.

2.3.4.4. Gas chromatography for monomer concentration

Gas chromatography analysis was performed on the monoconcentrated masterbatches and on color masterbatches in order to evaluate the monomer concentration by using a Perkin Elmer Clarus GC 580, following the ISO 11337 standard. The samples were solubilized in the Tetrafluoroethylene (TFE) with a concentration of 25 g·l^{-1} and the standard used for the quantitative analysis was ω-laurolactame. The measurements was performed in a glass column with a Nitrogen carrier flow of 35 to 60 ml/min, at 175 °C for 5 minutes and at 205° for 7 minutes.

Moreover the determination of monomer concentration was used to evaluate the thermal stability of the samples thermal treated at high temperature (260°C) at different residence time (3-13-23 minutes) [179, 180].

2.3.4.5. Mechanical testing on fibers

The mechanical properties of the industrial yarns were evaluated through quasi-static uniaxial tensile tests at break performed with a Mesdan Lab Autodyn 300 tensile machine, following the ISO 2062-EN standard. The sample length was 250 mm and the crosshead speed was set at 250 mm/min.

The two different yarns, prepared with standard and optimized monoconcentrated masterbatches, were tested, in order to evaluate the influence of pigment dispersion on the most important tensile properties of the final industrial product. From this analysis the elastic modulus (E), the tensile strength, the strain at break (ε_b) and the tenacity were evaluated. in particular, the elastic modulus (E) was calculated between 20 and 30% of deformation because the deformation until 20% is due to the crimp on the fibers [181] that confers the elasticity and the apparent volume needed in order to optimized the appearance on the final carpet.

Moreover, the mechanical properties were measured on the fibers after a thermal and UV aging in order to evaluate the thermal and UV stability of the yarns depending of the production process.

3. RESULTS AND DISCUSSION

3.1. MICROSTRUCTURAL PIGMENTS CHARACTERIZATION

3.1.1. SEM OBSERVATION

In Figure 3.1 SEM images of the eight color pigments powders considered in this work are reported. For each material different magnifications were used in order to evaluate the structure and the morphology of the primary particles.

Regarding inorganic pigments, the white pigment (PW6) and the carbon black (PBk7), shown in Figure 3.1a and 3.1b, are constituted by spherical primary particles with a diameters around 150 nm and 50 nm, respectively. On the contrary, the brown pigment (PBr24), reported in Figure 3.1c, shows big primary particles, with elongated shape, and their major dimension is approximately 300-400nm. The red pigment (PR101), represented in Figure 3.1d, is constituted by primary particles with acicular shape having the main dimension around 20 nm.

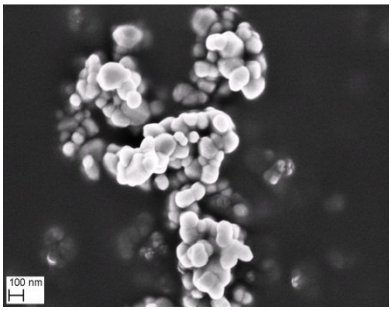

(a)

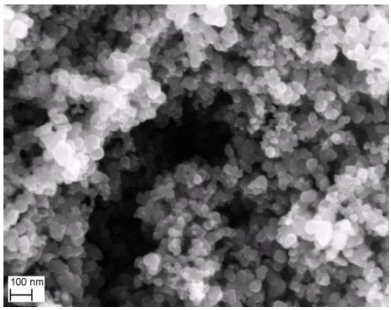

(b)

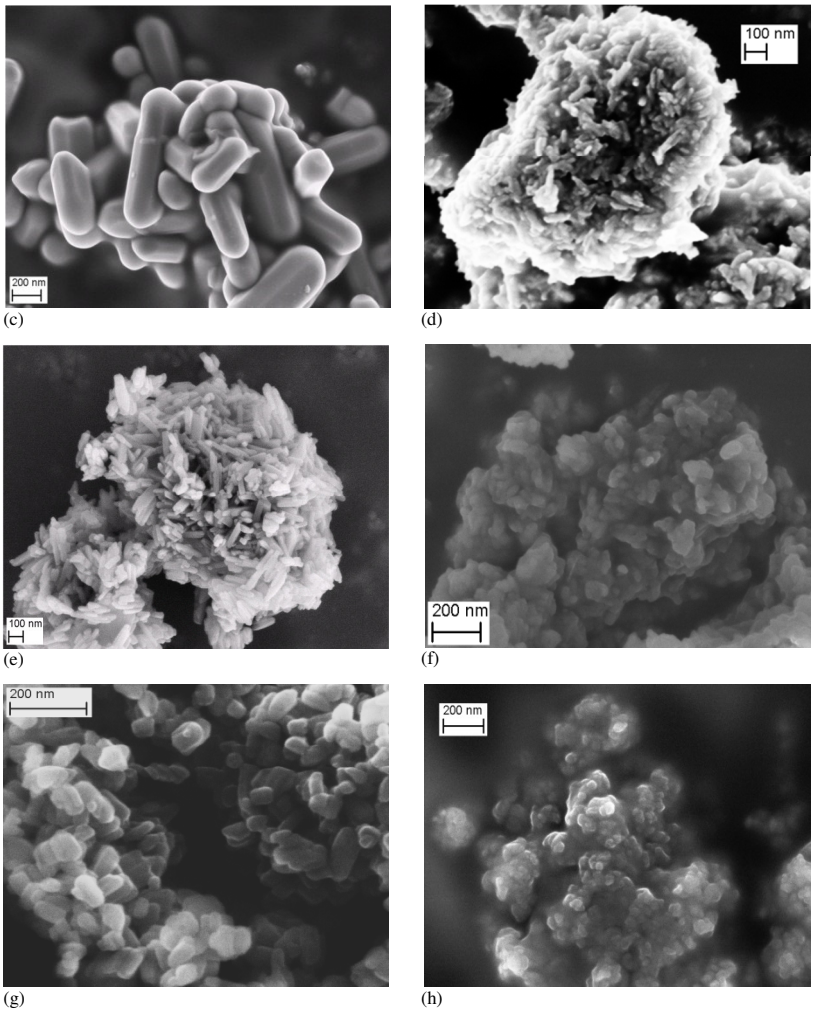

(c) (d)

(e) (f)

(g) (h)

Figure 3.1: SEM images of color pigments. (a) white pigment PW6; (b) black pigment PBk7; (c) brown pigment PBr24; (d) red pigment PR101; (e) blue pigment PB15:3; (f) green pigment PG7; (g) violet pigment PV23; (h) red pigment PR149

In the case of organic pigments, the primary particles of PB15:3 (Figure 3.1e) have acicular shape with the main axis of about 100 nm. The green PG7 and the violet PV23 pigments, represented in Figure 3.1f and 3.1g respectively, show platelet

primary particles with a dimension of around 70 nm. Finally, the red pigment PR149 (Figure 3.1h) has small round shape primary particles with a diameter of around 40 nm.

It is clear that the morphological properties of the pigments strongly affect the coloration capability.

3.1.2. DENSITY MEASUREMENTS

In the Figure 3.2 the results of the helium pycnometry measurements of the color pigments analyzed in this work are reported, while in Table 3.1 density results are summarized. For all the eight color pigments analyzed at least 200 measurements were necessary in order to reach a constant density value. This probably indicates that the surface of all pigments aggregates, except for the carbon black pigment (PBk7), has a diffused open porosity, among which helium molecules can penetrate and diffuse.

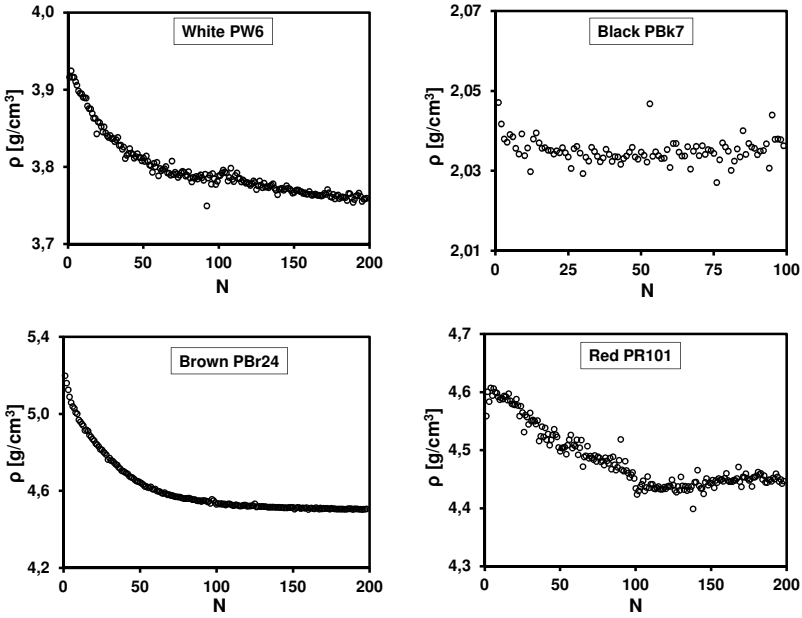

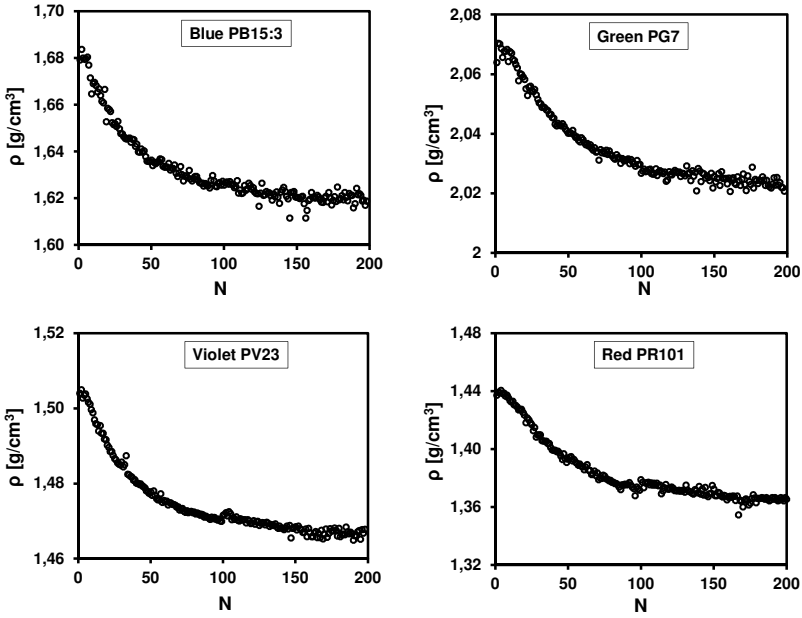

Figure 3.2: Density measurements on the different color pigments considered in this work

From Table 3.1, it is evident that density measured by helium picnometer on the color pigments are in accordance with the density reported in the datasheet.

Pigment	Density (datasheet) [g/cm³]	Density (measured) [g/cm³]
White PW6	3,80	3,76 ± 0,01
Black PBk7	2,00	2,02 ± 0,01
Brown PBr24	4,50	4,51 ± 0,01
Red PR101	5,00	4,44 ± 0,01
Blue PB15:3	1,60	1,62 ± 0,01
Green PG7	2,10	2,02 ± 0,01
Violet PV23	1,60	1,47 ± 0,01
Red PR149	1,40	1,36 ± 0,01

Table 3.1: Measured and Datasheet density

3.1.3. EVALUATION OF THE PIGMENT SURFACE PROPERTIES

Porosity measurements were performed in order to evaluate the surface properties of the color pigments.

In Figure 3.3 the evaluation of the porosity properties of the white pigment PW6 and the brown pigment PBr24 are reported. In particular, Figure 3.3a and 3.3d show the absorption/desorption curves, obtained during BET analysis. The absence of hysteresis between the two cycles means that these two color pigments are not internally porous and the porosity is constituted by interstitial spaces between primary particles fused together during the manufacturing process [143, 182, 183]. In the Figures 3.3b and 3.3e, from the extrapolation of the adsorbed gas volume at low relative pressure, the BET surface area of white and brown pigments were obtained and the results for all color pigments are reported in the Table 3.2.

Moreover, through the application of the BJH method it is possible to determine the pore volume contribution associated to pores with different dimension, and the resulting curves are represented in Figure 3.3c and in Figure 3.3f. In these cases and even for red pigment PR149, there are not peaks in the curves. This means that the greater contribution to the total pore volume is due to the pores with diameter smaller than 2 nm. The values of the mean pore diameter of all color pigments are reported in Table 3.2.

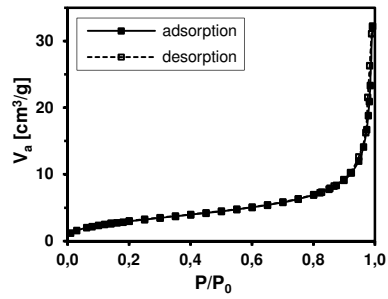

(a)

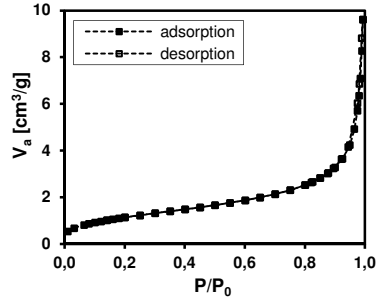

(d)

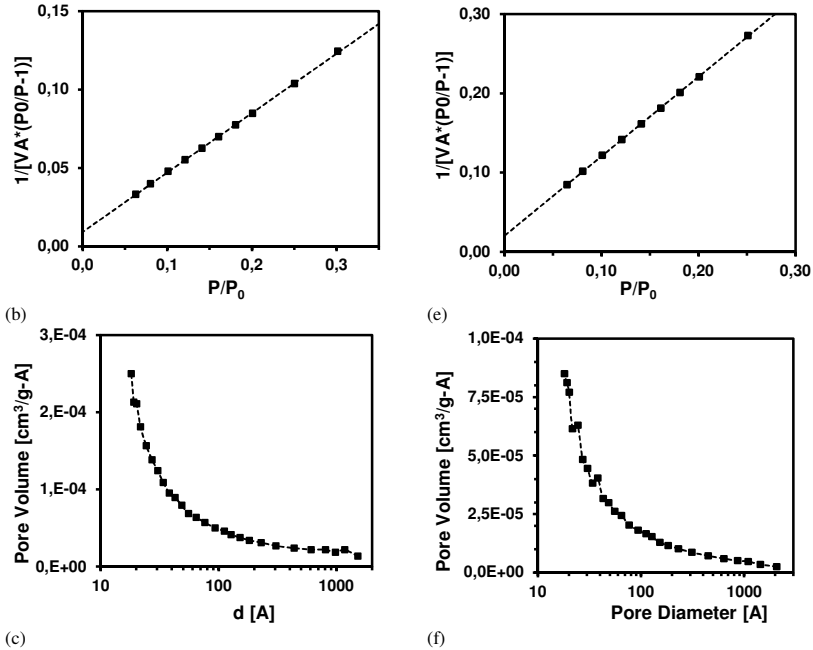

Figure 3.3: Porosity measurements of color pigment powders. Representative curves of the surface properties of Pigment White PW7 (a, b, c) and Brown PBr24 (d, e, f). (a-d) specific gas volume adsorbed vs relative pressure, (b-e) linear plot for the evaluation of the BET surface area, (c-f) pore volume distribution

A different behaviour can be detected by the surface properties measurements of the blue pigment PB15:3 and the violet pigment PV23, reported in Figure 3.4. From adsorption/desorption curves a little hysteresis at high relative pressure can be detected for both materials. The same behavior can be detected for the other organic pigments analyzed (PR149 and PG7) and even for the inorganic PR101 and carbon black PBk7. This is due to the capillary condensation phenomenon in the mesopores during pressurization and depressurization of the system. Probably these materials are internally porous and non-rigid slit-shaped pores can be found in correspondence of the aggregates of plate-like particles, formed during the synthesis of the particles [111, 184]. The curves related to pore volume distribution of the organic pigments, except PR149, and of inorganic PR101 and carbon black PBk7, reported in the

Figures 3.3c and 3.3f, show that the greatest contribution to the total pore volume is due to the presence of pores with a specific diameter, higher than 2 nm (Table 3.2).

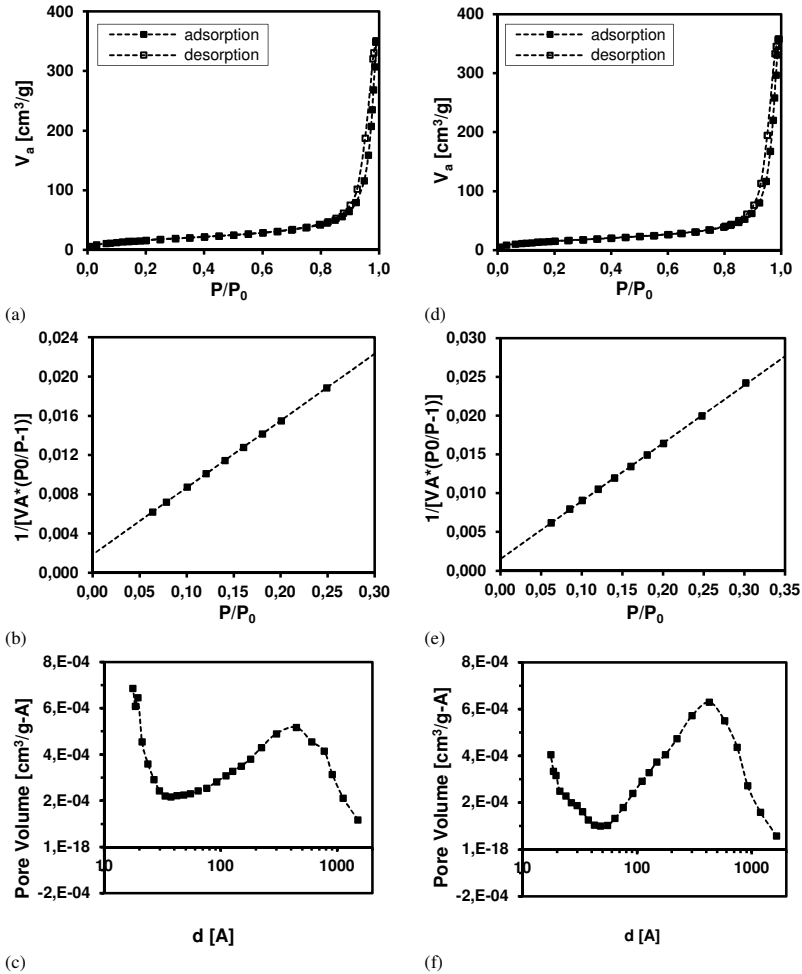

Figure 3.4: Porosity measurements of color pigment powders. Representative curves of the surface properties of Pigment Blue PB15:3 (a, b, c) and Violet PV23 (d, e, f). (a-d) specific gas volume adsorbed vs relative pressure, (b-e) linear plot for the evaluation of the BET surface area, (c-f) pore volume distribution

The surface properties of the color pigments, measured by BET surface analysis, are shown in the Table 3.2. The resulting specific surface area values are substantially in accordance with the values reported in the datasheets.

Pigment	BJH Adsorption Average Pore Diameter [nm]	BET Surface Area (measured) [m^2/g]	BET Surface Area (datasheet) [m^2/g]
PW6	17,76	11,22 ± 0,06	12
PBk7	36,42	103,58 ± 0,40	110
PBr24	14,16	4,21 ± 0,03	4
PR101	18,41	94,68 ± 0,20	-
PB15:3	35,33	61,49 ± 0,29	65
PG7	29,57	42,93 ± 0,15	61
PV23	38,80	57,11 ± 0,25	58
PR149	10,49	106,22 ± 0,67	76

Table 3.2: Results of the surface properties of color pigments

Moreover, through the specific surface area measured from BET analysis and the density evaluated by helium picnometry, the average primary particles diameter for all color pigments were calculated (Equation (17)). The results reported in the Table 3.3 are comparable with the dimension detectable from SEM micrographs.

Pigment	d_{BET} [nm]
PW6	142
PBk7	29
PBr24	317
PR101	16
PB15:3	60
PG7	69
PV23	72
PR149	41

Table 3.3: Primary particles diameters calculated through BET analysis and pycnometry measurements

3.1.4. LIGHT SCATTERING MEASUREMENTS

In Figure 3.5 the diameter distribution curves, obtained from light scattering measurements of the color pigments analyzed in this work, are summarized. From dynamic light scattering analysis the hydrodynamic diameters of the color pigment aggregates were evaluated and the results are summarized in the Table 3.4.

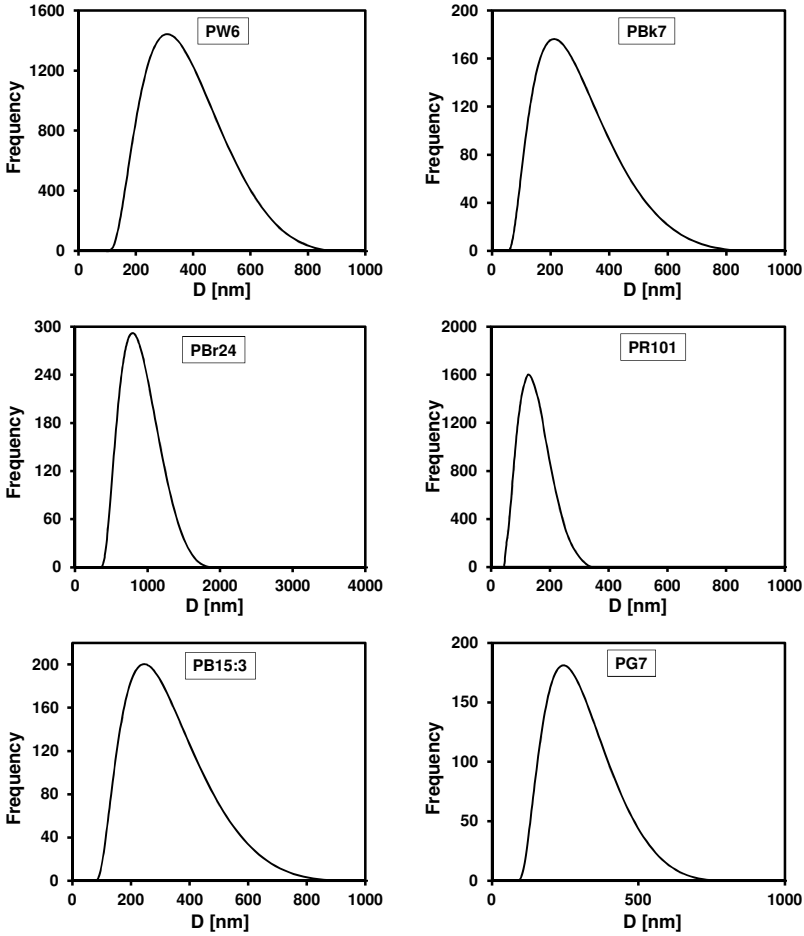

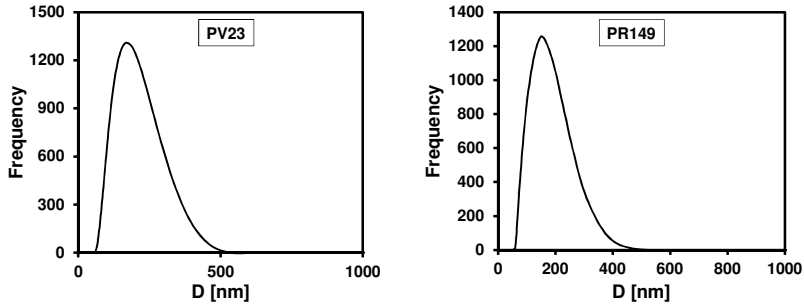

Figure 3.5: Color pigments diameter distribution from dynamic light scattering measurements

From Table 3.4 it can be noticed that the brown pigment PBr24 shows a larger aggregates diameter compared to the other pigments (around 1 μm). For this reason PBr24 is the most critical material in the fiber spinning process because of the intense filtration clogging. PW6 has an aggregate dimension of approximately 300 nm, while the other pigments have a diameter smaller than 250 nm.

Pigment	D_{50} [nm]
PW6	325
PBk7	224
PBr24	921
PR101	126
PB15:3	242
PG7	243
PV23	187
PR149	149

Table 3.4: Mean aggregate diameter (D_{50}) of color pigments from light scattering measurements

3.2. MONOCONCENTRATED MASTERBATCH SELECTION

The selection of the most critical monoconcentrated masterbatches was based on the Filter-Test measurements, performed keeping a constant pigment concentration and with a sintered filter of 25 μm. In Figure 3.6 the pressure curves of the most important and critical monoconcentrated masterbatches, used to produce carpet in automotive sector, are reported.

From Figure 3.6, it can be noticed that the brown masterbatch PBr24 shows a different clogging behaviour compared to the other masterbatches. In fact, the clogging phenomenon starts gradually and then it grows exponentially, without allowing the test to be finished. This is very critical from an industrial point of view, because this product tends to clog the filtration system during the melt spinning process and increases the breakage of the filament, reducing the production output.

The critical issue of brown masterbatch is due to the big primary particles that characterize the pigment PBr24, as highlighted by the SEM analysis, and so it is not related to the production.

On the other hand, the other monoconcentrated masterbatches show an important increase of pressure when the sample reaches the filter (i.e. after 5 minutes), and then the clogging rate is reduced. This is due to two concomitant and contrasting effects: the first is related to the color pigments that reach the filter, while the second regards the disaggregation of the pigment agglomerates due to the polymer flow through the filter. After the pressure peak, when only the polymer matrix is fed into the extruder, these masterbatches show a significant pressure reduction. This is due to the breakage of the pigment agglomerates and their subsequent flowing through the filter.

The significant pressure increase at the beginning of the test and the important pressure reduction at the end indicate that during the compounding process the primary particles form agglomerates, which could be critical for the subsequent industrial steps.

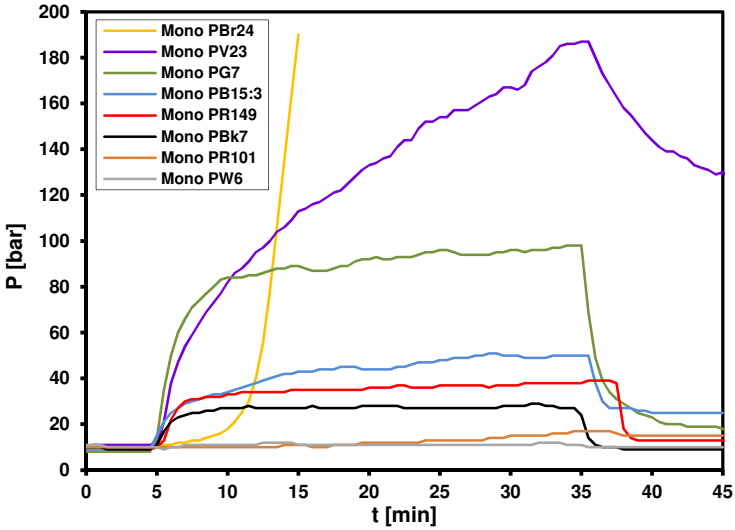

Figure 3.6: Pressure curves of the monoconcentrated masterbatches from Filter-Test measurements

Red (PR101) and white (PW6) monoconcentrated masterbatches did not show any important pressure variation during the analysis.

From this preliminary analysis, the six most problematic monoconcentrated masterbatches were selected. In particular: brown (PBr24), violet (PV23), green (PG7), blue (PB15:3), red (PR149) and black (PBk7) monoconcentrated masterbatches. On these materials a production process optimization analysis was performed, in order to reduce the clogging power and the filament breakage during melt spinning.

3.3. PRODUCTION PROCESS OPTIMIZATION OF MONOCONCENTRATED MASTERBATCHES

The eight monoconcentrated masterbatches studied in this research were obtained using different production process set up, as reported in Paragraph 2.2.1., in order to improve the dispersion of the color pigments in the polymer matrix and to reduce the dimension of their agglomerates. From an industrial point of view, this allows to reduce the clogging power of the color masterbatch, to reduce the filament breakage during spinning process and so to reduce the cost of production and increase the plant productivity.
All the prepared monoconcentrated masterbatches, were analyzed through Filter-Test, Relative Color Strength (RCS) and rheological measurements, in order to evaluate the pigment dispersion quality. On the other hand, viscosity analysis, end group determination and monomer concentration measurements allowed to evaluate the degradation phenomenon occurred during the processing and the thermal stability of the materials. Moreover, crystallization kinetics analysis was conducted to understand the effect of the color pigments on the thermal properties of PA6 and, indirectly, to evaluate the pigment dispersion.

In the following paragraphs the results obtained on the most critical monoconcentrated masterbatches and on a not problematic product (black monoconcentrated masterbatch) will be discussed in detailed. In particular the critical products analyzed were blue (PB15:3), green (PG7) and violet (PV23) monoconcentrated masterbatches, while a standard monoconcentrated masterbatch was the black one (PBk7). In Paragraph 3.3.5 Filter-Test and the Relative Color Strength (RCS) results, obtained on all monoconcentrated masterbatches studied in this work, will be briefly summarized.

3.3.1. BLUE MONOCONCENTRATED MASTERBATCH

3.3.1.1. Filter-Test measurements

In order to detect the process parameter combination that allows to limit the filter clogging during compounding and spinning processes, Filter-Test analysis was performed on blue monoconcentrated masterbatches produced with four different process set up (i.e. with different SME involved during extrusion).

From Filter-Test curves reported in Figure 3.7, three distinct regions can be detected: (i) a first plateau region in which the pressure remains constant due to the flow of neat (i.e. unfilled) PA6 matrix, (ii) a second zone characterized by a significant pressure increase due to the masterbatch flow through the filter. In this zone a marked pressure increase due to the presence of agglomerates can be initially detected, while a slope reduction due to subsequent disagglomeration promoted by the forcing polymer flow through the filter can be observed. (iii) In the third region, a final pressure drop due to the flowing of neat PA6, with the breakage of less stable agglomerates deposited on the filter surface, can be detected.

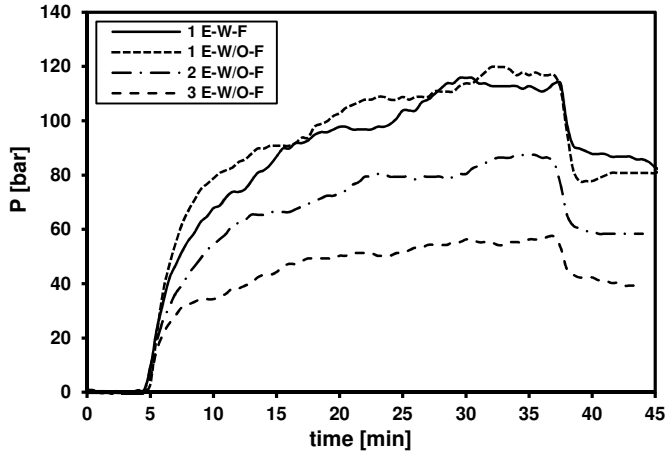

Figure 3.7: Representative Filter-Test curves of monoconcentrated blue masterbatches prepared with different processing set-up

In Figure 3.8 and in Table 3.5 the mean values of FPV, FPVII and the difference between them (ΔFPV) for each processing condition are summarized. The filtration process does not lead to substantial variations of the masterbatch filterability. In fact, considering standard deviation values, both FPV and FPVII values of filtered and unfiltered masterbatches are practically the same. It can be concluded that industrial filtration of these masterbatches is practically an unuseful processing step, that can be removed from the industrial layout of these products. Interestingly, an increase of the number of extrusions promotes a marked reduction of the aggregation tendency and thus of the filter clogging, with a significant reduction of both the FPV and FPVII values. For instance, 3 E-W/O-F sample shows an FPV reduction of the 50 % with respect of the 1 E-W-F compound. Furthermore, the ratio between FPV and FPVII values remains fairly constant for all the tested samples (around 1.4). This means that a change of the processing conditions does not alter the physical behavior of the filter clogging, but only reduces the aggregates size.

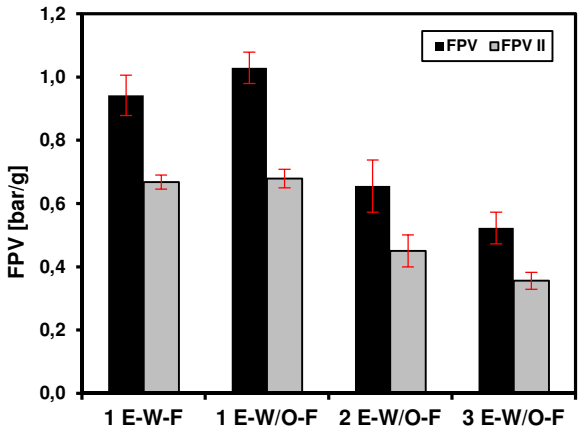

Figure 3.8: FPV and FPVII values of monoconcentrated blue masterbatches with different processing conditions

Mono PB15:3	FPV	FPV II	Δ FPV
1 E-W-F	0.942 ± 0.064	0.668 ± 0.022	-29%
1 E-W/O-F	1.029 ± 0.050	0.679 ± 0.029	-34%
2 E-W/O-F	0.655 ± 0.082	0.450 ± 0.051	-31%
3 E-W/O-F	0.523 ± 0.050	0.356 ± 0.027	-32%

Table 3.5: FPV and FPVII values of monoconcentrated blue masterbatches prepared with different processing conditions

3.3.1.2. Color Strength measurements

The results of color strength measurements are shown in Figure 3.9, in which the color strength of the 1 E-W-F compound was taken as reference. In accordance with Filter-Test analysis, the presence of the filter does not lead to significant changes in color strength, while an increase of the extrusion times leads to noticeable enhancements of the RCS values. For instance, RCS of the masterbatch extruded three times is about 10% higher than that of the 1 E-W-F sample. Once again, repeated extrusions improve pigment dispersion, decreasing the agglomerates size and thus, increasing the specific surface area of the filler, its light absorption capability was improved.

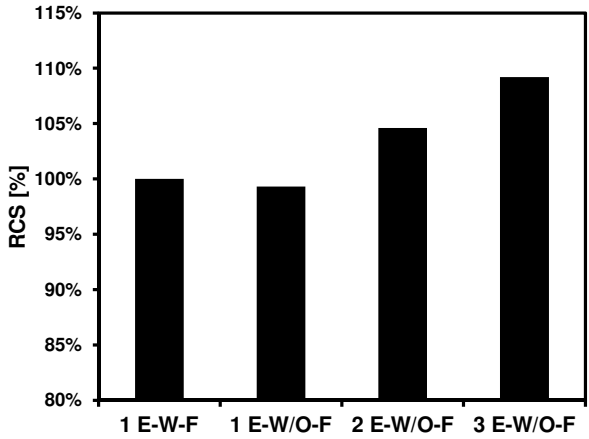

Figure 3.9: Relative Color Strength (RCS) of monoconcentrated blue masterbatches prepared with different processing parameters

From an industrial point of view, an increase of the Relative Color Strength of the masterbatch is a very interesting issue, because it allows to reduce the amount of the pigments in the compound, increasing masterbatch stability and the cost competitiveness of the coloration process.

3.3.1.3. Rheological measurements

Figure 3.10 shows the rheological curves of the neat polymer matrix and of the monoconcentrated masterbatch obtained with one extrusion without filter, at two residence times in the rheometer (3 and 23 minutes), while in Figure 3.11 the zero shear viscosity values of the different masterbatches processed at 3 and 23 minutes are summarized. A slight increase of the polymer viscosity can be detected for the neat PA6 system. This phenomenon is due to the post-condensation reactions occurring during the permanence in the rheometer, promoted by the moisture below the equilibrium concentration [94, 99, 100]. During the thermal processing the amino and carboxylic end groups react each other forming peptide groups and water. This reaction determines an increase of the molecular weight and thus of the apparent viscosity.

The introduction of the pigments in the polymer matrix generates an increase of the apparent viscosity over the whole range of tested shear rates, due to the constraining effect played by the primary particles aggregates. Interestingly, an increase of the processing time does not lead to substantial variations of the rheological curve. This probably means that blue pigment hinders post condensation reaction and/or promotes a slight thermo-oxidative degradation of the matrix. Also pigment flocculation at high residence times could be taken into account to explain this result. In Figure 3.11 the values of the zero shear rate viscosity, obtained through the interpolation of the rheological curves with the Cross model equation, are reported.

The presence of the filter does not affect the rheological behavior of the master, while a second and a third extrusion determine a marked decrease of the zero shear rate viscosity. This viscosity decrease can be explained considering

disagglomeration phenomena for repeated extrusions, detected in Filter-Tests and in RCS analysis.

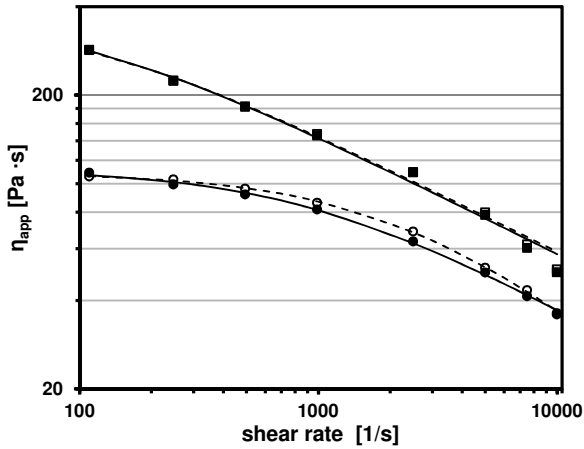

Figure 3.10: Rheological curves of neat PA6 matrix with a residence time of (●) 3 minutes and of (○) 23 minutes, and rheological curves of 1 E-W/O-F monoconcentrated blue masterbatch with a residence time of (■) 3 minutes and (□) 23 minutes.

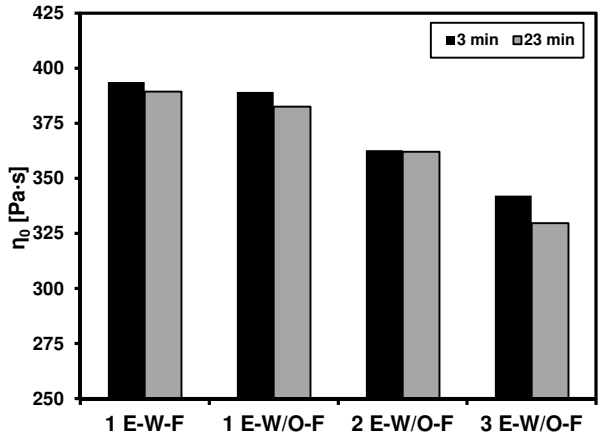

Figure 3.11: Zero shear viscosity values of monoconcentrated blue masterbatches processed at 3 and 23 minutes

As reported in a comprehensive review of Cassagnau, an improvement of the filler dispersion in particulate filled nanocomposites leads to an evident decrease of the melt viscosity of the system [185]. However, also the thermo-oxidative degradation effect due to a prolonged compounding should be taken into account. The results of rheological analysis and of the fitting with the Cross equation are reported in Table 3.6, while in Figure 3.12 a correlation between FPV values obtained from Filter-Tests and the C parameter of the Cross model is reported.

Mono PB15:3	Residence time	η_0	C	η (1000 s^{-1})
1 E-W-F	3 min	394	0,0103	144
	23 min	389	0,0093	140
1 E-W/O-F	3 min	389	0,0107	146
	23 min	383	0,0102	148
2 E-W/O-F	3 min	363	0,0057	144
	23 min	362	0,0086	134
3 E-W/O-F	3 min	342	0,0046	137
	23 min	330	0,0062	119

Table 3.6: Results of rheological measurements on monoconcentrated blue masterbatch and fitting parameters obtained through the application of the Cross model

A linear trend between these two parameters can be easily detected. Studies in literature demonstrate the existence of relationship between the filterability of a filled polymer and its rheological properties. In particular, the higher values of the coefficient C, proportional to the bonding energy between the particles under shear flow, the greater filler agglomeration and clogging effect of the filter [36]. This probably means that the viscosity decrease experienced for repeated extrusions is influenced by the pigment disagglomeration.

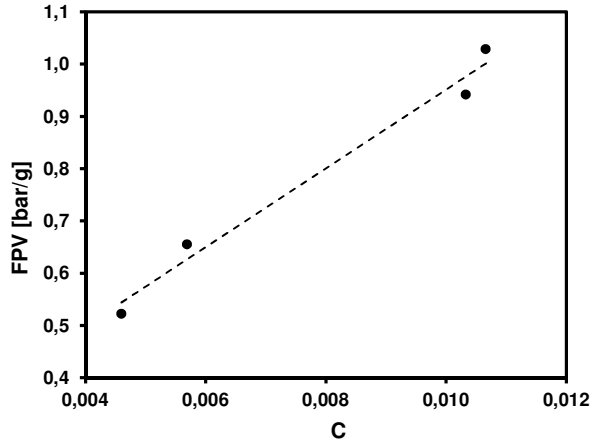

Figure 3.12: Correlation between FPV and C parameters of monoconcentrated blue masterbatch

3.3.1.4. Viscosity analysis

In Figure 3.13 a representative plots of reduced an inherent viscosity of the masterbatch extruded one time without filtration is represented, while in Figure 3.14 intrinsic viscosity values of all the prepared samples are reported.

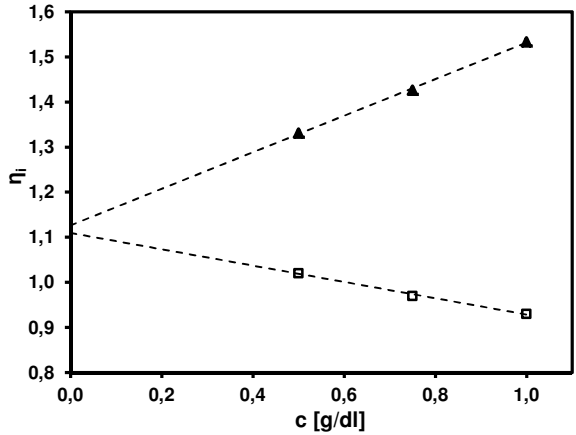

Figure 3.13: Intrinsic viscosity analysis of monoconcentrated blue masterbatch obtained through 1 Extrusion W/O-F. (▲) Reduced viscosity and (□) inherent viscosity

An important decrease of the η_i values can be detected only after the third extrusion of the masterbatch. Considering that intrinsic viscosity values depends only on the macromolecular coils (i.e. on their molecular weight) of the polymer matrix, it can be hypothesized that a prolonged thermo-mechanical processing of these samples leads to their partial thermo-oxidative degradation.

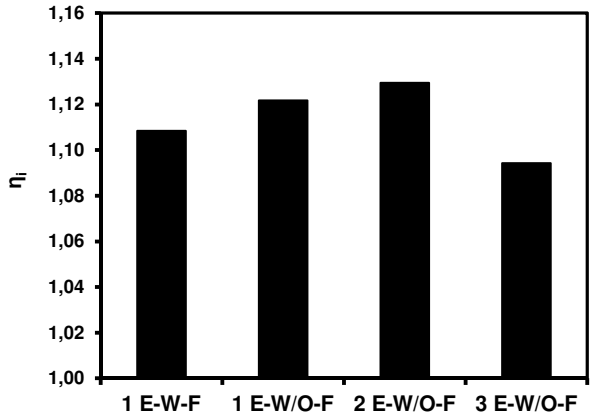

Figure 3.14: Intrinsic viscosity values of monoconcentrated blue masterbatch chips prepared with different processing set-up

3.3.1.5. End groups determination

End groups analyses were performed, and in Figure 3.15 the results of these tests, in terms of aminic and carboxylic functionalities, are reported. In can be seen that after the third extrusion an interesting decrease of the aminic groups associated to a corresponding increase of the carboxylic functionalities occurs, and the total number of the end groups slightly increases. According to literature references, thermo-oxidation of polyamides leads to a reduction of the aminic functionalities because of the generation of aldehydic groups that can be subsequently oxidized forming COOH functionalities [70]. Therefore, the total number of carboxylic groups

increases. It is therefore confirmed that the experienced intrinsic viscosity drop is related to a decrease of the molecular mass promoted by thermo-oxidation. Concluding, thermal re-processing of phthalocyanine blue masterbatches leads to a better pigments dispersion and to a partial thermo-oxidation of the polymer matrix. Both these aspects affect the rheological behavior of the resulting materials.

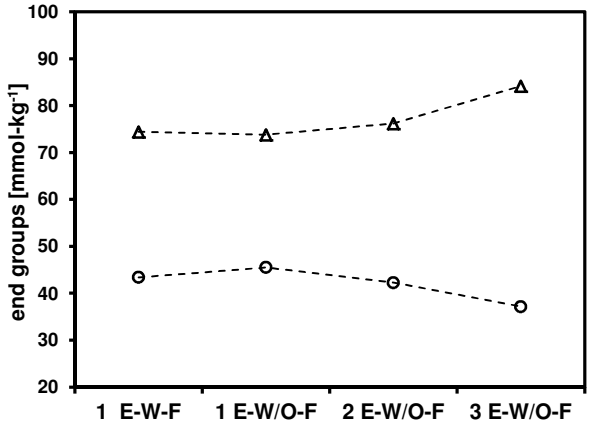

Figure 3.15: End groups analysis on monoconcentrated blue masterbatches with different process conditions. (●) aminic end groups and (▲) carboxylic end groups

3.3.1.6. Monomer concentration analysis

Gas Chromatography analysis was performed on the monoconcentrated blue masterbatches produced in the four different process conditions, in order to evaluate their monomer concentration. The concentration of caprolactame in the monoconcentrated masterbatches is an important parameter that allows to analyze the degradation phenomena occurred during the production and the thermal stability of the product.

The monomer concentration of the monoconcentrated blue masterbatches at different residence times in the rheometer at high temperature (260 °C) are reported in the Figure 3.16. The masterbatches obtained without filtration system show a lower monomer concentration after the production. This is probably due to the polymer flow stagnation induced by filter during production, that promoted thermo-oxidation degradation. After 23 minutes in the rheometer at 260 °C the masterbatches extruded one time have an higher monomer concentration compared to the masterbatches extruded two and three times. This can be explained by the fact that the subsequent processes stabilized the products, because of more degassing and water monomer extraction.

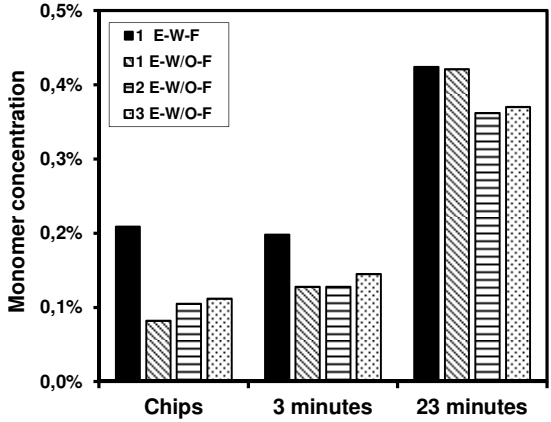

Figure 3.16: Monomer concentration of the monoconcentrated blue masterbatches at different residence times in the rheometer

3.3.1.7. DSC and Crystallization kinetics analysis

From DSC analysis the thermal properties of the monoconcentrated blue masterbatches, obtained through different process parameters, were measured. In Table 3.7 the thermal properties of the neat PA6 and of the standard

monoconcentrated blue masterbatch are summarized. It can be easily noticed that the presence of the phthalocyanine blue pigment leads to an important reduction of the melting enthalpy, during the first heating scan, and a significant increase of crystallization peak temperature, during the cooling scan. The pigment acts like an heterogeneous nucleus of crystallization because it increases the crystallization temperature but, probably, it reduce the mobility of polymer chain that results in a lower crystal content.

	1st Heating			Cooling		2nd Heating		
Sample	T_m [°C]	ΔH_m [J/g]	X_c [%]	T_c [°C]	ΔH_c [J/g]	T_g [°C]	T_m [°C]	ΔH_m [J/g]
AQ24401	226	86	45	159	59	55	221	58
Mono PB15:3	226	43	30	187	49	59	225	50

Table 3.7: Thermal properties of neat PA6 and monoconcentrated blue masterbatch from DSC tests

From isothermal crystallization kinetics analysis the activation energy of crystallization was evaluated, and the DSC cooling scan at different rates are reported in the Figure 3.17. Reducing the cooling rate, the crystallization peak temperature is shifted to higher value, because of longer time available for the polymer chains to form crystallites. At low cooling rate, it can be distinguished the two contributions of the crystallization temperature peaks related to the two crystalline structures (i.e. α and γ phases) [160]. The α phase is the most thermodynamically stable crystalline form, it could be obtained under the slow cooling condition and it is related to the shoulder at higher temperature in detectable Figure 3.17. Moreover the more pronounced peak at lower temperature is referred to the γ phase, that is obtained under fast cooling rate.

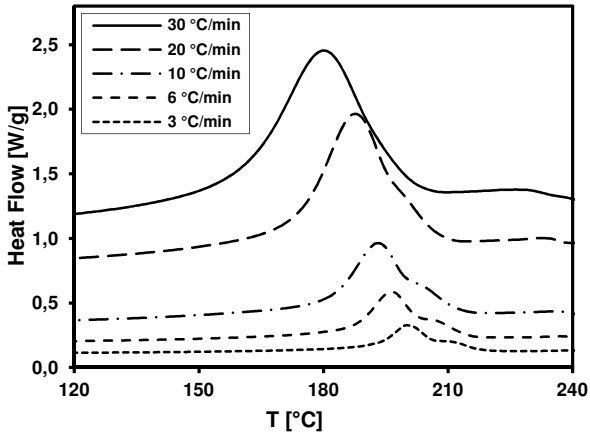

Figure 3.17: Cooling scan for monoconcentrated blue masterbatch at five different cooling rates from DSC tests

In Figure 3.18 the Arrhenius plot obtained from the crystallization kinetics analysis is reported. The slope of the curves increases from neat PA6 to monoconcentrated masterbatches and, moreover, it is increase with the second extrusion process.

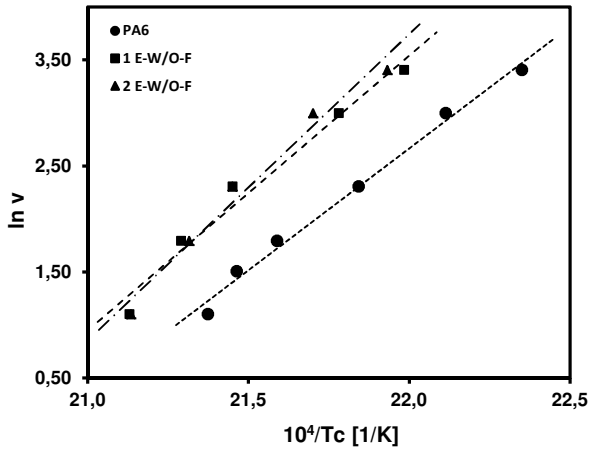

Figure 3.18: Arrhenius-type plot for PA6 and monoconcentrated blue masterbatches produced in two different conditions (1 E-W/O-F and 2 E-W/O-F)

In Table 3.8 the crystallization activation energy (ΔE_{act}) for neat PA6 and monoconcentrated blue masterbatches, derived from the slope of Arrhenius equation [186, 187] , are reported. The ΔE_{act} is negative because the transition from melt to crystalline state is an endothermic phenomenon. Moreover the magnitude of activation energy is related to the energy need for the macromolecules motion during transformation [160, 188]. The monoconcentrated masterbatch shows higher values of ΔE_{act} because the hindering effect of the nanocolorant on the polymer chain mobility.

From this analysis it was possible make some considerations about the pigment dispersion in the polymer matrix. A second extrusion further increases the crystallization activation energy. This can be related to the better pigment dispersion that leads to an higher filler surface in contact with the polymer that results in an higher nucleation effect but also in an higher hindrance to the macromolecules motion within the polymer matrix.

Sample	ΔE_{act} [kJ/mol]
PA6	-191 ± 8
Mono PB15:3 - 1 E-W/O-F	-215 ± 14
Mono PB15:3 - 2 E-W/O-F	-240 ± 13

Table 3.8: Crystallization activation energy from Arrhenius plot of DSC curves at different cooling rates of monoconcentrated blue masterbatches

3.3.2. GREEN MONOCONCENTRATED MASTERBATCH

3.3.2.1. Filter-Test measurements

In Figure 3.19 Filter-Test curves related to the four monoconcentrated green masterbatches, obtained with different process conditions, are reported. As for the monoconcentrated blue masterbatch, the curves of the green one show three distinct regions. The second region, after an important pressure increment, is characterized by a substantially zero slope curve, that is related to the perfect balance between the pigment agglomerates that reach the filtration system and their disaggregation due to the polymer flow. The third region shows an important pressure drop, higher than that displayed by monoconcentrated blue masterbatches. This is due to the bigger and more unstable agglomerates that the green phthalocyanine forms during the production.

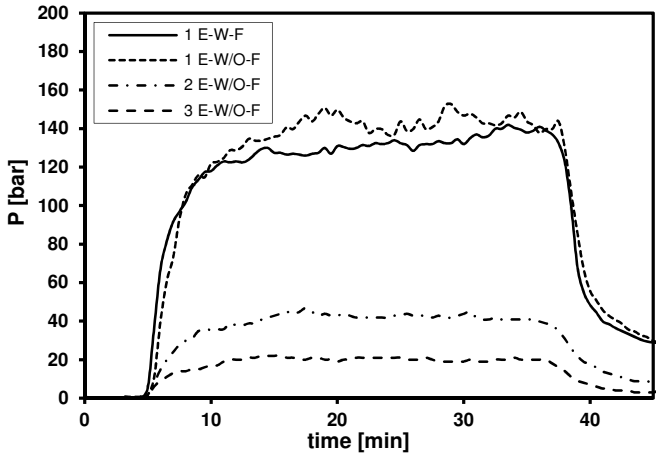

Figure 3.19: Representative Filter-Test curves of monoconcentrated green masterbatches

The mean values of FPV and FPVII for each processing condition are summarized in Figure 3.20 and in Table 3.9. As for the monoconcentrated blue masterbatch,

considering standard deviation values, the FPV and FPVII values of filtered and unfiltered masterbatches are practically the same. There are not important variations of the masterbatch filterability. The industrial filtration of the monoconcentrated green masterbatch is practically an useless processing step, that can be removed from the industrial layout of these products. The second extrusion produces an important reduction of the clogging power of this masterbatch and a third extrusion promotes a further FPV reduction. Interestingly, 3 E-W/O-F sample shows an FPV reduction of the 84 % with respect of the 1 E-W-F compound. The variation between FPV and FPVII, reported in Table 3.9, remains fairly constant for all the tested samples. This means that a change of the processing routes does not alter the physical behavior of the filter clogging, but only reduces the aggregates size.

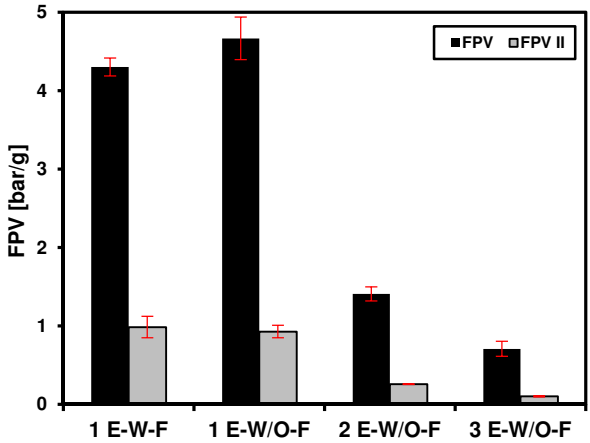

Figure 3.20: FPV and FPVII values of monoconcentrated green masterbatches with different processing conditions

Mono PG7	FPV	FPV II	Δ FPV
1 E-W-F	0,942 ± 0,064	0,668 ± 0,022	-78%
1 E-W/O-F	1,029 ± 0,050	0,679 ± 0,029	-80%
2 E-W/O-F	0,655 ± 0,082	0,450 ± 0,051	-82%
3 E-W/O-F	0,523 ± 0,050	0,356 ± 0,027	-85%

Table 3.9: FPV and FPVII values of monoconcentrated green masterbatches with different processing conditions

3.3.2.2. Color Strength measurements

In Figure 3.21 the results of Color Strength measurements are summarized and the color strength of the 1 E-W-F compound was taken as reference. These analysis confirmed the considerations obtained from the Filter-Test results. The presence of the filter does not lead to significant changes in color strength but, on the contrary, it seems to have a negative effect on this properties. With a second extrusion a significant increase in RCS was recorded. In fact, the 3 E-W/O-F shows a color strength 50% higher compared to the 1 E-W-F green masterbatch. This tinting strength enhancement is related to the pigment dispersion improvement, achieved with the higher specific mechanical energy involved during production. Industrially speaking, this pronounced RCS increase allows to reduce the use of the pigments in the compound, increasing masterbatch stability and reducing the cost of the coloration process.

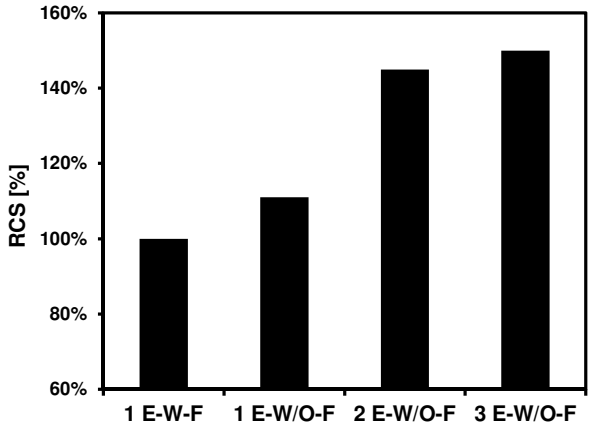

Figure 3.21: Relative Color Strength (RCS) of monoconcentrated green masterbatches prepared with different processing parameters

3.3.2.3. Rheological measurements

The rheological curves of the neat polymer matrix and of the monoconcentrated green masterbatch, obtained with one extrusion without filter, at two residence times in the rheometer (3 and 23 minutes) are reported in Figure 3.22, while Figure 3.23 shows the zero shear viscosity values of the different masterbatches processed at 3 and 23 minutes. As described in Paragraph 3.3.1.3, the neat PA6, after 23 minutes at high temperature, exhibits a slight increase of apparent viscosity because of post-condensation reaction that occurs inside the rheometer [94, 99, 100]. During the thermal processing the amino and carboxylic end groups react each other forming peptide groups and water. This reaction determines an increase of the molecular weight and thus of the apparent viscosity.

The green phthalocyanine pigment into the polyamide matrix markedly increases the apparent viscosity of the system for all shear rate range, during the test. This effect is due to the hindering effect promoted by the pigment aggregates into the polymer, that reduces the mobility of the polymer chains. After 23 minutes of residence time at 260°C an important reduction of viscosity was recorded. This is probably due to the thermo-oxidative degradation of the matrix, promoted by the color pigment, but also the flocculation phenomenon in the steady melt state could be taken into account to explain this result.

The values of the zero shear rate viscosity, obtained through the interpolation of the rheological curves with the Cross equation, are summarized in Figure 3.23. The filtration process does not have any influence on the rheological behavior of the monoconcentrated green masterbatch while, increasing the specific mechanical energy applied to the system with the second and the third extrusion, the zero shear rate viscosity was significantly reduced. This melt viscosity reduction can be due to the pigment dispersion enhancement, detected in Filter-Tests and in RCS analysis, as well explained by Cassagnau [185]. Moreover, the contribution of the thermo-

oxidative degradation, developed during the second and the third extrusions, must be taken into account.

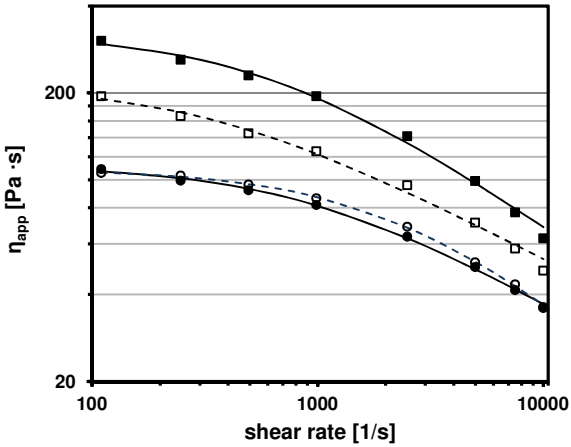

Figure 3.22: Rheological curves of neat PA6 matrix with a residence time of (●) 3 minutes and of (○) 23 minutes, and of the 1 E-W/O-F monoconcentrated green masterbatch with a residence time of (■) 3 minutes and (□) 23 minutes.

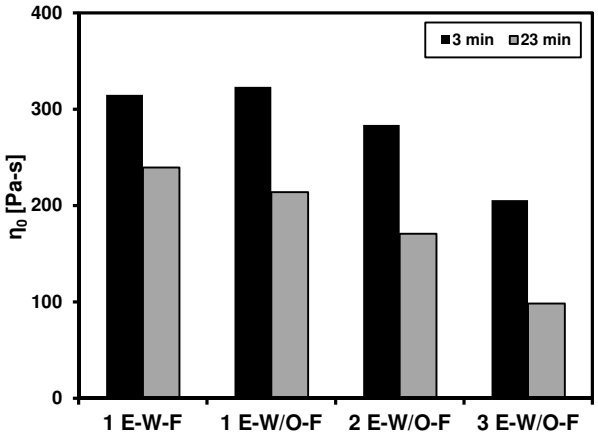

Figure 3.23: The zero shear viscosity values of the different monoconcentrated green masterbatches processed at 3 and 23 minutes

In Table 3.10 the results of rheological analysis and of the fitting with the Cross equation are shown. Figure 3.24 shows the correlation between FPV values obtained from Filter-Tests and the C parameter of the Cross model.

These two parameters are proportional and, as reported in literature [36], the higher values of the coefficient C, proportional to the bonding energy between the particles under shear flow, the greater filler agglomeration and clogging power of the masterbatch. This probably means that the viscosity decrease detected with repeated extrusions is due to the pigment disagglomeration.

Mono PG7	Residence time	η_0	C	η (1000 s^{-1})
1 E-W-F	3 min	315	0,0018	188
	23 min	239	0,0037	139
1 E-W/O-F	3 min	323	0,0019	195
	23 min	214	0,0029	126
2 E-W/O-F	3 min	284	0,0015	168
	23 min	171	0,0022	105
3 E-W/O-F	3 min	206	0,0012	133
	23 min	98	0,0013	75

Table 3.10: Results of rheological measurements on monoconcentrated green masterbatch and fitting parameters obtained through the application of the Cross model

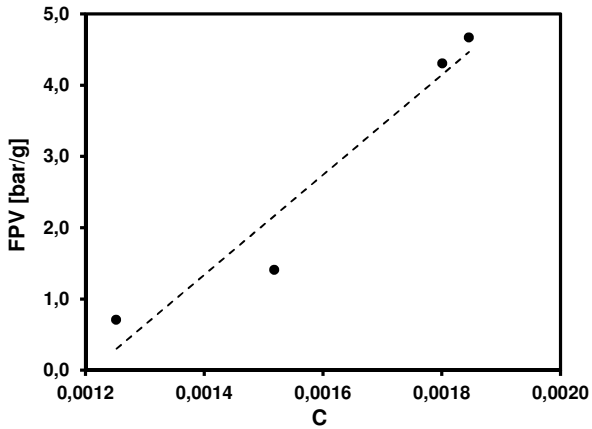

Figure 3.24: Correlation between FPV and C parameters detected for the green monoconcentrated masterbatches prepared with different production set-up

3.3.2.4. Viscosity analysis

A representative plots of reduced an inherent viscosity of 1 E-W/O-F monoconcentrated green masterbatch, that converge at zero concentration into intrinsic viscosity is reported in Figure 3.25. In Figure 3.26 the intrinsic viscosity values of all the prepared samples are summarized.

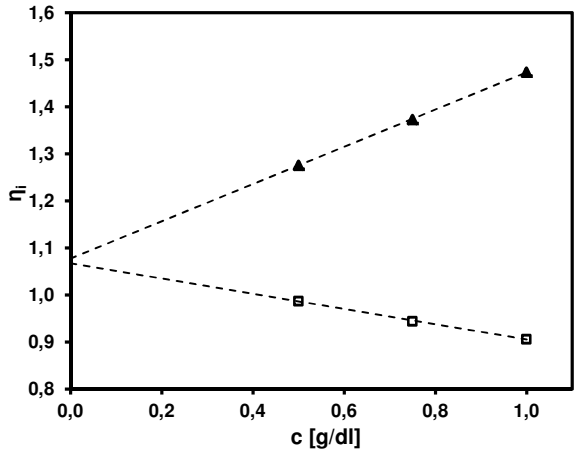

Figure 3.25: Intrinsic viscosity analysis of 1 Extrusion W/O-F monoconcentrated green masterbatch. (▲) Reduced viscosity and (□) inherent viscosity

The intrinsic viscosity of the monoconcentrated green masterbatch slightly decreases removing the filtration system from the industrial lay-out and even with the second extrusion process. Moreover, an important reduction of intrinsic viscosity is detected after the third extrusion, as can be noticed in Figure 3.26. This can be related to the thermo-oxidative degradation that occurred inside the extruder during the third step, because of the prolonged thermo-mechanical processing.

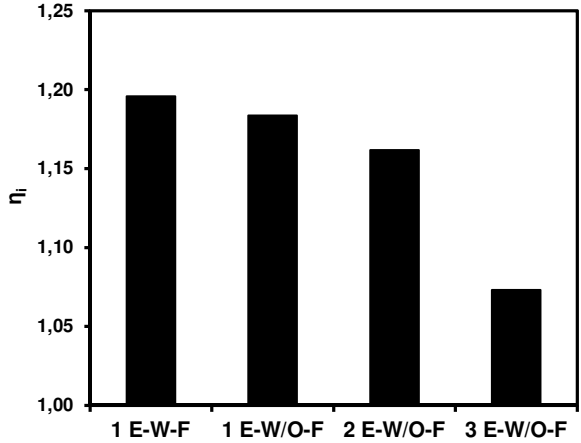

Figure 3.26: Intrinsic viscosity values of monoconcentrated green masterbatch chips

3.3.2.5. End groups determination

In Figure 3.27 the number of carboxylic and aminic terminal functionalities of polyamide macromolecules, measured by end groups analysis, are reported. Both functionalities are not affected by the filtration system and, as confirmed from previous tests, the filter can be removed from the industrial layout. The second and the third extrusions determine an important increase of -COOH functionalities and a reduction of -NH end groups. These variations are associated to a thermo-oxidation reaction of the polymer matrix [70] that occurred during prolonged thermo-mechanical process. This results are in accordance with the rheological behaviour and with the intrinsic viscosity of monoconcentrated green masterbatches obtained following different process conditions.

The re-processing of the monoconcentrated green masterbatch allows to improve the pigments dispersion within the polyamide but even promotes a thermo-oxidative degradation of the polymer matrix. Both these aspects affect the rheological behavior of the resulting materials.

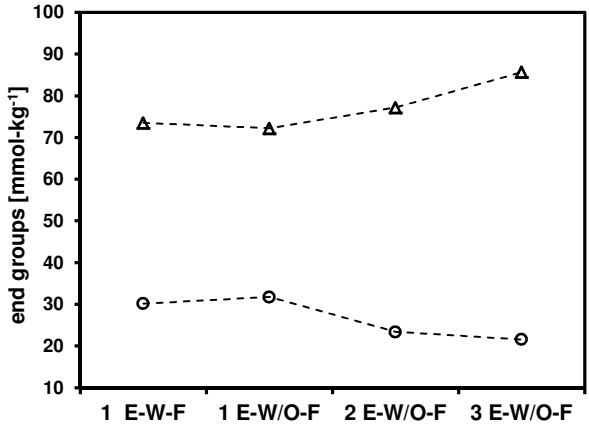

Figure 3.27: End groups analysis on monoconcentrated green masterbatches with different process conditions. (●) aminic end groups and (▲) carboxylic end groups

3.3.2.6. Monomer concentration analysis

The study of the degradation and of the thermal stability of the monoconcentrated green masterbatch was performed by evaluating the monomer concentration in the four products, related to the different production conditions, using Gas Chromatography. In Figure 3.28 the monomer concentration of the four monoconcentrated green masterbatches at different residence time in the rheometer at high temperature (260 °C) are summarized. Regarding the masterbatch as produced in chips form, the monomer concentration is reduced by removing the filter and by increasing the number of extrusions. The products are more stable because probably the monomer was removed during the cooling step in the water batch after extrusion. On the contrary, increasing the residence time at high temperature, after 23 minutes, the products underwent to prolonged thermo-mechanical process, and thus show an higher monomer formation compare to the standard monoconcentrated green masterbatch. Concluding, the production with higher specific mechanical energy stabilizes the monoconcentrated green

masterbatch but, after a long residence time at high temperature, it seems to be more sensitive to thermo-oxidative degradation.

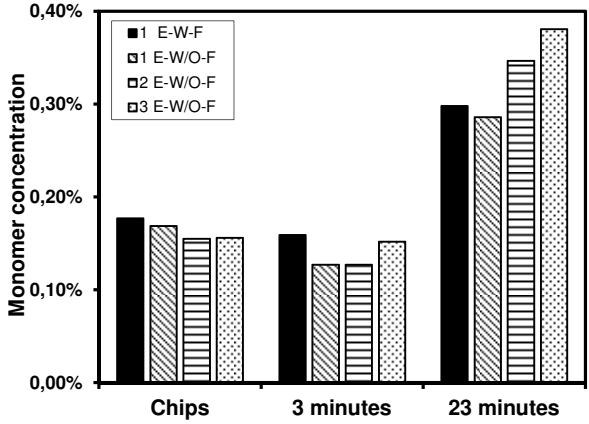

Figure 3.28: Monomer concentration of the monoconcentrated green masterbatches at different residence time in the rheometer

3.3.2.7. DSC and Crystallization kinetics analysis

Table 3.11 shows the thermal properties of the neat PA6 and of the standard monoconcentrated green masterbatch (1 E-W-F), obtained from DSC test. The halogenated copper phthalocyanine green acts as an heterogeneous nucleus of crystallization, increasing the crystallization peak temperature, but it hinders the mobility of polymer chains that results in a reduction of total crystalline phase.

	1st Heating			Cooling		2nd Heating		
Sample	T_m [°C]	ΔH_m [J/g]	X_c [%]	T_c [°C]	ΔH_c [J/g]	T_g [°C]	T_m [°C]	ΔH_m [J/g]
AQ24401	226	86	45	159	59	55	221	58
Mono PG7	224	51	36	190	51	54	221	52

Table 3.11: Thermal properties of neat PA6 and monoconcentrated green masterbatch from DSC analysis

In Figure 3.29, DSC curves at five cooling rates for the monoconcentrated green masterbatch produced by one extrusion without filtration system are reported. Reducing the cooling rate the crystallization peak temperature is shifted to higher value, because of longer time available for the polymer chains to move and to form crystallites. At low cooling rate the crystallization peak becomes larger and starts to split into two contribution, α and γ phases [160], but, differently to the monoconcentrated blue masterbatch, this phenomenon is less pronounced. The α phase is the most thermodynamically stable crystalline form, it could be obtained under the slow cooling condition and it is related to the small shoulder peak detectable at higher temperature in Figure 3.29. Moreover, the more pronounced peak at lower temperature is referred to the γ phase, that is obtained under fast cooling rate.

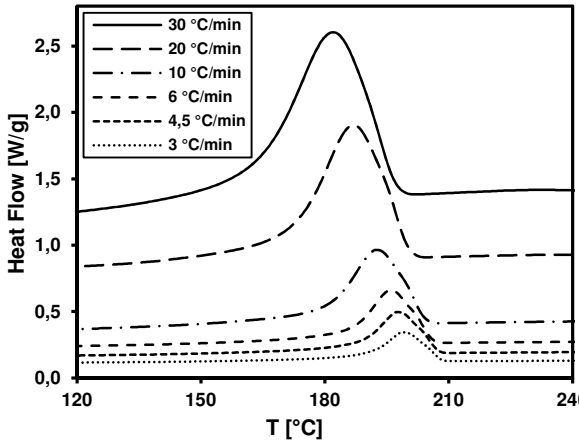

Figure 3.29: DSC Cooling scan for monoconcentrated green masterbatch at five different cooling rates

The Arrhenius plot of the crystallization kinetics analysis on the PA6 and on the monoconcentrated green masterbatch extruded one and two times is reported in Figure 3.30. The presence of the green phthalocyanine pigments in the polyamide 6 determines an increment of the Arrhenius curve slope that means an increase of the crystallization activation energy. Moreover, the second extrusion produces a further

slope increase, because a better pigment dispersions increase the heterogeneous nucleation during cooling.

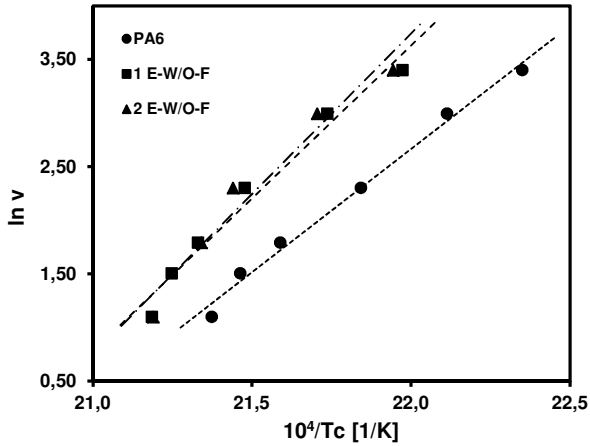

Figure 3.30: Arrhenius-type plot for PA6 and monoconcentrated green masterbatches produced in two different conditions (1 E-W/O-F and 2 E-W/O-F)

The crystallization activation energy values for the polyamide 6 and for the monoconcentrated green masterbatches obtained with one and two extrusions were calculated from the slope of the Arrhenius curves [186], and reported in Table 3.12.

As for the monoconcentrated blue masterbatches, the ΔE_{act} is negative because the transition from melt to crystalline state is an endothermic phenomenon. The monoconcentrated green masterbatch shows higher magnitude of activation energy compared to the neat PA6 and this is related to the higher energy required to the macromolecules motion during crystallization [160, 188]. This is due to the hindering effect played by the nanocolorant on the polymer chain.

From Table 3.12, it can be notice that the activation energy of crystallization is increased with the green color pigment addition and a further enhancement was registered after the second thermo-mechanical process. This can be explained by the fact that the second extrusion improves the pigment dispersion in the polymer

matrix, this results in a larger surface area in contact with the polymer. In these conditions, the heterogeneous nucleation can be increased.

Sample	ΔE_{act} [kJ/mol]
PA6	-191 ± 8
Mono PG7 - 1 E-W/O-F	-237 ± 14
Mono PG7 - 2 E-W/O-F	-249 ± 16

Table 3.12: Crystallization activation energy of neat PA6 and green monoconcentrated masterbatches at different processing conditions

3.3.3. VIOLET MONOCONCENTRATED MASTERBATCH

3.3.3.1. Filter-Test measurements

The monoconcentrated violet masterbatch was identified, from the preliminarily selection, ad one of the most critical pigment in terms of clogging power. In order to reduce its tendency to clog the filtration system during the production and during the more sensible melt spinning process, it was produced in four different conditions and tested by Filter-Test analysis.

In Figure 3.31 the pressure curves of the four monoconcentrated violet masterbatches are reported. This masterbatch is characterized by a different second region with a different behaviour compared to the previous monoconcentrated masterbatches. In fact, there is not a typical marked pressure increase when the pigment starts to reach the filter and the subsequent slope reduction that is typical for phthalocyanine pigments. The pressure continues to increase without showing the pressure plateau. This behavior is very problematic, because it is difficult to predict and to control during the industrial process. In the third region, the final pressure drop, due to the flowing of neat PA6, is less pronounced compared to the other pigments taken into account.

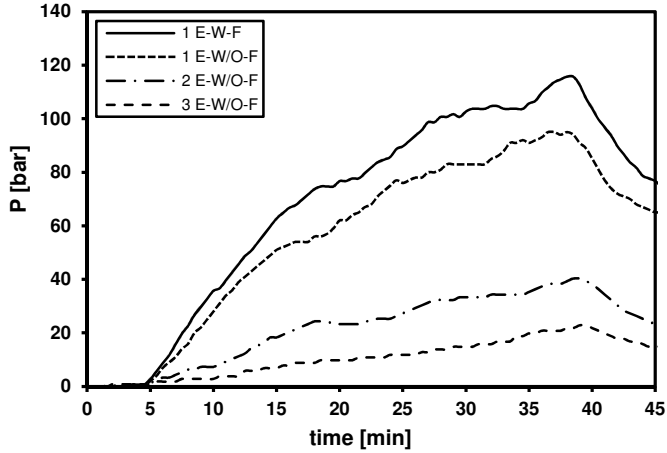

Figure 3.31: Representative Filter-Test curves of monoconcentrated violet masterbatches

In Figure 3.32 and in Table 3.13 the mean values of FPV and FPVII for each processing conditions are summarized. The filtration process shows a negative effect in terms of clogging power because the monoconcentrated violet masterbatch, produced without filter, is characterized by significant lower FPV and FPVII values. For this reasons, the industrial filtration must be removed from the industrial layout of these products. Increasing the number of extrusions and so the specific mechanical energy applied to the system during production, the clogging power of the masterbatch was markedly reduced, and was therefore decreased the aggregation tendency of the violet color pigment. For instance, with the third extrusion it is possible to reduce the FPV of about 82% compared to the monoconcentrated violet masterbatch produced in the standard way. The change of the production process conditions does not alter the behaviour of the clogging phenomenon, but only reduces the aggregates dimension. This is demonstrated by the relative variation

between FPV and FPVII, that remains fairly constant for all the tested samples (around 45%).

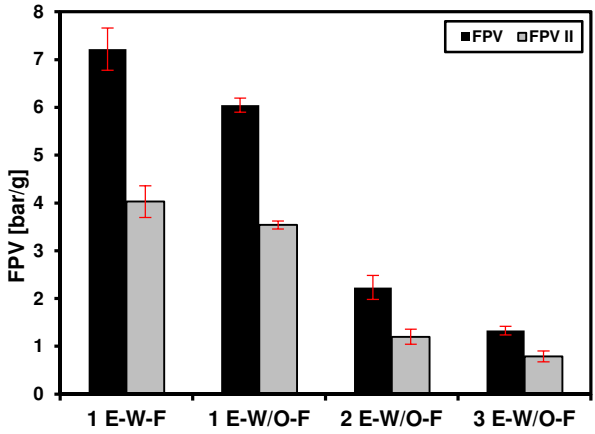

Figure 3.32: FPV and FPVII values of monoconcentrated violet masterbatches with different processing conditions

Mono PV23	FPV	FPV II	Δ FPV
1 E-W-F	7,219 ± 0,444	4,028 ± 0,331	-44%
1 E-W/O-F	6,048 ± 0,145	3,540 ± 0,085	-41%
2 E-W/O-F	2,231 ± 0,251	1,200 ± 0,155	-46%
3 E-W/O-F	1,329 ± 0,089	0,788 ± 0,115	-41%

Table 3.13: FPV and FPVII values of monoconcentrated violet masterbatches with different processing conditions

3.3.3.2. Color Strength measurements

The Relative Color Strength of the four monoconcentrated violet masterbatches, obtained using different specific mechanical energy values, taking the 1 E-W-F sample as a reference, are summarized in the Figure 3.33.

It can be noticed that the filtration process slightly reduces the RCS of the masterbatch, but the second and the third extrusions leads to an important and a positive effect on the product tinting strength. This is due to the better pigment dispersion in the polymer matrix due to the higher energy involved in the process. This consideration is in accordance with the results obtained through Filter-Test. The third extrusion allows to increase the Relative Color Strength of the monoconcentrated violet masterbatch obtained with one extrusion without filtration (about 20%). Economically speaking, this improvement of RCS leads to a reduction of production cost and to a higher masterbatch stability.

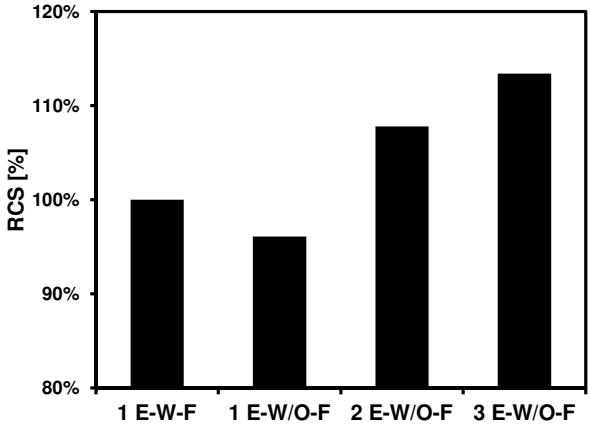

Figure 3.33: Relative Color Strength (RCS) of monoconcentrated violet masterbatches prepared with different processing parameters

3.3.3.3. Rheological measurements

Figure 3.34 shows the rheological curves of the monoconcentrated violet masterbatch and of the neat polyamide after 3 and 23 minutes of residence time at 260 °C in the rheometer. The dioxazine violet pigment produces an important improvement of the apparent viscosity of the polyamide 6 at low shear rate because

of the reduction of the polymer chain mobility due to the hindering effect promoted by the pigment aggregates into the matrix. The rheological curve of the monoconcentrated violet masterbatch after a residence time of 23 minutes at high temperature is shifted at lower apparent viscosity value. This is due to the thermo-oxidative degradation.

Regarding PA6, as well described in Paragraph 3.3.1.3, its viscosity is increased after 23 minutes of residence time, at shear rate higher than 1000 s^{-1}, because of the post-condensation reaction that occurs inside the rheometer [94, 99, 100].

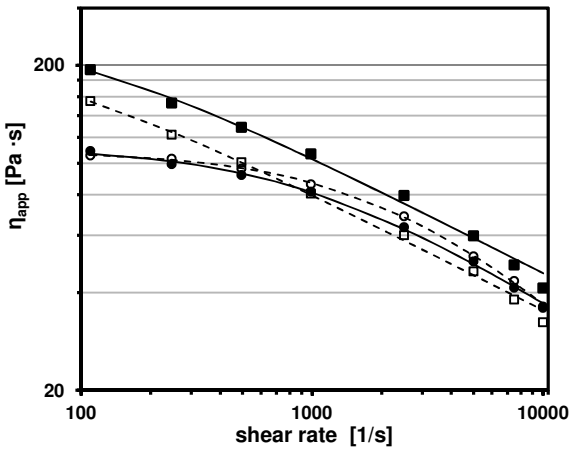

Figure 3.34: Rheological curves of neat PA6 matrix with a residence time of (●) 3 minutes and of (○) 23 minutes, and rheological curves of 1 E-W/O-F monoconcentrated violet masterbatch with a residence time of (■) 3 minutes and (□) 23 minutes.

The viscosity value at zero shear rate, obtained from interpolation of the rheological curves through the Cross equation, are reported in the Figure 3.35. The filtration process seems to play a negative effect on the system viscosity. In fact, the masterbatch produced without filter shows an higher viscosity. This is probably due to the elevated shear stresses, developed into the filtration system during the production, that promote degradative phenomena in the matrix. Contrary to the

color masterbatches based on phthalocyanine pigment, the monoconcentrated violet masterbatch shows a slight increment in zero shear rate viscosity increasing the number of extrusions. This is probably due to the important reduction of the pigment aggregate dimension.

As explained by Cassagnau [185], better distributed aggregates are more able to link the macromolecules within the aggregates, increasing the chain blocking effect in the polymer matrix. Once again, an increase of the compounding time lead to a systematic reduction of the zero shear rate viscosity values, because of the thermo-oxidative degradation of the matrix.

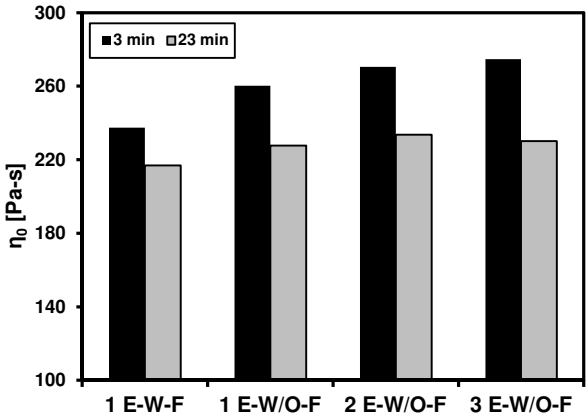

Figure 3.35: Zero shear viscosity values of the different monoconcentrated violet masterbatches processed at 3 and 23 minutes

The value of zero shear rate viscosity, the apparent viscosity al 1000 s^{-1} and the C parameter obtained from the fitting of the rheological curves through the Cross equation are reported in Table 3.14. It can be noticed that the C parameter, proportional to the bonding energy between the particles under shear flow, related to the rheological curve after 3 minutes of residence time is reduced with the specific mechanical energy involved in the production process. This is due to the higher degree of pigment disagglomeration achieved with prolonged extrusions, and it is in

accordance with the Filter-Test analysis. The correlation between FPV values obtained from Filter-Tests and the C parameter of the Cross model is shown in Figure 3.36 and, as reported in literature [36], they are directly proportional. The clogging power of the monoconcentrated violet masterbatch is reduced with the number of extrusions and consequently even the C coefficient and the FPV value are reduced.

Mono PV23	Residence time	η_0	C	η (1000 s^{-1})
1 E-W-F	3 min	**237**	0,0156	**94**
	23 min	**217**	0,0137	**78**
1 E-W/O-F	3 min	**260**	0,0119	**107**
	23 min	**228**	0,0174	**81**
2 E-W/O-F	3 min	**271**	0,0095	**113**
	23 min	**234**	0,0204	**86**
3 E-W/O-F	3 min	**275**	0,0086	**111**
	23 min	**230**	0,0185	**87**

Table 3.14: Results of rheological measurements on monoconcentrated violet masterbatches with the fitting parameters according to Cross Equation

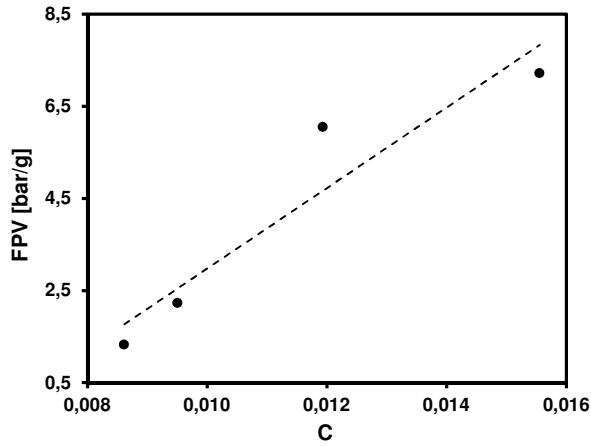

Figure 3.36: Correlation between FPV and C parameters of monoconcentrated violet masterbatches prepared with different processing conditions

3.3.3.4. Viscosity analysis

Figure 3.37 shows reduced and inherent viscosity curves of the monoconcentrated violet masterbatch, obtained from the relative viscosity values of the solution polymer. At zero concentration they converge into the intrinsic viscosity and the values for the four samples produced by using different processing conditions are summarized in Figure 3.38.

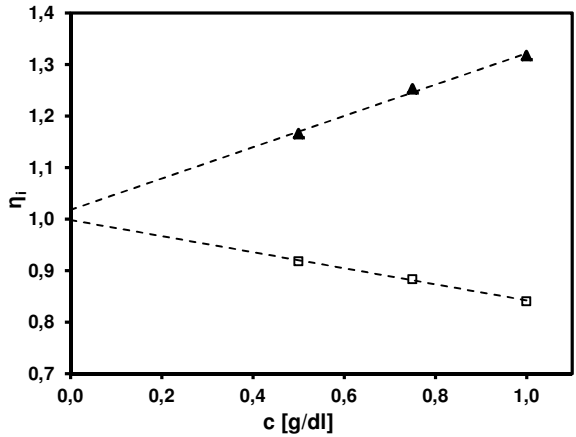

Figure 3.37: Intrinsic viscosity analysis of 1 Extrusion W/O-F monoconcentrated violet masterbatch. (▲) Reduced viscosity and (□) inherent viscosity

The intrinsic viscosity of the monoconcentrated violet masterbatch increases removing the filtration system, and it increases with the second and the third extrusion (Figure 3.38). These results are in accordance with the rheological measurements and can be due to the post condensation reaction that occurred during the production in the monoconcentrated violet masterbatch.

Considering that η_i values mainly depend on the molecular weight distribution within the polyamide matrix, the experienced increase of intrinsic viscosity values

for repeated extrusions can be explained considering the post condensation reaction that occurred in the matrix during the production of the monoconcentrated violet masterbatch. It is also possible that the presence of the filler could increase the kinetics of the post condensation reaction.

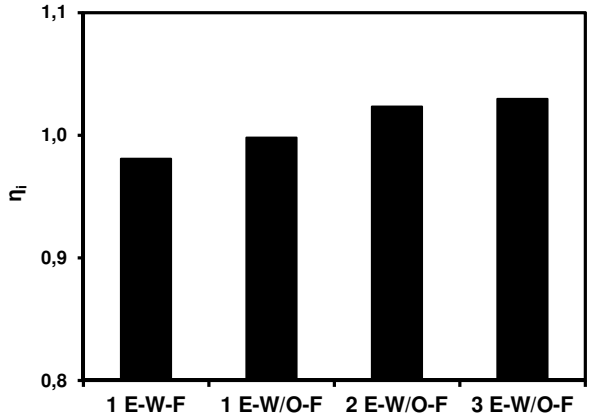

Figure 3.38: Intrinsic viscosity values of monoconcentrated violet masterbatch chips prepared with different processing conditions

3.3.3.5. End groups determination

The number of carboxylic and aminic terminal functionalities of polyamide macromolecules, measured by end groups analysis, are shown in Figure 3.39.
According to the rheological and relative viscosity measurements the carboxylic and aminic end groups are slightly reduced by removing the filtration system and by increasing the number of extrusions. This means that a post-condensation reaction take place during the production. Concluding, re-processing of the monoconcentrated violet masterbatch allows to improve pigments dispersion and to promote the kinetics of post condensation reaction within the matrix.

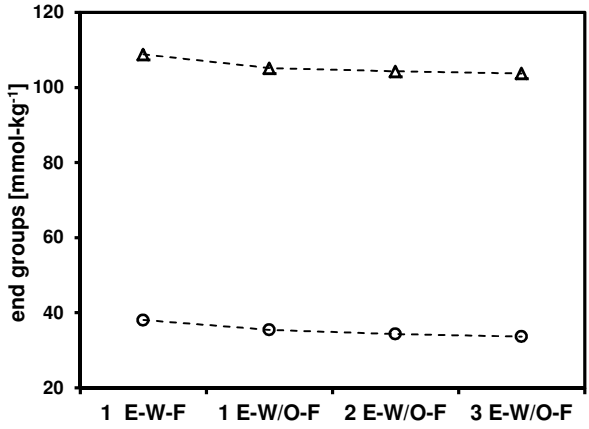

Figure 3.39: End groups analysis on monoconcentrated violet masterbatches with different process conditions. (●) aminic end groups and (▲) carboxylic end groups

3.3.3.6. Monomer concentration analysis

Gas Chromatography analysis was performed on the monoconcentrated violet masterbatches produced in four different process conditions, in order to evaluate their monomer concentration. The concentration of caprolactame in the monoconcentrated masterbatches is an important parameter that allows to evaluate the degradation phenomena occurred during the production and the thermal stability of the products.

Figure 3.40 shows the monomer concentration of the monoconcentrated violet masterbatches, obtained by using different process conditions, at different residence times in the rheometer and at elevated temperatures (260 °C). The filtration system has a negative effect on the monomer formation, in fact the monoconcentrated violet masterbatches produced without filter shows a lower monomer concentration after the production. This is probably due to the polymer flow stagnation induced by filters during production, that promoted thermo-oxidative degradation. After 23 minutes of residence time in the rheometer the monomer concentration in the

masterbatches is reduced. It can be concluded that the subsequent thermo-mechanical process stabilized the monoconcentrated violet masterbatch.

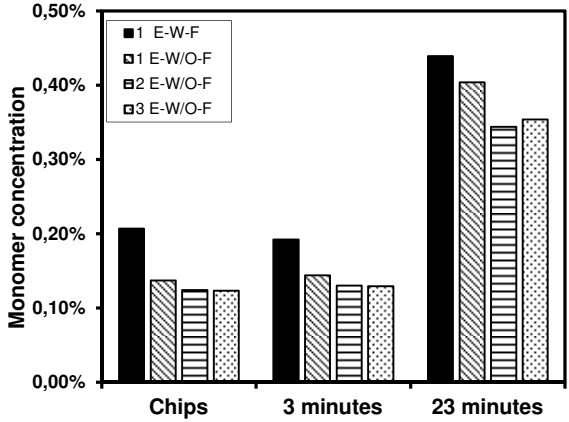

Figure 3.40: Monomer concentration of the monoconcentrated violet masterbatches at different residence times in the rheometer

3.3.3.7. DSC and Crystallization kinetics analysis

The thermal properties of the neat polyamide 6 and the monoconcentrated violet masterbatch, obtained by 1 E-W-F process, are summarized in Table 3.15.

As for the other organic color pigments, the dioxazine violet increases the crystallization peak temperature of the polyamide because it acts like an heterogeneous nucleus of crystallization. Hindering the mobility of the macromolecules, the violet pigment produces a reduction of the crystalline phase.

	1st Heating			Cooling		2nd Heating		
Sample	T_m [°C]	ΔH_m [J/g]	X_c [%]	T_c [°C]	ΔH_c [J/g]	T_g [°C]	T_m [°C]	ΔH_m [J/g]
AQ24401	226	86	45	159	59	55	221	58
Mono PV23	224	51	36	191	51	58	222	51

Table 3.15: Thermal properties of neat PA6 and monoconcentrated violet masterbatch

The DSC cooling curves of the monoconcentrated violet masterbatch produced by one extrusion without filtration at five different cooling rate are reported in the Figure 3.41. The crystallization peak temperature is shifted at higher temperature reducing the cooling rate. This is due to the longer time available for the macromolecules to crystallize. From the curve obtained at 3 °C/min of cooling rate, it is easily detectable that the crystallization peak starts to be splitted into its two contributions, α and γ phases [160]. This can be explained by the fact that the more stable α phase, related to the small shoulder of the crystallization peak, is produced under slow cooling rate. Furthermore, the other contribution is represented by the γ phase, that it is usually obtained under fast cooling rate.

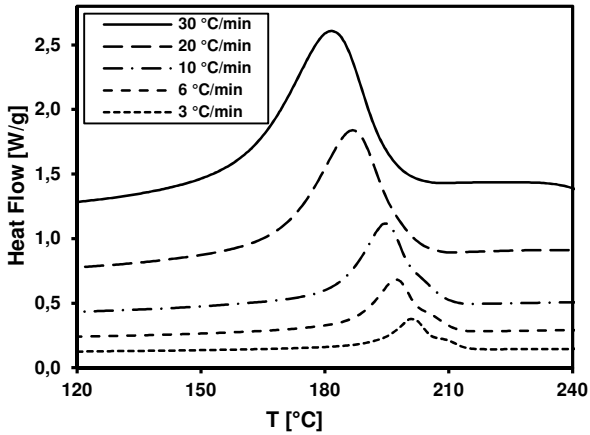

Figure 3.41: Cooling scan for monoconcentrated violet masterbatch at five different cooling rate

Figure 3.42 shows the Arrhenius curves from the crystallization analysis performed on the polymer matrix and on the monoconcentrated violet masterbatch obtained by one and two extrusions. The increment of the curve slope with the introduction of dioxazine violet pigment into PA6 is easily detectable. Regarding the process condition, increasing the specific mechanical energy involved during production, a slight slope increase can be registered.

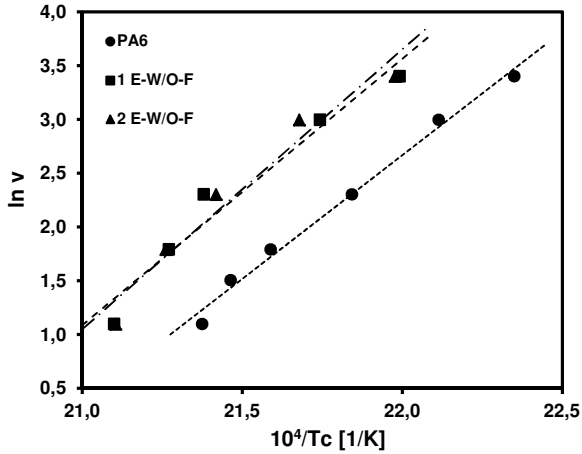

Figure 3.42: Arrhenius-type plot for PA6 and monoconcentrated violet masterbatches produced in two different conditions (1 E-W/O-F and 2 E-W/O-F)

In Table 3.16 the crystallization activation energies, calculated from the Arrhenius plot [186], for the PA6 and for the monoconcentrated violet masterbatches are summarized. The presence of the dioxazine violet pigment increases the activation energy because it acts like an heterogeneous nucleus of crystallization, but the nanocolorants dispersion increase the energy required for the polymer chain motion [160, 188].

Improving the pigment dispersion in the polymer matrix by a second extrusion, the curve slope is slightly more increase. This confirms the conclusions obtained from Filter-Test and Color Strength results.

Sample	ΔE_{act} [kJ/mol]
PA6	-191 ± 8
Mono PV23 - 1 E-W/O-F	-206 ± 19
Mono PV23 - 2 E-W/O-F	-216 ± 19

Table 3.16: Crystallization activation energy of neat PA6 and of monoconcentrated violet masterbatches from the Arrhenius plot of DSC curves at different cooling rates

3.3.4. BLACK MONOCONCENTRATED MASTERBATCH

The monoconcentrated black masterbatch was taken as a reference sample, in order to explain the behavior of the other masterbatches that were found to be not markedly influenced by the production processing conditions. The increase of the specific mechanical energy during the production did not lead to a clogging power reduction and color strength increase. The properties of the monoconcentrated black masterbatch did not substantially change passing from one to two extrusion process and, for these reasons, a third thermo-mechanical treatment was not performed. The same behavior was found for the white (PW7), brown (PBr24), red (PR101) and red (PR149) monoconcentrated masterbatches.

3.3.4.1. Filter-Test measurements

The monoconcentrated black masterbatch was produced by using different processing conditions in order to reduce its clogging power and tested by Filter-Test analysis. Figure 3.43 shows the representative pressure curves of the monoconcentrated black masterbatch related to the three different production processes. As for the previous masterbatches described, this product shows three distinct regions in the pressure curves. In the first zone the pressure is constant due to the neat polyamide 6 flow. The second region is characterized by an important pressure increase, when the pigment reaches the filter, and after it by a curve slope reduction. In the third region a marked pressure drop is recorded. This means that the black pigment agglomerates, that generate the filter clogging during test, were unstable and were broken down by the polymer flow.

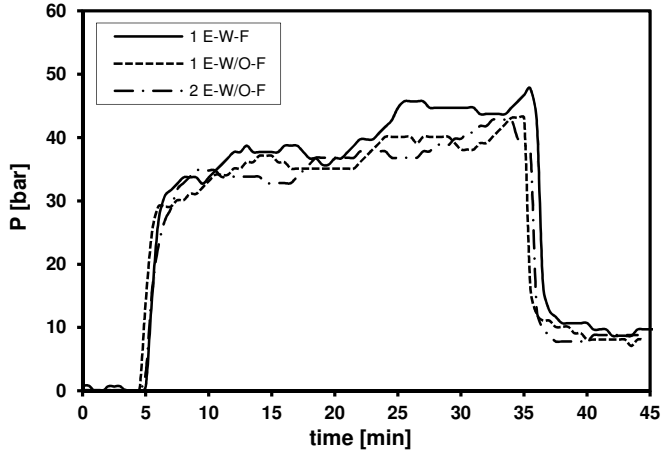

Figure 3.43: Representative Filter-Test curves of monoconcentrated black masterbatches

The mean values of FPV and FPVII for each processing condition, calculated from the pressure curves, are reported in Figure 3.44 and in Table 3.17. The filtration process seems to be useless regarding the clogging power of the masterbatch and even the second extrusion does not produce any important variation in the product filtration properties. In fact, considering the standard deviation of the Filter-Test measurements, their results are similar. The industrial filtration results to have only a negative effect in terms of production output and in terms of waste production. Generally speaking, it reduces the productivity of the plant and, for this reason, it can be removed from the industrial layout. In this case, increasing the specific mechanical energy in the process, the pigment dispersion does not change, and the process based on one extrusion without filtration is sufficient in order to obtain an optimal pigment distribution.

The relative difference between the FPV and FPVII values, reported in the Table 3.17, remains fairly constant for all three processes (around 76%). This means that the different conditions do not alter the clogging phenomenon behavior. These results suggest that the filter clogging is due to the presence of unstable agglomerates and the filter can be easily cleaned by flowing neat polymer matrix.

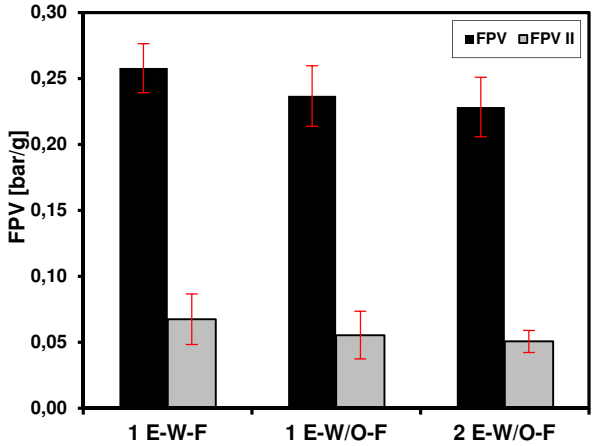

Figure 3.44: FPV and FPVII values of monoconcentrated black masterbatches with different processing conditions

Mono PBk7	FPV	FPV II	Δ FPV
1 E-W-F	0,258 ± 0,019	0,068 ± 0,019	-74%
1 E-W/O-F	0,237 ± 0,023	0,056 ± 0,018	-77%
2 E-W/O-F	0,229 ± 0,023	0,051 ± 0,008	-78%

Table 3.17: FPV and FPVII values of monoconcentrated masterbatches prepared with different processing conditions

3.3.4.2. Color Strength measurements

The relative color strength values of the three monoconcentrated black masterbatches are reported in Figure 3.45, taking the 1 E-W-F compound as reference. According to the Filter-Test results, the second extrusion does not improve the pigment dispersion in the polymer matrix because the relative color strength of the monoconcentrated black masterbatch are fairly constant changing the process conditions. Also the RCS analysis confirmed that the filtration system is an unuseful step in the industrial layout.

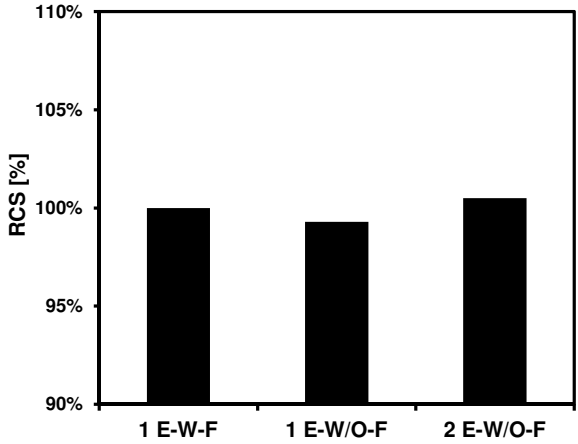

Figure 3.45: Relative Color Strength (RCS) of monoconcentrated black masterbatches prepared with different processing conditions

3.3.4.3. Rheological measurements

The rheological curves of the monoconcentrated black masterbatch and of the neat polyamide 6, related to two different residence times (3 and 23 minutes) into rheometer at 260°C, are reported in Figure 3.46.

Carbon black pigment producs a consistent increase of apparent viscosity, in fact the apparent viscosity of monoconcentrated masterbatch are shifted to higher values compared to the curve of the neat polyamide 6. This is due to the hindering effect of the pigments that reduce the mobility of the macromolecules and their alignment during the polymer flow through rheometer capillary. The effect of the carbon black is more pronounced compared to the previous organic pigments and even to the other pigments analyzed in this work. This can be explained by the fact that carbon black shows higher specific surface area values, therefore carbon black nanoparticles present a higher interaction with the polymer matrix. Moreover, the ratio between the aggregates and primary particles dimension is higher compared to the other pigments and it means a higher number of particles composing the aggregate. As

explained to Cassagnau [185], this morphological feature allows to blind the polymer chains into the aggregates/agglomerates, reducing the mobility and, therefore, the viscosity of the compound.

The monoconcentrated black masterbatch shows a good thermal stability, and the rheological curve, after a prolonged thermal treatment, does not substantially change with respect to the standard curve.

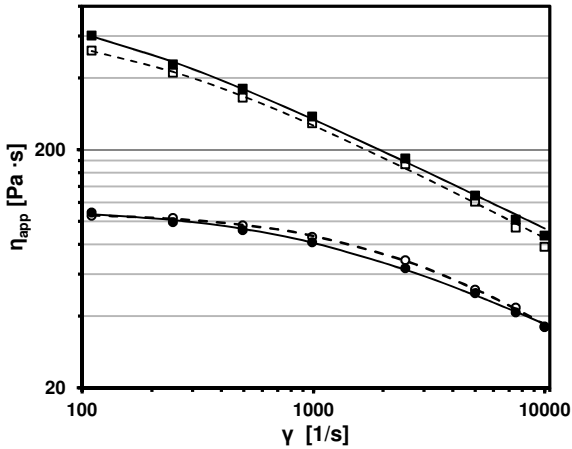

Figure 3.46: Rheological curves of neat PA6 matrix with a residence time of (●) 3 minutes and of (○) 23 minutes, and rheological curves of 1 E-W/O-F monoconcentrated black masterbatch with a residence time of (■) 3 minutes and (□) 23 minutes.

3.3.4.4. End groups determination

Figure 3.47 shows the variation of the terminal functionalities for the monoconcentrated black masterbatch and for the neat polyamide 6, from 3 to 23 minutes of residence time, in order to evaluate the thermal stability of the product.

It is easy to notice that the end groups of polyamide 6 after a prolonged thermal treatment are reduced, because a post condensation reaction that occurred in the rheometer at high temperature, in accordance with the rheology measurements. Regarding monoconcentrated black masterbatch, the terminal functionalities did not change after more 20 minutes of residence time. Probably the effect of post

condensation on the polymer matrix is neutralized by a little thermo-oxidative degradation.

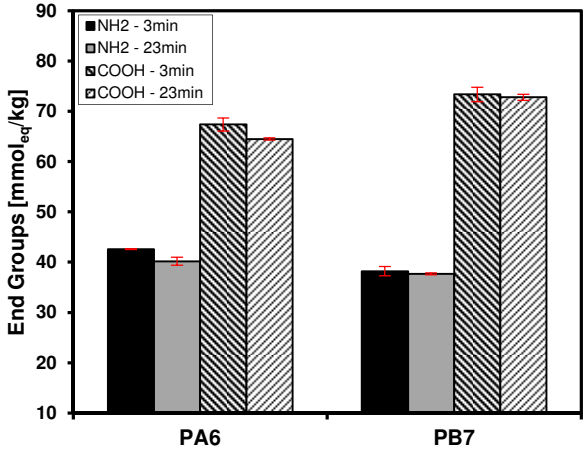

Figure 3.47: End groups analysis on neat PA6 and on monoconcentrated black masterbatches at a residence time of 3 and 23 minutes

3.3.4.5. DSC analysis

In Table 3.18 the thermal properties of the neat polyamide 6 and of the monoconcentrated black masterbatch, obtained by 1 E-W-F process, are reported. Accordingly to the other pigments, the presence of carbon black into the polyamide 6 matrix produces an increment of the crystallization peak temperature. This is due to the nucleating effect played by this color pigment. Moreover, it does not alter the amount of crystallinity in the polymer, for the first heating and neither in the second heating ramp.

	1st Heating			Cooling		2nd Heating			
Sample	T_m [°C]	ΔH_m [J/g]	X_c [%]	T_c [°C]	ΔH_c [J/g]	T_g [°C]	T_m [°C]	ΔH_m [J/g]	X_c [%]
AQ24401	224	69	36,6	182	73	55	221	74	38,9
Mono PBk7	226	70	36,6	190	72	52	222	74	38,9

Table 3.18: Results of DSC tests on neat PA6 and monoconcentrated black masterbatch

3.3.5. CONCLUSIONS ON PRODUCTION PROCESS OPTIMIZATION

In order to have a general overview on the experimental results obtained in the production process optimization analysis, in Figure 3.48 the FPV values of the six monoconcentrated masterbatches, that showed higher FPV in the preliminary selection, are summarized. The relative color strength (RCS) values of the same monoconcentrated masterbatches, prepared by using different production conditions, are reported in Figure 3.49.

Brown (PBr24), black (PBk7) and red (PR149) monoconcentrated masterbatches do not change their clogging power and the color strength applying different specific mechanical energy values to the system during extrusion. This means that the standard production process is sufficient in order to obtain a good pigment distribution into the polymer matrix. On the basis of these considerations, the filtration can be removed from the industrial layout, and the new production process for these monoconcentrated masterbatches is based on one extrusion without filtration. This operation allows to reduce the production waste, to increase the productivity, and thus to reduce the costs of production.

Regarding blue (PB15:3), green (PG7) and violet (PV23) monoconcentrated masterbatches, they were the most problematic products because their color pigments are very difficult to be homogeneously dispersed into the polyamide carrier [35, 41, 59]. For these products, the increase of specific mechanical energy in the process leads to an important reduction of the clogging power and an increase of the tinting strength. This is due to the better pigments dispersive mixing achieved, that consistently reduces the dimension of the pigment agglomerates, leading to a lower FPV value, and increasing the surface that absorbs light. Therefore the process composed by two extrusions without filtration was found to be the best compromise between the materials properties enhancement and the production costs.

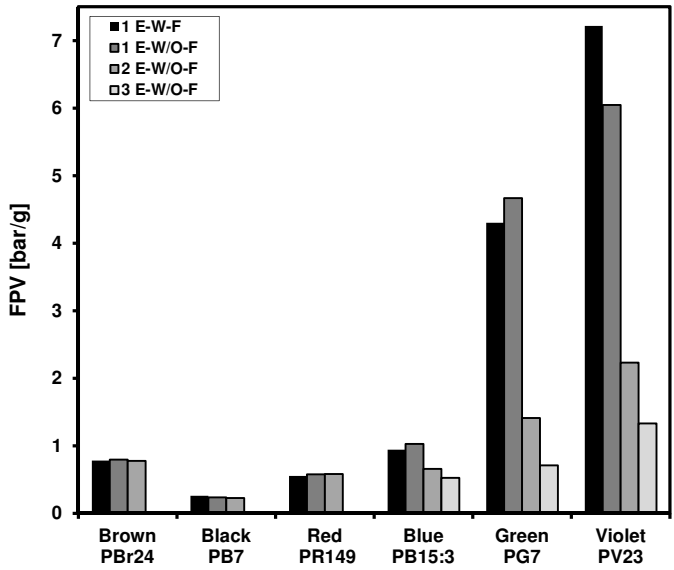

Figure 3.48: FPV values of the monoconcentrated masterbatches

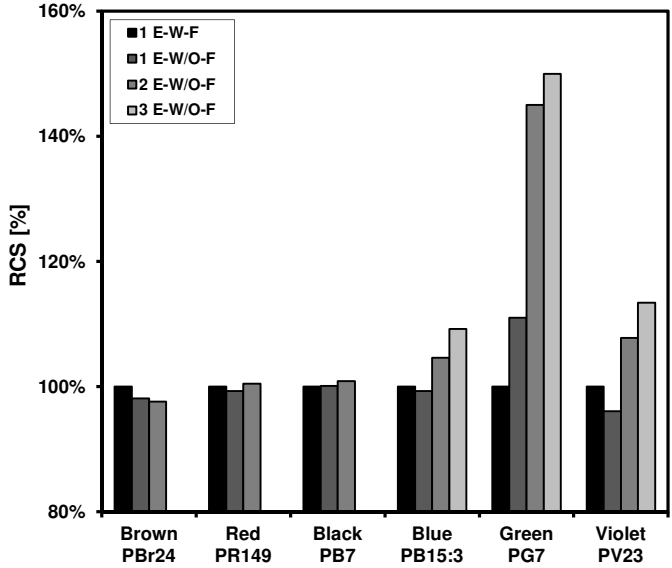

Figure 3.49: RCS values of the monoconcentrated masterbatches

3.4. CHARACTERIZATION OF COLOR MASTERBATCHES

In order to evaluate the effect of the production process optimization on the subsequent manufacturing step, a blue color masterbatch was selected because its formulation contained also the blue (PB15:3) and the violet (PV23) monoconcentrated masterbatches (see Paragraph 2.2.2). This kind of color masterbatch has the peculiarity to clog the filtration system during spinning process and therefore a frequent change of the filters is required. This obviously reduces the production output of industrial plant and reduces the stability and quality of the final product. Moreover, it can promote the drop formation in the spinneret during melt spinning and, consequently, the fibers breakage.

3.4.1. FILTER-TEST ANALYSIS

In Figure 3.50 the pressure curves of Standard Blue Masterbatch (BM-S) and Optimized Blue Masterbatch (BM-O), obtained with Filter-Test, are reported. The improvement of the pigment dispersion into the most problematic monoconcentrated masterbatches, present in the blue masterbatch formulation, allows to significantly reduce the clogging power of this product.
The extrusion employed to mix the different monoconcentrated masterbatches in the color masterbatch production has the aim to obtain a good distributive mixing, and so to obtain an homogeneous dispersion of the color pigments into the polymer matrix. For these reasons, the clogging power reduction experienced through monoconcentrated masterbatches production optimization, was transferred to the final color masterbatch, as demonstrated by Filter-Test.

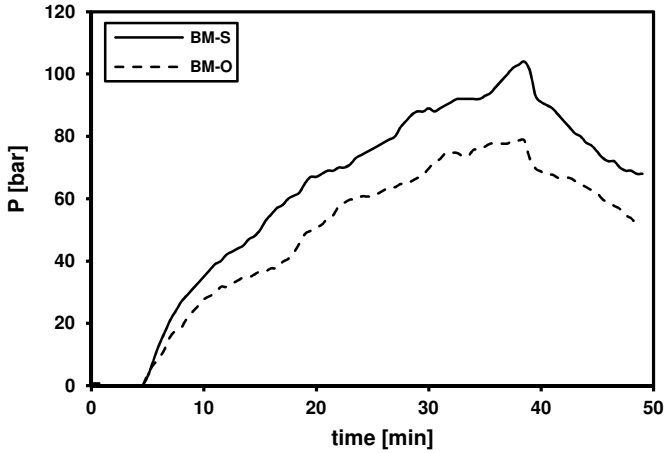

Figure 3.50: Pressure curves of Standard Blue Masterbatch (BM-S) and Optimized Blue Masterbatch (BM-O)

The FPV values of the blue color masterbatches, obtained using the standard and the optimized monoconcentrated masterbatches, are reported in Figure 3.51.

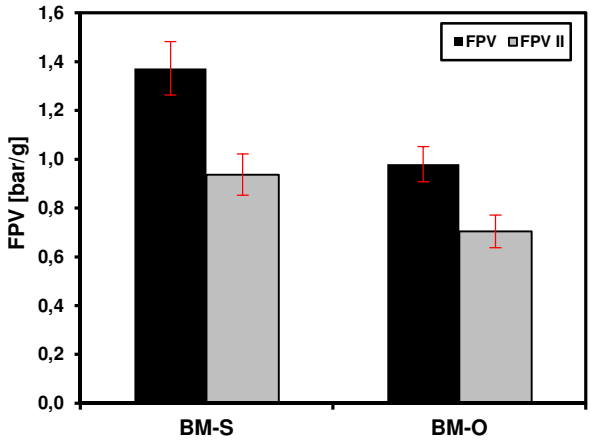

Figure 3.51: FPV and FPVII values of Standard Blue Masterbatch (BM-S) and Optimized Blue Masterbatch (BM-O)

In Table 3.19 the FPV and FPVII values are reported. The clogging power of the Blue Masterbatch is reduced of about 30%, and the difference between FPV and FPVII remains fairly constant, meaning that the physical mechanism of the filter clogging remains the same.

Once again, the reduction of the clogging tendency during the melt spinning process is very important from industrial point of view. In fact, this allows to increase the lifetime of the spinneret, reducing the stops of the machine and increasing the efficiency of the process. Moreover, this aspect is directly related to the degradation phenomenon that occurs during the thermal treatment. A reduction of clogging power leads to a reduction of the shear stresses applied to the matrix near the filter and, consequently, to a reduction of polymer degradation and drop formation under the spinneret. This leads to a lower filament breakage during spinning, increasing the productivity.

	FPV	**FPV II**	**Δ FPV**
BM-S	1,373 ± 0,110	0,937 ± 0,085	-32%
BM-O	0,980 ± 0,072	0,704 ± 0,067	-28%

Table 3.19: FPV and FPVII values of Standard Blue Masterbatch (BM-S) and Optimized Blue Masterbatch (BM-O)

3.4.2. RHEOLOGICAL MEASUREMENTS

Figure 3.52 shows the rheological curves of the Standard Blue Masterbatch at three different residence times, in order to evaluate the thermal stability of the product. The apparent viscosity of the BM-S is significantly reduced with the time at high temperature, because of the thermo-oxidative degradation that occurs into the rheometer.

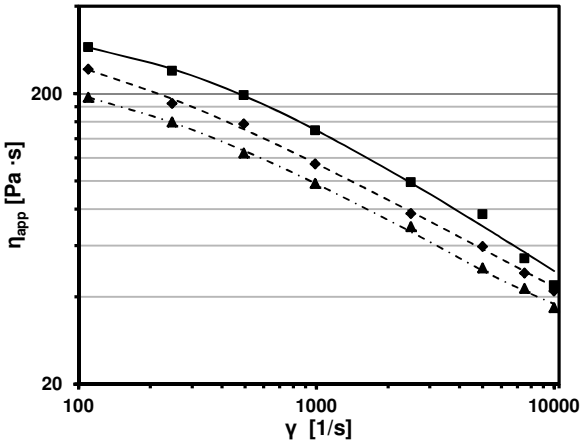

Figure 3.52: Rheological curves of Blue Masterbatch Standard (BM-S) with a residence time of (■) 3 minutes, of (◆) 13 minutes and of (▲) 23 minutes

The rheological curves of the Optimized Blue Masterbatch are reported in Figure 3.53. The curve related to 3 minutes of residence time is shifted to lower apparent viscosity values compared to that of BM-S. This is probably due to the additional thermo-mechanical processes that reduces the molecular weight of the polymer, because of thermo-oxidative degradation. Moreover, it is possible to notice that the variations of apparent viscosity with the residence time are negligible. The pigment dispersion optimization reached in the monoconcentrated masterbatches allows to

increase the thermal stability of the final color masterbatch, improving its processability.

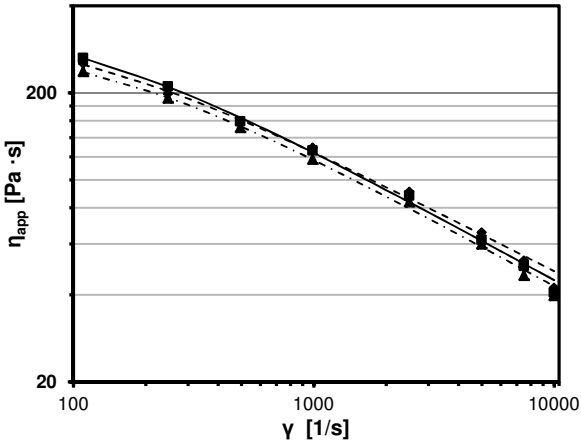

Figure 3.53: Rheological curves of Blue Masterbatch Optimized (BM-O) with a residence time of (■) 3 minutes, of (◆) 13 minutes and of (▲) 23 minutes

3.4.3. VISCOSITY ANALYSIS

The intrinsic viscosity values of the Blue Masterbatch, obtained from the relative viscosity measurements, are reported in Figure 3.54. Accordingly with the rheological measurements, the BM-S shows a reduction of intrinsic viscosity with the residence time, because of the thermal degradation reaction that occurred into the rheometer, while, on the contrary, the BM-O is thermally stable. In fact, only a slight viscosity variation can be recorded for the optimized product increasing the residence time.

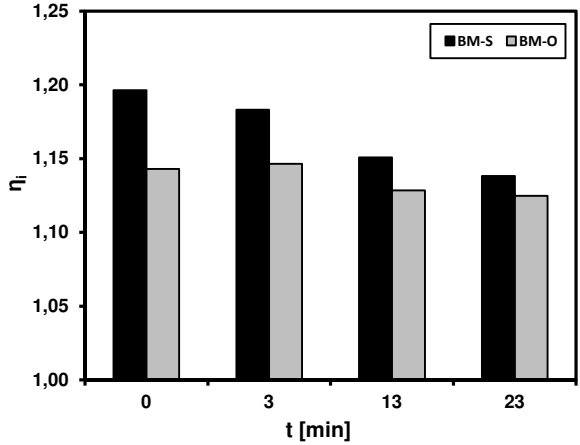

Figure 3.54: Intrinsic viscosity values of BM-S and BM-O as produced and after 3, 13 and 23 minutes of residence time at 260°C

3.4.4. END GROUPS DETERMINATION

End groups analysis, performed through titration methods, were performed on the BM-S and on BM-O in order to evaluate the thermal stability of these masterbatches. The sum of the end groups, measured on standard and optimized blue masterbatches, are reported in Figure 3.55.

For both materials, after three minutes an important end groups reduction is recorded. This is due to the post condensation reaction that characterized polyamide 6 at high temperature, when the moisture content is under the equilibrium concentration [70]. Increasing the residence time in the rheometer at 260°C, the sum of the terminal functionalities does not vary significantly for both Blue Masterbatches, but the optimized sample shows a lower reduction after thermal treatment. The pigment dispersion improvement, and the repeated extrusion steps reduces the tendency to post condensate, stabilizing the final color masterbatch.

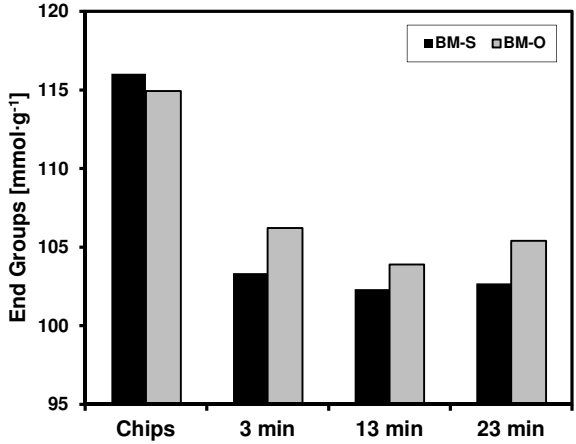

Figure 3.55: End groups variation of BM-S and of BM-O blue color masterbatches

3.4.5. MONOMER CONCENTRATION ANALYSIS

The monomer concentration of the Blue Masterbatches, produced by using the standard and the optimized processes, was evaluated through gas chromatography analysis.

In Figure 3.56 the variation of monomer concentration for BM-S and BM-O, at different residence time at 260 °C, is reported. It is easily detectable that the caprolactame concentration increases with the time because of degradation. The terminal amino groups react with the first peptide groups in the macromolecules, forming a monomer ring. This is in accordance with the intrinsic viscosity determination because the formation of monomer reduces the molecular weight of the polymer without affecting the number of the final terminal functionalities.

The concentration of caprolactame in the color masterbatches is an important parameter that allows to analyze the degradation phenomena occurred during the production and the thermal stability of the product. It directly influences the drop

formation under the spinneret during the melt spinning process and so the productivity of the industrial plant. The optimized blue masterbatch shows a systematic lower monomer concentration compared to the standard one.

Once again, the optimization of the processing parameters in the color masterbatch leads to an higher thermal degradation stability of the product.

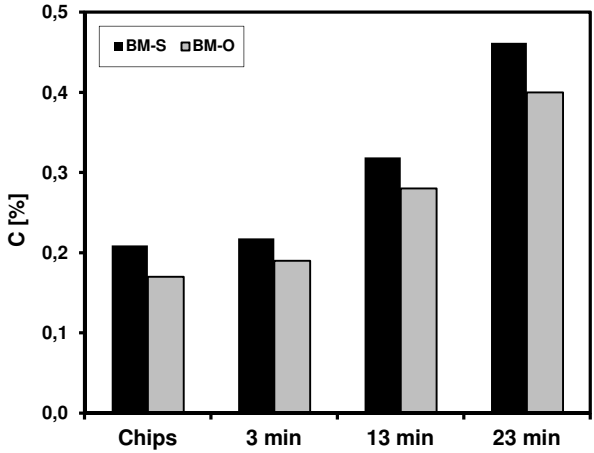

Figure 3.56: Monomer concentration of the BM-S and BM-O at different residence time in the rheometer

3.5. CHARACTERIZATION OF FIBERS

Finally, in order to evaluate the influence of the pigment dispersion on the final industrial product (i.e. colored yarns), a bulk continuous filament spinning process was performed on the industrial plant at Aquafil SpA.
The Standard and the Optimized Blue Masterbatches were used to color the related yarns by mass pigmentation process, and their coloration and mechanical properties were investigated.

3.5.1. QUASI-STATIC TENSILE TESTS ON FIBERS

In Figure 3.57 representative stress-strain curves of Standard and Optimized Blue Yarns, derived from quasi-static tensile tests, are reported, while in Table 3.20 the most important tensile properties are summarized.
It is clear that, improving the color pigment dispersion into the polyamide fibers, an important improvement of the mechanical properties can be achieved. The Optimized Blue Yarn showed a significant enhancement of Elastic Modulus (E), a slightly increase of tensile strength and a slightly reduction of the deformation at break (ε_b). The tenacity, defined as the force exerted on the specimen based on the linear density of the unstrained material [189], remained fairly constant.
The color pigments studied in this work showed an intermediate properties between micro- and nano-fillers. It is well known that the addition of high modulus fillers increases the modulus and the strength of a polymer, but in micro composites filler addition generally leads to a reduction in ductility and in impact strength, because of the stress concentrations caused by the fillers [190-197]. Improving the dispersion of nanoparticles it is possible to improve the stiffness and the strength of the pristine material, maintaining or even improving ductility, because their small size does not promote significant stress concentrations [198-201].

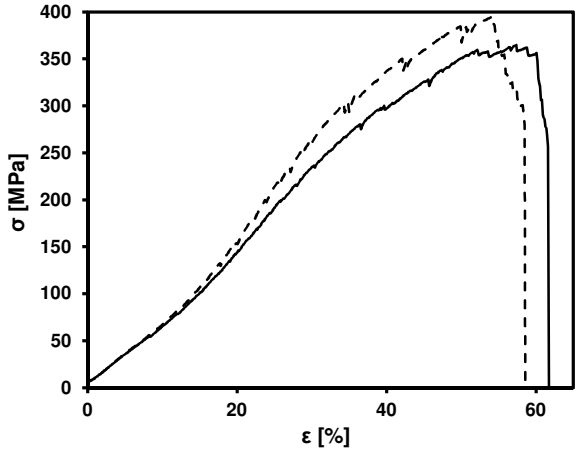

Figure 3.57: Representative Stress-Strain curves of Blue Yarn.
Standard (—) and Optimized (---)

Sample	Elastic Modulus [MPa]	Tensile Strength [MPa]	Deformation at break [%]	Tenacity [cN/tex]
BY-S	953 ± 29	369,6 ± 8,4	52,4 ± 2,1	32,4 ± 0,7
BY-O	1075 ± 18	383,9 ± 10,1	49,6 ± 2,1	32,9 ± 0,8

Table 3.20: Quasi-static tensile properties of Standard and Optimized Blue Yarn

3.5.2. MICROSTRUCTURAL CHARACTERIZATION

In Figure 3.58 a representative FT-IR spectrum of the polyamide 6, performed on the industrial yarn, is reported. Its characteristic peaks are well visible and in particular the peaks related to the α crystalline phase, at around 1200 cm^{-1}, and the peaks related to the γ crystalline phase, and the amorphous phase at around 1170 cm^{-1} [2].

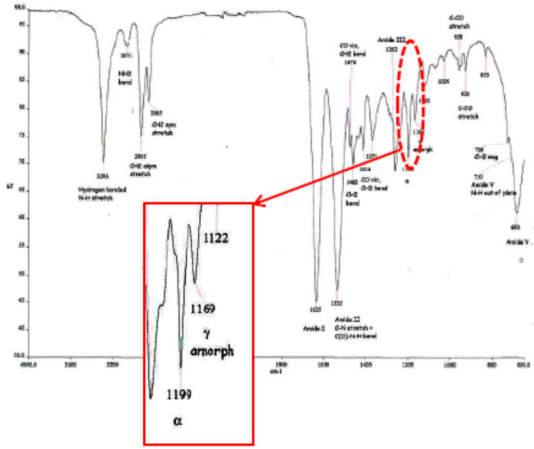

Figure 3.58: FT-IR spectrum of polyamide 6 with the characteristic peaks of α-phase and γ-phase

The results of FT-IR analysis in term of α/γ ratio for the Standard Blue Yarn and for the Optimized Blue Yarn are reported in Figure 3.59.

The yarn colored through mass pigmentation process by optimized blue masterbatch showed an increase of the α/γ ratio of about 5%. This can be associated to the pigment dispersion improvement. The activity of heterogeneous nucleus of crystallization was enhanced by the larger pigment surface in contact with the polymer, as confirmed by the kinetic crystallization analysis performed on the Blue Masterbatches. This considerations could explain even the results obtained with the

quasi-static tensile test. The higher α/γ ratio, the higher elastic modulus and the tensile strength.

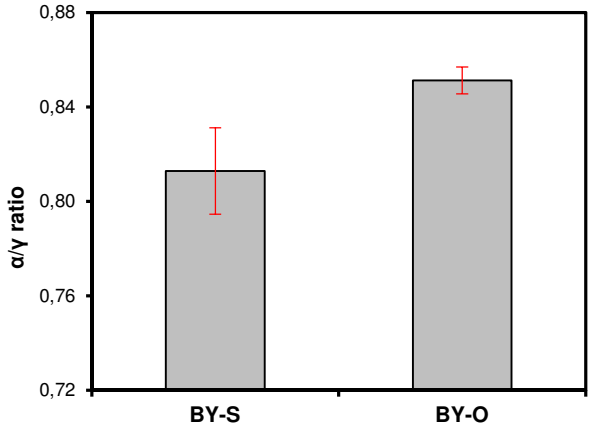

Figure 3.59: α/γ ratio of BY-S and of BY-O from FT-IR analysis

3.5.3. THERMAL-AGING RESISTANCE

An important feature of the industrial yarn used in the carpet manufacturing is the thermal aging resistance. The carpet used in residential and, in the automotive sector undergo to thermal stresses during their service life, and their durability is one of the most critical issues for the costumers.

In order to evaluate the thermal stability of the yarns, the samples were treated in the oven at 160 °C at different set of residence times (1-2-4-8-16-24-32 hours), and their morphology, mechanical and color properties were analyzed. In Figure 3.60 the effect of residence time at 160 °C on the α/γ ratio of the industrial yarn is reported.

It possible to notice that the α/γ ratio increases after the first hours of thermal treatment because of the secondary crystallization that occurs in the polyamide 6 at high temperature, while after 4 hours at 160 °C the ratio remains fairly constant. Moreover, the Optimized Blue Yarn showed higher α/γ ratio values over the entire

residence time interval, because of the pigment dispersion improvement, as explained in the previous paragraph.

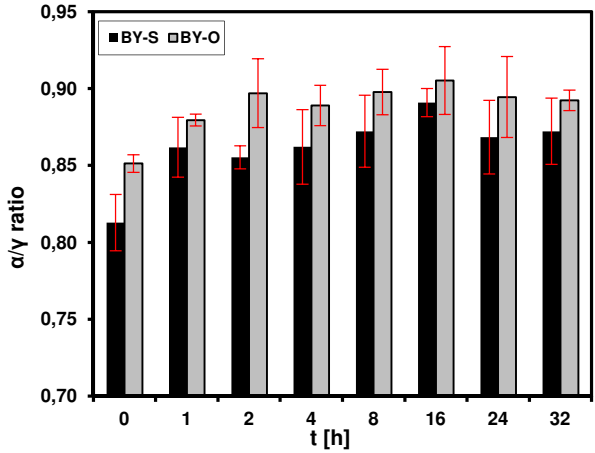

Figure 3.60: α/γ ratio of the BY-S and BY-O thermally treated at different residence times

The elastic modulus of the BY-S and BY-O thermal treated with different residence time at 160°C are reported in Figure 3.61.

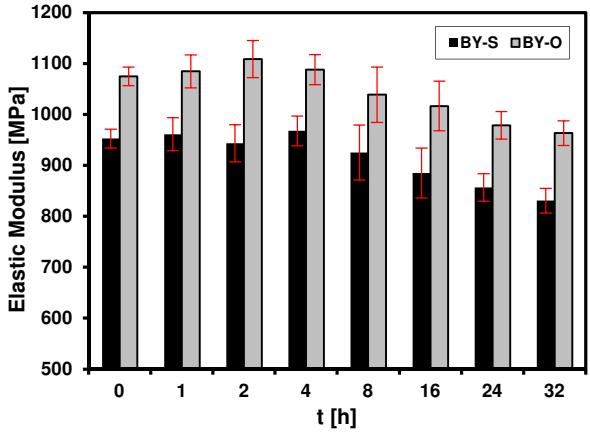

Figure 3.61: Elastic modulus of BY-S and BY-O thermally treated at different residence times

For both samples it remains fairly constant until 4 hour in the oven while after higher residence time the elastic modulus start to be reduced because of the degradation effect. For the first hours probably there is a concomitant and contrasting effects: the increase of α/γ, noticed in the FT-IR analysis and the thermo-oxidative degradation. Moreover, the yarn with the optimized pigment dispersion show better mechanical properties over the entire tested residence time interval.

The tensile strength, the deformation at break (ε_b) and the tenacity (Figure 3.62) are reduced with the exposure time at high temperature because of degradation phenomenon. In Figure 3.62 it can be seen that there are not any important differences between the tenacity of the two samples over the entire time range.

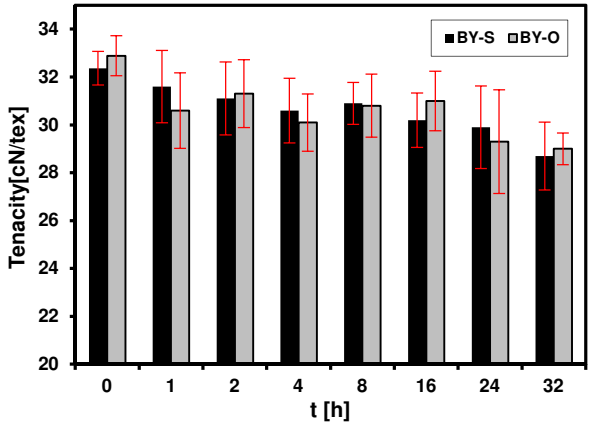

Figure 3.62: Tenacity of BY-S and BY-O thermally treated at different residence times

The mechanical properties of the Standard Blue Yarn are summarized on Table 3.21 while those of the Optimized Blue Yarn in Table 3.22.

BY-S				
Residence time [h]	Elastic Modulus [MPa]	Tensile Strength [MPa]	Deformation at break [%]	Tenacity [cN/tex]
0	953 ± 29	369,6 ± 8,4	52,4 ± 2,1	32,4 ± 0,7
1	961 ± 32	362,2 ± 17,1	47,5 ± 3,8	31,6 ± 1,5
2	943 ± 24	354,9 ± 15,9	47,1 ± 4,2	31,1 ± 1,5
4	968 ± 32	351,0 ± 16,3	44,2 ± 3,6	30,6 ± 1,3
8	925 ± 20	354,4 ± 8,8	42,8 ± 1,5	30,9 ± 0,9
16	885 ± 21	345,9 ± 13,2	42,2 ± 3,8	30,2 ± 1,1
24	857 ± 33	341,6 ± 15,8	39,6 ± 3,1	29,9 ± 1,7
32	831 ± 17	327,1 ± 16,5	38,3 ± 3,6	28,7 ± 1,4

Table 3.21: Tensile properties of BY-S at different residence times

BY-O				
Residence time [h]	Elastic Modulus [MPa]	Tensile Strength [MPa]	Deformation at break [%]	Tenacity [cN/tex]
0	1075 ± 18	383,9 ± 10,1	49,6 ± 2,1	32,9 ± 0,8
1	1085 ± 32	367,2 ± 17,7	41,1 ± 2,2	30,6 ± 1,6
2	1108 ± 37	365,4 ± 16,2	40,7 ± 3,0	31,3 ± 1,4
4	1088 ± 29	359,2 ± 15,7	39,7 ± 2,6	30,1 ± 1,2
8	1039 ± 54	359,6 ± 13,5	38,3 ± 3,7	30,8 ± 1,3
16	1017 ± 49	360,5 ± 14,4	38,2 ± 3,9	31,0 ± 1,2
24	979 ± 27	347,5 ± 14,2	35,0 ± 3,1	29,3 ± 2,2
32	963 ± 24	339,4 ± 6,8	35,8 ± 1,3	29,0 ± 0,7

Table 3.22: Tensile properties of BY-O at different residence times

The thermal aging resistance was evaluated by measuring the color variation with the exposure time at high temperature, taken the yarn just produced as a reference, and the results are reported in Figure 3.62.

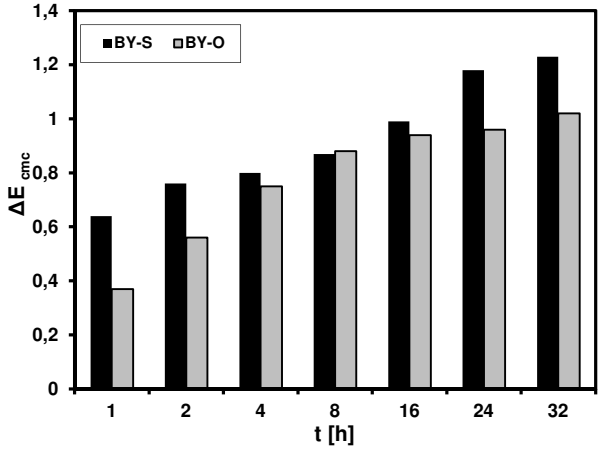

Figure 3.63: Color difference variation with the residence time in the oven at 160 °C

Usually the thermo-oxidative degradation promote the formation of double bond in the polymer chain that act like chromophore groups, increasing the yellow index and the color difference (ΔE_{cmc}).

The Standard Blue Yarn showed an important variation of color just after one hour at 160°C and then it continues to increase with the time. On the other hands, for the Optimized Blue Yarn, the color variation is reduced and seems to be substantially stable after eight hour of exposure.

3.5.4. UV-AGING RESISTANCE

The UV aging resistance is another important feature of carpet requested by the costumers. The UV radiation is very dangerous for the plastic products because it can cause a degradation of mechanical and color properties during the service life. The Standard and the Optimized Blue Yarn were underwent to a UV radiation with a power of 600 Wm^2, for 110 and 220 hours. The UV aging resistance was evaluated

by measuring the morphology, mechanical and color properties of the treated samples.

The variation of the α/γ ratio of the industrial yarn after UV radiation exposure time is reported in Figure 3.64. The morphology seems to be unchanged even after 220 hours of treatment, in fact the α/γ ratio remains fairly constant over the entire time interval. As reported before the Optimized Blue Yarn has an higher α/γ crystalline phase ratio compared to the Standard one.

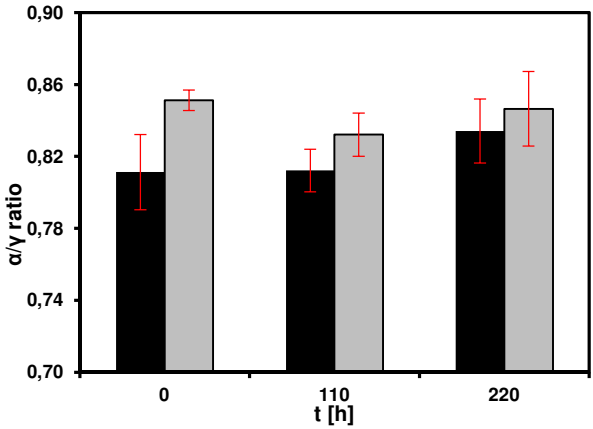

Figure 3.64: α/γ ratio of the BY-S and BY-O UV treated at different UV treatment times

Figure 3.65 shows the elastic modulus of the BY-S and BY-O yarns UV treated for 110 and 220 hours. No significant variations are recorded for the two residence times, but the Optimized Blue Yarn shows higher elastic modulus values with respect to the standard yarn.

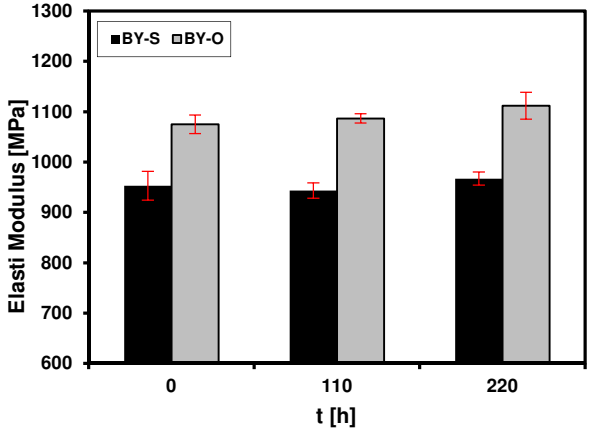

Figure 3.65: Elastic modulus of BY-S and BY-O UV treated at different times

In Figure 3.66 the tenacity of the BY-S and BY-O UV treated at different times is reported. The tenacity is reduced after 110 hour of exposure, because of UV degradation, and then it remains constant. Both samples, considering the standard deviation, show similar tenacity values at all the UV exposure times.

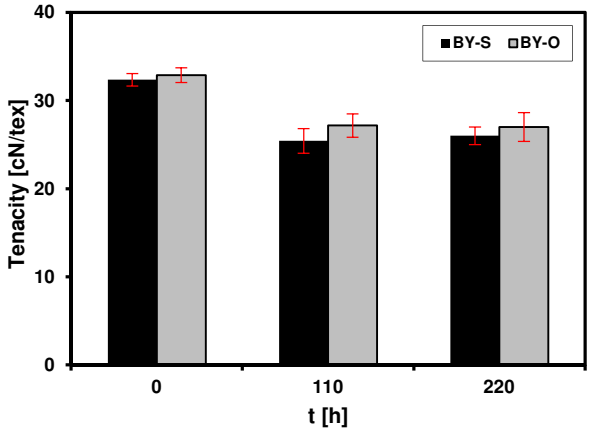

Figure 3.66: Tenacity of BY-S and BY-O UV treated at different times

The mechanical properties of the Standard Blue Yarn and of the Optimized Blue Yarn, at different time of UV exposure, are respectively reported in Table 3.23 and in Table 3.24.

BY-S			
Exposure time [h]	0	110	220
Elastic Modulus [MPa]	953 ± 29	943 ± 15	967 ± 13
Tensile strength [MPa]	369,6 ± 8,4	289,8 ± 13,8	295,2 ± 10,3
Deformation at break [%]	52,4 ± 2,1	35,0 ± 2,5	33,6 ± 1,6
Tenacity [cN/tex]	32,4 ± 0,7	25,4 ± 1,4	26,0 ± 1,0

Table 3.23: Mechanical properties of BY-S at different UV exposure times

BY-O			
Exposure time [h]	0	110	220
Elastic Modulus [MPa]	1075 ± 18	1087 ± 9	1112 ± 27
Tensile strength [MPa]	383,9 ± 0,1	316,7 ± 17,5	314,6 ± 20,4
Deformation at break [%]	49,6 ± 2,1	32,6 ± 1,9	32,4 ± 2,2
Tenacity [cN/tex]	32,9 ± 0,8	27,2 ± 1,3	27,0 ± 1,6

Table 3.24: Mechanical properties of BY-O at different UV exposure times

The resistance to the UV radiation was also studied in terms of color variation with the exposure time, taken the yarn just produced as a reference. The results are reported in Figure 3.67.

The UV degradation usually produces a color variation because of the formation of new chromophoric groups that increase the yellow index and the color difference (ΔE_{cmc}). After 110 h of UV radiation exposure both yarns show only slight color variations compared to the untreated samples. For the Standard Blue Yarn a slight increase of the color difference after 220 h of residence time is recorded, while in

the Optimized Blue Yarn the color difference after 220 h resulted substantially stable.

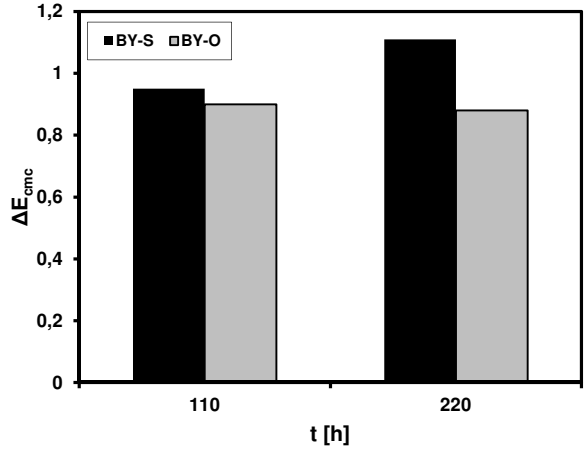

Figure 3.67: Color differences variation with the UV exposure times

3.5.5. GENERAL COMPARISON

In Table 3.25 the most important properties of the optimized and standard Blue Yarns are compared. It is possible to notice that the optimized production process allows to obtain a yarn with higher mechanical properties, probably due to the higher α crystalline phase present in the fiber microstructure.

The optimized product shows higher thermal and UV stability, in fact the microstructure (α/γ ratio) is less affected by the environmental stresses due to the application of these treatments. Moreover, even the mechanical properties undergo to lower reduction after both thermal and UV exposure.

	BY-S	BY-O
t = 0h		
α/γ ratio	0,813	0,851
Elastic Modulus [MPa]	953 ± 29	1075 ± 18
Tensile Strength [MPa]	369,6 ± 8,4	383,9 ± 0,1
Thermal treatment: t = 32h		
α/γ ratio	107,3%	104,7%
Elastic Modulus	87,2%	89,6%
Tensile Strength	88,5%	88,4%
Tenacity	88,6%	88,1%
UV exposure: t = 220h		
α/γ ratio	102,9%	99,4%
Elastic Modulus	101,5%	103,4%
Tensile Strength	79,8%	81,9%
Tenacity	80,2%	82,1%

Table 3.25: Comparison between the physical properties of standard and optimized blue yarns. The percentages are calculated from Table 3.21, 3.22, 3.23 and 3.24.

3.6. INDUSTRIAL TEST

In order to confirm the interesting experimental results obtained on the optimized blue yarn at the laboratory scale, an industrial test was performed and the most problematic aspect of the process were critically analyzed. During the industrial melt spinning process there are two critical points that depend on the masterbatch properties and, in particular, on the color pigment dispersion in the polyamide matrix. The first is the clogging phenomenon that occurred on the extruder filter that causes the increase of pressure, while the second is the filament breakage under the spinneret.

3.6.1. CLOGGING PHENOMENON AT THE EXTRUDER FILTER

In Figure 3.68 the industrial layout of solution dyed bulk continuous filament process is represented. The polyamide 6 matrix and the color masterbatch are mixed together by an extrusion and, before going into the melt pump, the resulting compound is forced to pass through a filter with a dimension of 60 µm.

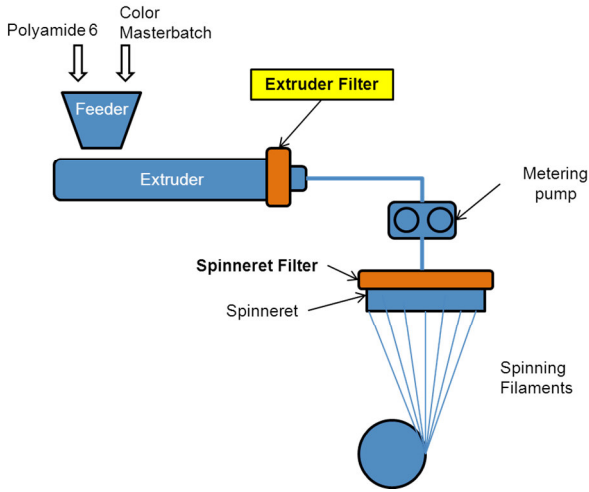

Figure 3.68: Industrial layout of solution dyed bulk continuous filament

The filtration process has the aim to remove impurities, gels and large additive agglomerates that could clog the spinneret filter and promote the fibers breakage under the spinneret [76, 77]. Some of the most problematic color masterbatches, like the blue one, tend to rapidly clog the extruder filter, determining an important increase of the pressure. This make necessary to stop the production in order to change the filter. From an industrial point of view, this operation means a reduction of production output, an increase of the cost and a reduction of the processability.

In order to evaluate the effect of the pigment dispersion improvement in the Blue Masterbatch on the extruder filter clogging phenomenon, the Standard and the Optimized products were used to color yarns during an industrial production.

In Figure 3.69 the pressure variation on the extruder filter, registered during the two productions, is reported. It is easy detectable that the use of the optimized blue masterbatch allows to markedly reduce the clogging rate of about 70%, passing from 1.06 bar/h to 0.27 bar/h. This result is in accordance with the clogging power results, measured through filter test method. The pigment dispersion improvement, obtained increasing the specific mechanical energy involved in the monoconcentrated masterbatch production, has a positive influence also on the final production step, increasing the productivity and the stability of the plant and reducing the production cost.

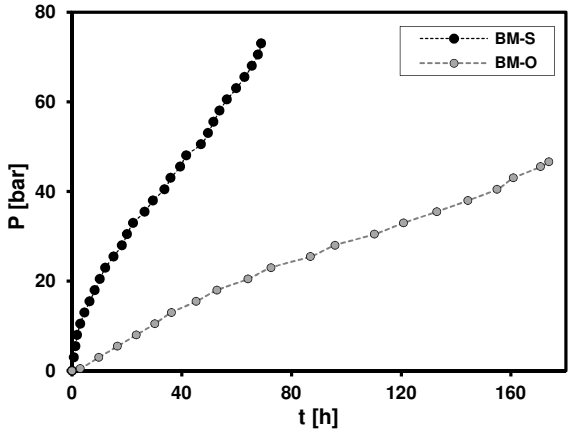

Figure 3.69: Pressure variation on the extruder filter during production by using BM-s and BM-O

3.6.2. FILAMENT BREAKAGE UNDER THE SPINNERET

Another crucial aspect that can be affected by the quality of the color masterbatch is the filament breakage during the melt spinning process. In Figure 3.70 a representation of the industrial layout of solution dyed bulk continuous filament is shown, evidencing where the filament breakage could occurs, i.e. under the spinneret, when the melt flow comes out from the holes. This phenomenon is probably related to the presence of monomer and low molecular weight component that can form drops under the spinneret and that can fall down breaking the filament.

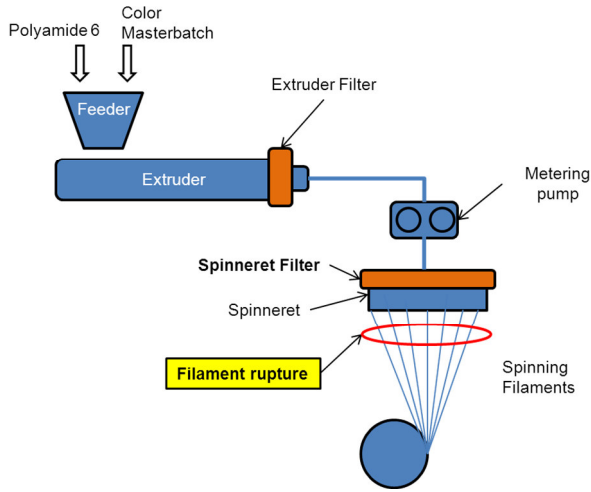

Figure 3.70: Industrial layout of solution dyed bulk continuous filament

Industrially speaking, the filament breakage leads to a reduction of productivity because of the consequent production stop. The blue masterbatch is a critical product even for the filament breakage point of view. For this reason, during the industrial production of the standard and of the optimized blue yarn, the filament rupture under the spinneret were monitored.

A significant filament breakage reduction is registered for the production where the optimized blue masterbatch was used, passing from 7.3 to 4 breakage per tons, with a relative improvement of about 45%. This result is probably due to the thermal stability enhancement of the optimized product that leads to a lower monomer concentration and, in general, to a higher degradation resistance.

4. CONCLUSIONS

The industrial yarns used in the carpet sector and automotive market are made by polyamide 6 and colored by a so called mass pigmentation process. The color pigment are added into the polymer matrix during the melt spinning through the use of color masterbatches. They are obtained mixing different monoconcentrated masterbatches constituted by polymer and one type of color pigment, in order to achieved the color requested by the costumer.

- In this work, the most important and common monoconcentrated masterbatches were industrially produced and analyzed in order to optimized the processing set-up and to improve the pigment dispersion in polymer matrix, without affecting the thermal stability of the final product. The filtration process after the extrusion was find to be useless for all the products. On the basis of these considerations it was removed from the industrial layout allowing an important reduction of production waste and an increase of productivity.

- The phthalocyanines PG7 and PB15:3 and the dioxazine PV23 are the most problematic monoconcentrated masterbatches, as well known in literature, in terms of clogging power. The increase of the specific mechanical energy involved during the extrusion allowed to improve the dispersive and distributive mixing of the color pigments. This led to an important reduction of the clogging power and to a significant increase of the relative color strength of the products. Obviously, the prolonged thermo-mechanical treatment lead to a partial thermo-oxidative degradation of the matrix, reducing the apparent and intrinsic viscosity, increasing the end groups of the macromolecules and the monomer formation. This aspect did not negatively affect the subsequent production steps.

- Blue Masterbatch is a problematic product because it tends to clog the extruder filter during the melt spinning process and to promote the formation of drops under the spinneret that can cause an increase of filament breakage during the production. For these reasons, it was produced using the standard monoconcentrated masterbatches and the optimized one, obtained through the new process setup (i.e. 2 extrusions without filtration), in order to evaluate if the pigment dispersion improvement could positively influence the quality of the final product. The use of the optimized blue masterbatch to color the industrial yarn allowed to markedly reduce the clogging phenomenon on the extruder filter of about 70%, reducing the number of filter substitutions and so the production stops. Moreover, the filament breakage were reduced of about 45%, increasing the productivity of the process, the stability of the product and reducing the production cost.

- Finally, even the yarns produced were characterized in order to evaluate the effect of the pigment dispersion on the final product. The optimized yarn showed an improvement of the mechanical properties, in particular the elastic modulus, compared with the standard product. This is a very important issue from an industrial point of view, because the higher elastic modulus, the higher carpet resistant to the compressive stresses during its service life. The pigment dispersion improvement enhanced the heterogeneous nucleation of the polyamide 6 during the melt spinning, resulting in a higher content of the more stable α phase with respect to the γ crystalline phase. Moreover, both the thermal and UV degradation resistance were improved.

5. REFERENCES

1. http://www.aquafil.com.
2. Kohan M.I., *Nylon Plastics Handbook*. 2nd ed. 1995, New York: Hanser/Gardner Publications.
3. Aharoni S.M., *n-Nylons, their synthesis, structure, and properties*. 1997, Hoboken (NJ): Wiley & Sons.
4. Thomas S. and M V.P., *Handbook of Engineering and Specialty Thermoplastics, Nylons*. 2011: Wiley & Sons.
5. Page I.B., *Polyamides as Engineering Thermoplastic Materials*. 2000, Shawbury: Rapra Technology.
6. Jackman D.R., Dixon M.K. and Condra J., *The Guide to Textiles for Interiors*. 2003, Winnipeg (CA): Portage & Main Press.
7. http://www.reach.gov.it/.
8. Nassau K., *The physics and chemistry of color: the fifteen causes of color*. 2001, New York: Wiley & Sons.
9. Christie R.M. and Chemistry R.S.o., *Colour Chemistry*. 2001, Cambridge: Royal Society of Chemistry.
10. Zollinger H., *Color Chemistry: Syntheses, Properties, and Applications of Organic Dyes and Pigments*. 2003, Zurich: Wiley & Sons.
11. Judd D.B. and Wyszecki G., *Color in Business, Science, and Industry*. 1967, Hoboken (NJ): Wiley & Sons.
12. Drobny J.G., *Radiation Technology for Polymers*. 2 ed. 2012, Boca Raton (FL): Taylor & Francis.
13. Overheim R.D. and Wagner D.L., *Light and Color*. 1982, London: Evans Brothers.
14. Malacara D., *Color Vision and Colorimetry: Theory and Applications*. 2002, Miami: Society of Photo Optical.

15. Cheshire G., *Light and Color*. 2006, North Mankato (MN): Smart Apple Media.
16. Flesch P., *Light and Light Sources: High-Intensity Discharge Lamps*. 2007, Berlin: Springer.
17. Tilley R.J.D., *Colour and The Optical Properties of Materials: An Exploration of the Relationship Between Light, the Optical Properties of Materials and Colour*. 2010, Chichester: Wiley & Sons.
18. Ariño I., Kleist U. and Rigdahl M., *Color of pigmented plastics - Measurements and predictions.* Polymer Engineering & Science, 2004. **44**(1): p. 141-152.
19. Rohatgi-Mukherjee K.K., *Fundamentals of Photochemistry*. 1978, New Dehli: Wiley & Sons.
20. Goldstein E.B., *Sensation and Perception*. 2013, Andover (UK): Wadsworth.
21. Freberg L., *Discovering Biological Psychology*. 2010, Belmont: Wadsworth, Cengage Learning.
22. McDonald R., *Colour physics for industry*. 1997, Bradford: Society of Dyers and Colourists.
23. Burger W. and Burge M., *Principles of Digital Image Processing: Core Algorithms*. 2010, London: Springer.
24. Schubert E.F., *Light-emitting Diodes*. 2003, Cambridge: Cambridge University Press.
25. Rigg B., *Color difference formulas-Recent developments*. Second ed. 1997: Aatcc. 109-112.
26. Kang H.R., *Computational Color Technology*. 2006, Miami: Society of Photo Optical.
27. Luo M.R., *Development of colour-difference formulae.* Review of Progress in Coloration and Related Topics, 2002. **32**(1): p. 28-39.
28. Sharma G. and Bala R., *Digital Color Imaging Handbook*. 2002, Boca Raton (FL): CRC Press.

29. McDonald R. and Smith K.J., *CIE94-A new color-difference formula at COLOR TECHNOLOGY in the textile industry*. Second ed. 1997: Aatcc. 113-117.
30. Ambasta B.K., *Chemistry for Engineers*. 2006, New Delhi: Laxmi Publications.
31. Randall D.L., *Instrumentation for the measurement of color*. Second ed. 1997: Aatcc. 9-15.
32. Homann J.P., *Digital Color Management: Principles and Strategies for the Standardized Print Production*. 2008, Berlin: Springer.
33. Hao Z. and Iqbal A., *Some aspects of organic pigments.* Chemical Society Reviews, 1997. **26**(3): p. 203-213.
34. Sargent W., *The Enjoyment and Use of Color*. 1923, New York: Dover Publications.
35. Deshmukh S.P., Parmar M.B., Rao A.C., et al., *Polymer- and wax-based monoconcentrate predispersed pigments in the colouring of plastics.* Coloration Technology, 2010. **126**(4): p. 189-193.
36. Marcinčin A., *Modification of fiber-forming polymers by additives.* Progress in Polymer Science, 2002. **27**(5): p. 853-913.
37. Sugimoto T., *Monodispersed Particles*. 2001, Amsterdam: Elsevier.
38. Otterstedt J.E. and Brandreth D.A., *Small Particles Technology*. 1998, New York: Springer.
39. Parfitt G.D., *Dispersion of Powders in Liquids: With Special Reference to Pigments*. 1981, London: Elsevier.
40. Liu M., *Coating Technology of Nuclear Fuel Kernels: A Multiscale View*. Modern Surface Engineering Treatments. 2013.
41. Ahmed S.I., Shamey R., Christie R.M., et al., *Comparison of the performance of selected powder and masterbatch pigments on mechanical properties of mass coloured polypropylene filaments.* Coloration Technology, 2006. **122**(5): p. 282-288.

42. Van de Velde K., Van Wassenhove V. and Kiekens P., *Optical analyses of pigment particles in colour concentrates and polypropylene yarns.* Polymer Testing, 2002. **21**(6): p. 675-689.
43. Ajayan P.M., Schadler L.S. and Braun P.V., *Nanocomposite Science and Technology*. 2006, Weinheim: Wiley & Sons.
44. Ahmed M., *Polypropylene fibers, science and technology*. 1982, Oxford: Elsevier.
45. Bart J.C., *Plastics Additives: Advanced Industrial Analysis*. 2006, Amsterdam: IOS Press.
46. Karger K.J., *Polypropylene: An A-Z Reference*. 1999, Norwell: Kluwer.
47. Lee Wo D. and Tanner R., *The impact of blue organic and inorganic pigments on the crystallization and rheological properties of isotactic polypropylene.* Rheologica Acta, 2010. **49**(1): p. 75-88.
48. Fillon B., Lotz B., Thierry A., et al., *Self-nucleation and enhanced nucleation of polymers. Definition of a convenient calorimetric "efficiency scale" and evaluation of nucleating additives in isotactic polypropylene (α phase).* Journal of Polymer Science Part B: Polymer Physics, 1993. **31**(10): p. 1395-1405.
49. Ziabicki A., *Theoretical analysis of oriented and non isothermal crystallization.* Colloid and Polymer Science, 1974. **252**(3): p. 207-221.
50. Wlochowicz A. and Broda J., *SAXS and WAXS investigations of mass coloured polyamide fibres.* Acta Polymerica, 1992. **43**(5): p. 252-257.
51. Ujhelyiová A., Marcinčin A., Kišš M., et al., *Nucleation and crystallization of polypropylene filled with BaSO4.* Journal of thermal analysis, 1996. **46**(2): p. 619-626.
52. Heuvel H.M. and Huisman R., *Effects of winding speed, drawing and heating on the crystalline structure of nylon 6 yarns.* Journal of Applied Polymer Science, 1981. **26**(2): p. 713-732.

53. Lu F.M. and Spruiell J.E., *The role of crystallization kinetics in the development of the structure and properties of polypropylene filaments.* Journal of Applied Polymer Science, 1993. **49**(4): p. 623-631.
54. Herbst W. and Hunger K., *Industrial Organic Pigments: Production, Properties, Applications*. 2006: Wiley & Sons.
55. Lewis P.A., *Pigment Handbook: Properties and economics*. 1988, Hoboken (NJ): Wiley & Sons.
56. Murphy J., *Additives for Plastics Handbook*. 2001, Oxford: Elsevier.
57. Zweifel H., Maier R.D. and Schiller M., *Plastics Additives Handbook*. 2009, Munich: Hanser Publishers.
58. Harris R.M., *Coloring Technology for Plastics*. 1999, New York: William Andrew.
59. Joshi A., Rathi S. and Deshpande S., *Analysis of the wetting behaviour of pigments and the effectiveness of surfactants.* Coloration Technology, 2009. **125**(2): p. 99-103.
60. Knor N., Walter R. and Haupert F., *Mechanical and thermal properties of nano-titanium dioxide-reinforced polyetheretherketone produced by optimized twin screw extrusion.* Journal of Thermoplastic Composite Materials, 2011. **24**(2): p. 185-205.
61. Mather R.R., *Fractal analysis of the surfaces of anisometric pigment particles.* Colloids and Surfaces A: Physicochemical and Engineering Aspects, 1995. **98**(3): p. 191-195.
62. Mather R.R., *The effect of crystal properties on the manufacture and application performance of copper phthalocyanine pigments.* Journal of Porphyrins and Phthalocyanines, 1999. **3**(6-7): p. 643-646.
63. Fryer J.R., McKay R.B., Mather R.R., et al., *The technological importance of the crystallographic and surface properties of copper phthalocyanine pigments.* Journal of Chemical Technology and Biotechnology, 1981. **31**(1): p. 371-387.

64. Giles H.F., Wagner J.R. and Mount E.M., *Extrusion: The Definitive Processing Guide and Handbook*. 2013, Oxford: Elsevier
65. De Filippi A.M., *Fabbricazione di componenti in materiali polimerici*. 2004, Milano: Hoepli.
66. Harris H.E., *Extrusion Control: Machine-process-product*. 2004, Munich: Hanser Publishers.
67. Rosato D.V., *Extruding Plastics: A Practical Processing Handbook*. 1998, Norwell: Chapman & Hall.
68. Kent R.J., *Plastics Profile Extrusion*. 1998, Shawbury: Rapra Technology.
69. Filippo C., *Proprietà e lavorazione delle materie plastiche. Guida pratica per i tecnici dell'industria*. 2005, Palermo: EuroPass.
70. Ciaperoni A. and Mula A., *Chimica e tecnologia delle poliammidi*. 2001, Pisa: Pacini
71. Rauwendaal C., *Polymer Extrusion*. 2001, Munich: Hanser Publishers.
72. Saechtling H. and Baucia G., *Manuale delle materie plastiche*. 2006, Milano: Tecniche Nuove.
73. Michaeli W., *Plastics Processing: An Introduction*. 1995, Munich: Hanser Publishers.
74. Chung C.I., *Extrusion of Polymers: Theory and Practice*. 2000, Munich: Hanser Publishers.
75. Eichhorn S.J. and Institute T., *Handbook of textile fibre structure: Fundamentals and manufactured polymer fibres. Vol. 1*. 2009, Cambridge: Woodhead Publishing.
76. Lewin M. and Sello S.B., *Handbook of Fiber Science and Technology: Fiber chemistry*. 1985, New York: Marcel Dekker.
77. Griskey R.G., *Polymer Process Engineering*. 1995, New York: Chapman & Hall.
78. Gupta V.B. and Kothari V.K., *Manufactured Fibre Technology*. 1997, London: Chapman & Hall.

79. Bunsell A.R. and Institute T., *Handbook of Tensile Properties of Textile and Technical Fibres*. 2009, Cambridge: Woodhead Publishing.

80. Agassant J.F., Avenas P., Sergent J.P., et al., *Polymer Processing: Principles and Modeling*. 1991, Cincinnati (OH): Hanser Publishers.

81. Jeon Y.P. and Cox C.L., *Simulation of multifilament semicrystalline polymer fiber melt-spinning.* Journal of Engineered Fibers and Fabrics, 2009. **4**(1): p. 34-43.

82. Kalb B. and Pennings A.J., *Maximum strength and drawing mechanism of hot drawn high molecular weight polyethylene.* Journal of Materials Science, 1980. **15**(10): p. 2584-2590.

83. Ciferri A. and Ward I.M., *Ultra-High Modulus Polymers*. 1979: Applied Science Publishers.

84. Zachariades A.E. and Kanamoto T., *New model for the high modulus and strength performance of ultradrawn polyethylenes.* Journal of Applied Polymer Science, 1988. **35**(5): p. 1265-1281.

85. Takajima T., Kajiwara K. and McIntyre J.E., *Advanced Fiber Spinning Technology*. 1994, Cambridge: Woodhead Publishing.

86. Akron C.D., *Rheology and Processing of Polymeric Materials*. Vol. 2. 2007, Oxford: Oxford University Press.

87. Doufas A.K., McHugh A.J. and Miller C., *Simulation of melt spinning including flow-induced crystallization: Part I. Model development and predictions.* Journal of Non-Newtonian Fluid Mechanics, 2000. **92**(1): p. 27-66.

88. Shimizu J., Okui N., Kikutani T., et al., *High speed melt spinning of Nylon 6.* Sen'i Gakkaishi, 1981. **37**(4): p. T143-T152.

89. Beyreuther R. and Brünig H., *Dynamics of Fibre Formation and Processing: Modelling and Application in Fibre and Textile Industry*. 2006, Berlin: Springer.

90. Kothari V.K., *Textile Fibres: Developments and Innovations*. 2000: IAFL Publications.

91. Mukhopadhyay S.K. and Institute T., *The Structure and Properties of Typical Melt-spun Fibres: A Critical Appreciation of Recent Developments*. 1989, Manchester: Textile Institute.

92. Ziabicki A. and Kawai H., *High-Speed Fiber Spinning: Science and Engineering Aspects*. 1991, Malabar (FL): Krieger Publishing Company.

93. Hsiao S., Wang H., Chou J., et al., *Synthesis and characterization of novel organosoluble and thermally stable polyamides bearing triptycene in their backbones.* Journal of Polymer Research, 2012. **19**(7): p. 9902-9911.

94. Buccella M., Dorigato A., Pasqualini E., et al., *Thermo-mechanical properties of Polyamide 6 chemically modified by chain extension with Polyamide/Polycarbonate blend.* Journal of Polymer Research, 2012. **19**(8): p. 1-9.

95. Papaspyrides C.D. and Vouyiouka S.N., *Solid State Polymerization*. 2009, Hoboken (NJ): Wiley & Sons.

96. Sperling L.H., *Introduction to Physical Polymer Science*. 2005, Haboken (NJ): Wiley & Sons.

97. Wagner W., *Process for the Production of Polyamide-6 Filament Yarns, Polyamide-6,6 Filament Yarns and Polyester Filament Yarns*. 1977: Bayer.

98. *Fibres and Plastics*. 1961: L. Hill Technical Group.

99. Buccella M., Dorigato A., Caldara M., et al., *Thermo-mechanical behaviour of Polyamide 6 chain extended with 1,1'-carbonyl-bis-caprolactam and 1,3-phenylene-bis-2-oxazoline.* Journal of Polymer Research, 2013. **20**(9): p. 1-9.

100. Buccella M., Dorigato A., Pasqualini E., et al., *Chain extension behavior and thermo-mechanical properties of polyamide 6 chemically modified with 1,1'-carbonyl-bis-caprolactam.* Polymer Engineering & Science, 2013. **54**(1): p. 158-165.

101. Lave L., Conway S.N., Harvey J., et al., *Recycling Postconsumer Nylon Carpet.* Journal of Industrial Ecology, 1998. **2**(1): p. 117-126.

102. Braun M., Levy A.B. and Sifniades S., *Recycling nylon 6 carpet to caprolactam.* Polymer-Plastics Technology and Engineering, 1999. **38**(3): p. 471-484.

103. Kojima Y., Usuki A., Kawasumi M., et al., *Mechanical properties of nylon 6-clay hybrid.* Journal of Materials Research, 1993. **8**(5): p. 1185-1189.

104. Bunn C.W. and Garner E.V., *The crystal structures of two polyamides ('Nylons').* Proceedings of the Royal Society of London. Series A, Mathematical and Physical Sciences, 1947. **189**(1016): p. 39-68.

105. Holmes D.R., Bunn C.W. and Smith D.J., *The crystal structure of polycaproamide: Nylon 6.* Journal of Polymer Science, 1955. **17**(84): p. 159-177.

106. Arimoto H., Ishibashi M., Hirai M., et al., *Crystal structure of the γ-form of nylon 6.* Journal of Polymer Science Part A, 1965. **3**(1): p. 317-326.

107. http://www.specialchem4coatings.com/tc/color-handbook.

108. Buxbaum G., *Industrial Inorganic Pigments*. 2008, New York: Wiley & Sons.

109. Lee Y.J., Feke D.L. and Manas Z.I., *Dispersion of titanium dioxide agglomerates in viscous media.* Chemical Engineering Science, 1993. **48**(19): p. 3363-3372.

110. Koleske J.V., *Paint and Coating Testing Manual: Fourteenth Edition of the Gardner-Sward Handbook*. 1995: ASTM.

111. Dorigato A., *Viscoelastic and fracture behaviour of polyolefin based nanocomposites*, in *PhD Thesis at Department of Materials Engineering and Industrial Technologies*. 2009, University of Trento: Trento.

112. Medalia A.I. and Richards L.W., *Tinting strength of carbon black.* Journal of Colloid and Interface Science, 1972. **40**(2): p. 233-252.

113. Stacy C.J., Johnson P.H. and Kraus G., *Effect of carbon black structure aggregate size distribution on properties of reinforced rubber.* Rubber Chemistry and Technology, 1975. **48**(4): p. 538-547.

114. Gregory P., *High-Technology Applications of Organic Colorants*. 2012, London: Springer.

115. Giesen V. and Eisenlohr R., *Pigment printing.* Review of Progress in Coloration and Related Topics, 1994. **24**(1): p. 26-30.

116. Fryberg M., *Dyes for ink–jet printing.* Review of Progress in Coloration and Related Topics, 2005. **35**(1): p. 1-30.

117. Brown C.J., *Crystal structure of [small beta]-copper phthalocyanine.* Journal of the Chemical Society A: Inorganic, Physical, Theoretical, 1968(0): p. 2488-2493.

118. McKay R.B., *The development of organic pigments with particular reference to physical form and consequent behaviour in use.* Review of Progress in Coloration and Related Topics, 1979. **10**(1): p. 25-32.

119. Craver C. and Carraher C., *Applied Polymer Science*. 2000, Oxford: Elsevier.

120. Peters A.T. and Freeman H.S., *Modern Colorants: Synthesis and Structures*. 1995, Glasgow: Blackie Academic & Professional.

121. Beebe G., *Colorants for Plastics*, in *Encyclopedia of Chemical Technology*. 2000, Wiley & Sons: New Jersey.

122. Faulkner E.B. and Schwartz R.J., *High Performance Pigments*. 2009, Weinheim: Wiley & Sons.

123. Kutz M., *Applied Plastics Engineering Handbook: Processing and Materials*. 2011, London: Elsevier.

124. Manas-Zloczower I., *Mixing and Compounding of Polymers: Theory and Practice*. 2009, Munich: Hanser Publishers.

125. Charvat R.A., *Coloring of Plastics: Fundamentals*. 2005, New Jersey: Wiley & Sons.

126. Kohlgrüber K. and Bierdel M., *Co-rotating Twin-screw Extruders*. 2008, New York: Carl Hanser Publishers.

127. Levy S. and Carley J.F., *Plastics Extrusion Technology Handbook*. 1989, New York: Industrial Press.

128. Hensen F. and Berghaus U., *Plastics Extrusion Technology*. 1997, Munich: Hanser Publishers.

129. Godavarti S. and Karwe M.V., *Determination of specific mechanical energy distribution on a twin-screw extruder.* Journal of Agricultural Engineering Research, 1997. **67**(4): p. 277-287.

130. Liang M., Huff H.E. and Hsieh F.H., *Evaluating energy consumption and efficiency of a twin-screw extruder.* Journal of Food Science, 2002. **67**(5): p. 1803-1807.

131. Eise K., Herrmann H., Jakopin S., et al., *An analysis of twin-screw extruder mechanisms.* Advances in Polymer Technology, 1981. **1**(2): p. 18-39.

132. Ilo S., Tomschik U., Berghofer E., et al., *The effect of extrusion operating conditions on the apparent viscosity and the properties of extrudates in twin-screw extrusion cooking of maize grits.* LWT - Food Science and Technology, 1996. **29**(7): p. 593-598.

133. Domenech T., Peuvrel-Disdier E. and Vergnes B., *The importance of specific mechanical energy during twin screw extrusion of organoclay based polypropylene nanocomposites.* Composites Science and Technology, 2013. **75**(0): p. 7-14.

134. Gropper M., Moraru C.L. and Kokini J.L., *Effect of specific mechanical energy on properties of extruded protein-starch mixtures.* Cereal Chemistry, 2002. **79**(3): p. 429-433.

135. Wildi R.H. and Maier C., *Understanding Compounding*. 1998, Munich: Hanser Publishers.

136. Domenech T., Peuvrel D.E. and Vergnes B., *The importance of specific mechanical energy during twin screw extrusion of organoclay based polypropylene nanocomposites.* Composites Science and Technology, 2013. **75**(0): p. 7-14.

137. Villmow T., Kretzschmar B. and Pötschke P., *Influence of screw configuration, residence time, and specific mechanical energy in twin-screw extrusion of polycaprolactone/multi-walled carbon nanotube composites.* Composites Science and Technology, 2010. **70**(14): p. 2045-2055.

138. Ciardelli F., Crescenzi V., Pezzin G., et al., *Macromolecole. Scienza e tecnologia*. 2007, Pisa: Nuova Cultura.

139. Ciardelli F., *Macromolecole: scienza e tecnologia*. 1983, Pisa: Pacini.

140. Ghosh P., *Polymer Science and Technology: Plastics, Rubbers, Blends and Composites*. 2001, New Delhi: McGraw-Hill.

141. Ebewele R.O., *Polymer Science and Technology*. 2000, Boca Raton (FL): Taylor & Francis.

142. Kwak S.Y., Kim J.H., Kim S.Y., et al., *Microstructural investigation of high-speed melt-spun nylon 6 fibers produced with variable spinning speeds.* Journal of Polymer Science Part B: Polymer Physics, 2000. **38**(10): p. 1285-1293.

143. Condon J.B., *Surface Area and Porosity Determinations by Physisorption: Measurements and Theory*. 2006, Oxford: Elsevier.

144. Brunauer S., Emmett P.H. and Teller E., *Adsorption of gases in multimolecular layers.* Journal of the American Chemical Society, 1938. **60**(2): p. 309-319.

145. Barrett E.P., Joyner L.G. and Halenda P.P., *The determination of pore volume and area distributions in porous substances. I. Computations from nitrogen isotherms.* Journal of the American Chemical Society, 1951. **73**(1): p. 373-380.

146. Jonasz M. and Fournier G., *Light Scattering by Particles in Water: Theoretical and Experimental Foundations: Theoretical and Experimental Foundations*. 2011, London: Elsevier.

147. Berne B.J. and Pecora R., *Dynamic Light Scattering: With Applications to Chemistry, Biology, and Physics*. 2000, Toronto: Dover Publications.

148. Johnson C.S. and Gabriel D.A., *Laser Light Scattering*. 1994, New York: Dover Publications.

149. Mishchenko M.I., Hovenier J.W. and Travis L.D., *Light Scattering by Nonspherical Particles: Theory, Measurements, and Applications*. 1999, San Diego: Academic Press.

150. Goldburg W.I., *Dynamic light scattering.* American Journal of Physics, 1999. **67**(12): p. 1152-1160.

151. Xu R., *Particle Characterization: Light Scattering Methods*. 2001, New York: Springer.

152. Rahbar R.S. and Mojtahedi M.R.M., *Influence of hot multistage drawing on structure and mechanical properties of nylon 6 multifilament yarn* Journal of Engineered Fibers and Fabrics, 2011. **6**(2): p. 7-15.

153. Kaiserberger E., *NETZSCH Annual for Science and Industry: DSC-TG-DMA-TMA : DSC, TG, DMA and TMA Results of Investigations of Thermoplastics, Thermosets, Elastomers and Additives. TA for polymer engineering*. 1994: NETZSCH-Gerätebau GmbH.

154. Brandrup J., Immergut E.H. and Grulke E.A., *Polymer Handbook*. 4th ed. 1999: Wiley & Sons.

155. Fambri L., Incardona S.D., Migliaresi C., et al., *Crystallization kinetics of J-1 polymer under different thermal treatments.* Journal of Materials Science, 1994. **29**(18): p. 4678-4682.

156. Fambri L., Pegoretti A., Gleria M., et al., *Thermal and mechanical characterization of poly[bis(4-benzylphenoxy)phosphazene].* Polymer, 1994. **35**(22): p. 4813-4818.

157. Qiu S., Zheng Y., Zeng A., et al., *Non-isothermal crystallization of monomer casting polyamide 6/functionalized MWNTs nanocomposites.* Polymer Bulletin, 2011. **67**(9): p. 1945-1959.

158. Durmus A. and Yalçınyuva T., *Effects of additives on non-isothermal crystallization kinetics and morphology of isotactic polypropylene.* Journal of Polymer Research, 2009. **16**(5): p. 489-498.

159. Şanlı S., Durmus A. and Ercan N., *Effect of nucleating agent on the nonisothermal crystallization kinetics of glass fiber- and mineral-filled polyamide-6 composites.* Journal of Applied Polymer Science, 2012. **125**(S1): p. E268-E281.

160. Şanlı S., Durmus A. and Ercan N., *Isothermal crystallization kinetics of glass fiber and mineral-filled polyamide 6 composites.* Journal of Materials Science, 2012. **47**(7): p. 3052-3063.

161. Zhang Y., Wang B. and Hu G., *Isothermal crystallization kinetics and melting behavior of polyamide 11/silica nanocomposites prepared by in situ melt polymerization.* Journal of Applied Polymer Science, 2012. **123**(1): p. 273-279.

162. Yang Z., Huang S. and Liu T., *Crystallization behavior of polyamide 11/multiwalled carbon nanotube composites.* Journal of Applied Polymer Science, 2011. **122**(1): p. 551-560.

163. Ludtge C., *Quality recipe for high-quality masterbatches.* Kunststoffe-Plast Europe, 2005. **95**(9): p. 176-177.

164. Klein G.A., *Industrial Color Physics*. 2010, New York: Springer.

165. Lewin M., *Handbook of Fiber Chemistry, Third Edition*. 2010, Boca Raton (FL): Taylor & Francis.

166. Dijkstra D.J., *Guidelines for rheological characterization of polyamide melts.* Pure and Applied Chemistry, 2009. **81**(2): p. 339-349.

167. Cross M.M., *Polymer rheology: Influence of molecular weight and polydispersity.* Journal of Applied Polymer Science, 1969. **13**(4): p. 765-774.

168. Dealy J.M. and Larson R.G., *Structure and Rheology of Molten Polymers: From Structure to Flow Behavior and Back Again*. 2006, Berlin: Hanser Publishers.

169. Barnes H.A., Hutton J.F. and Walters K., *An Introduction to Rheology*. 1989, Oxford: Elsevier.

170. Dealy J.M. and Saucier P.C., *Rheology in Plastics Quality Control*. 2000, Berlin: Hanser Publishers.

171. Tadros T.F., *Rheology of Dispersions: Principles and Applications*. 2011, Hoboken (NJ): Wiley & Sons.

172. Gupta R.K., *Polymer and Composite Rheology*. Second ed. 2000, New York: Marcel Dekker.

173. Ferry J.D., *Viscoelastic Properties of Polymers*. 1980, New York: Wiley.

174. Holding S.R. and Meehan E., *Molecular Weight Characterisation of Synthetic Polymers*. 1995, Shawbury: Rapra Technology.

175. Shah V., *Handbook of Plastics Testing and Failure Analysis*. 2007, Hoboken (NJ): Wiley & Sons.

176. Rutgers R., *Relative viscosity and concentration.* Rheologica Acta, 1962. **2**(4): p. 305-348.

177. Pamies R., Hernández C.J.G., Martínez C.M., et al., *Determination of intrinsic viscosities of macromolecules and nanoparticles. Comparison of single-point and dilution procedures.* Colloid and Polymer Science, 2008. **286**(11): p. 1223-1231.

178. Steve L., *Characterization and Failure Analysis of Plastics*. 2003, Cleveland (OH): ASM International.

179. Asua J., *Polymer Reaction Engineering*. 2008, Oxford: Wiley & Sons.

180. Berezkin V.G., Alishoev V.R. and Nemirovskai I.B., *Gas Chromatography of Polymers*. 2011, Amsterdam: Elsevier.

181. Brown R., *Handbook of Polymer Testing: Physical Methods*. 1999, New York: Taylor & Francis.

182. Lowell S., *Characterization of Porous Solids and Powders: Surface Area, Pore Size and Density*. 2004, Norwell: Kluwer Academic Publishers.

183. Rouquerol J., Rouquerol F., Llewellyn P., et al., *Adsorption by Powders and Porous Solids: Principles, Methodology and Applications*. 2013, Oxford: Elsevier.

184. Roquerol F., Roquerol J. and Singh K., *Adsorption by powders and porous solids*. 1999, San Diego: Academic Press.

185. Cassagnau P., *Melt rheology of organoclay and fumed silica nanocomposites.* Polymer, 2008. **49**(9): p. 2183-2196.

186. Tung C.M. and Dynes P.J., *Morphological characterization of polyetheretherketone–carbon fiber composites.* Journal of Applied Polymer Science, 1987. **33**(2): p. 505-520.

187. Yuan Q., Awate S. and Misra R.D.K., *Nonisothermal crystallization behavior of polypropylene–clay nanocomposites.* European Polymer Journal, 2006(42): p. 1994-2003.

188. Li J., Fang Z., Zhu Y., et al., *Isothermal crystallization kinetics and melting behavior of multiwalled carbon nanotubes/polyamide-6 composites.* Journal of Applied Polymer Science, 2007. **105**(6): p. 3531-3542.

189. ASTM, D123-9, *Standard Terminology Relating to Textiles*, ASTM International, West Conshohocken (PA), 2009

190. Landel R.F. and Nielsen L.E., *Mechanical Properties of Polymers and Composites*. 2nd ed. 1993, New York: Marcel Dekker.

191. Mallick P.K., *Fiber-Reinforced Composites: Materials, Manufacturing, and Design, Second Edition*. 1993, New York: Marcel Dekker.

192. Ahmed S. and Jones F.R., *A review of particulate reinforcement theories for polymer composites.* Journal of Materials Science, 1990. **25**(12): p. 4933-4942.

193. Bigg D.M., *Mechanical properties of particulate filled polymers.* Polymer Composites, 1987. **8**(2): p. 115-122.

194. Jancar J., Dianselmo A. and Dibenedetto A.T., *The yield strength of particulate reinforced thermoplastic composites.* Polymer Engineering & Science, 1992. **32**(18): p. 1394-1399.

195. Galeski A., *Strength and toughness of crystalline polymer systems.* Progress in Polymer Science, 2003. **28**(12): p. 1643-1699.

196. Kryszewski M., Galeski A. and Martuscelli E., *Polymer Blends: Processing, Morphology and Properties*. 1999, New York: Springer.

197. Nielsen L.E., *Simple theory of stress-strain properties of filled polymers.* Journal of Applied Polymer Science, 1966. **10**(1): p. 97-103.

198. Varghese S., Gatos K.G., Apostolov A.A., et al., *Morphology and mechanical properties of layered silicate reinforced natural and polyurethane rubber blends produced by latex compounding.* Journal of Applied Polymer Science, 2004. **92**(1): p. 543-551.

199. Kontou E. and Niaounakis M., *Thermo-mechanical properties of LLDPE/SiO2 nanocomposites.* Polymer, 2006. **47**(4): p. 1267-1280.

200. Ou C.F. and Hsu M.C., *Preparation and properties of cycloolefin copolymer/silica hybrids.* Journal of Applied Polymer Science, 2007. **104**(4): p. 2542-2548.

201. Wichmann M.H.G., Schulte K. and Wagner H.D., *On nanocomposite toughness.* Composites Science and Technology, 2008. **68**(1): p. 329-331.

6. PUBLICATIONS

(Updated to April 13th, 2014)

- Buccella M., Dorigato A., Pasqualini E., Caldara M., Fambri L., ***Thermo-mechanical properties of Polyamide 6 chemically modified by chain extension with Polyamide/Polycarbonate blend***. Journal of Polymer Research, 2012. **19**(8): p. 1-9.

- Buccella M., Dorigato A., Caldara M., Pasqualini E., Fambri L., ***Thermo-mechanical behaviour of Polyamide 6 chain extended with 1,1'-carbonyl-bis-caprolactam and 1,3-phenylene-bis-2-oxazoline***. Journal of Polymer Research, 2013. **20**(9): p. 1-9.

- Buccella M., Dorigato A., Pasqualini E., Caldara M., Fambri L., ***Chain extension behavior and thermo-mechanical properties of polyamide 6 chemically modified with 1,1'-carbonyl-bis-caprolactam***. Polymer Engineering & Science, 2013. **54**(1): p. 158-165.

- Buccella M., Dorigato A., Crugnola F., Caldara F., Fambri L., ***Effect of the extrusion processes on rheological, chemical and coloration properties of a copper phthalocyanine based masterbatch***. Coloration Technology, submitted.

- Buccella M., Dorigato A., Crugnola F., Caldara M., Fambri L., ***Influence of the processing parameters on the dispersion and coloration behaviour of a halogenated copper phthalocyanine based masterbatch***. Journal of Material Science, submitted.

- Buccella M., Dorigato A., Crugnola F., Caldara M., Fambri L., ***Coloration properties and chemo-rheological characterization of a dioxazine pigment based monodispersed masterbatch,*** Journal of Applied Polymer Science, submitted.

- Buccella M., Dorigato A., Caldara M., Fambri L., ***Rheological and molecular characterization of regraded Nylon-6 obtained in different reactive compounding***. International Journal of Polymer Analysis and Characterization, in preparation.

7. CONGRESS CONTRIBUTIONS

(Updated to April 13th, 2014)

- Fambri L., Buccella M., Dorigato A., Pasqualini E., Caldara M., "***Rheological and Molecular Characterization of regraded Nylon-6 obtained in Different Reactive Compounding",*** 24th International Symposium on Polymer Analysis and Characterization, June 6-8th, 2011, Torino (Italy)

- Fambri L., Lorenzi D., Buccella M., Giacomelli G., Comperatore L., ***"Preparation of nanofilled polyamides for spinning and drawing",*** EuroFillers 2011, August 21-25th, 2011, Dresden (Germany)

- Buccella M., Dorigato A., Pasqualini E., Giacomelli G., Caldara M., Fambri L., **"*Rigradazione di poliammidi industriali: caratterizzazione reologica e termo-meccanica",*** XX Convegno Italiano di Scienza e Tecnologia delle Macromolecole, September 4-8th 2011, Terni (Italy)

- Buccella M, Dorigato A., Caldara M., Fambri L., ***"Re-gradation of industrial polyamide 6. Comparison of different chain-extenders."*** European Polymer Federation Congress 2013, 16-21st June 2013, Pisa (Italy)

- Buccella M., Dorigato A., Fambri F., Caldara M., **"Evaluation of color pigment dispersion in polyamide 6 matrix",** 27th International Symposium on Polymer Analysis and Characterization, June 16-18th, 2014, Les Diablerets (Switzerland) - submitted

8. ACKNOWLEDGEMENTS

First of all, I would like to thank my academic tutors, Prof. Luca Fambri and Ing. Andrea Dorigato, PhD (Department of Industrial Engineering, University of Trento, Italy) for their constant support throughout my experimental work.
I would gratefully thank my industrial tutor Dott. Mauro Caldara (Aquafil S.p.A., Arco, Italy) who allowed me to develop the doctorate project into an important multinational company like Aquafil and for his precious support.

I would like to thank all the people which worked with me in the Polymers and Composites Laboratory of the Department of Industrial Engineering (University of Trento, Italy).
A particular thank is devoted to the Aquafil management that gave me this significant opportunity, to work and to grow in an international and multidisciplinary industrial environment. Moreover, I would like to thank all the people in Aquafil that collaborated with me during this experience.

Last but not least, I would gratefully thank my parents, Gemma and Paolo, and my Annalisa for their loving support trough all of these years.

Trento, April 2014